Local electrochemical formation and selective detection of reactive oxygen species

(Lokale elektrochemische Bildung und selektiver Nachweis von reaktiven Sauerstoffspezies)

Von der Fakultät für Mathematik und Naturwissenschaften
der Carl von Ossietzky Universität Oldenburg
zur Erlangung des Grades und Titels eines

Doktors der Naturwissenschaften (Dr. rer. nat.)
angenommene Dissertation

von Herrn **Saustin Dongmo,** M.Sc.
geboren am 25. 07. 1985 in Douala, Kamerun

Oldenburg, Dezember 2016

This work was carried out from April 2013 to June 2016 at the Carl von Ossietzky University of Oldenburg, Faculty of Mathematics and Natural Science, Institute of Chemistry under the supervision of Prof. Dr. Gunther Wittstock. The research was enriched by different collaborations, particularly with Prof. Dr. Christiane Richter-Landsberg and Janina Leyk of the Department of Neuroscience, Molecular Neurobiology, and Research Center Neurosensory Science and Julia Witt of the Wittstock group at the University of Oldenburg. Prof. Dr. Ulla Wollenberger of the Institut of Biochemistry and Biology, University of Postdam introduced me to biosensors based on cytochrome c. Additionally, I had occasionally the possibility to work with colleagues in different projects such as lithium-oxygen batteries with Patrick Schwager of the Wittstock group at the University of Oldenburg and oxygen reduction reaction at the liquid|liquid interface with Justyna Jedraszko, of the group of Prof. Dr. Marcin Opallo at the Institute of Physical Chemistry, Polish Academy of Sciences, Warsaw, Poland.

Gutachter:	Prof. Dr. Gunther Wittstock
Zweitgutachter:	Prof. Dr. Rüdiger Beckhaus
Tag der Disputation:	03.02.2017

“If we knew what it was we were doing, it would not be called research, would it?”
Albert Einstein

Abstract

Oxygen reduction reaction (ORR) is undeniable the most common reactions taking place in our environment within biological or technical systems. However, the reduction reaction of dioxygen produces not only hydrogen peroxide (uptake of 2 electrons) or water (uptake of 4 electrons) but also a broad range of oxygen-derived species. These products are characterized by their short lifetime and high reactivity and are named reactive oxygen species (ROS). This thesis describes different approaches to produce and detect the formation of ROS during ORR. The ORR at a plumbagin (PLG) polymer-modified glassy carbon (GC) electrode or microelectrode (ME) prepared using a new approach yields superoxide radicals ($O_2^{\bullet-}$). At pH 7, the generation of $O_2^{\bullet-}$ illustrated a one-electron pathway. The formation of $O_2^{\bullet-}$ and hydrogen peroxide (H_2O_2) were demonstrated using fluorescence microscopy. A selective and sensitive dye was used for each ROS during fluorescence detection. Moreover, the diffusion of $O_2^{\bullet-}$ was followed by using a PLG polymer-modified GC ME placed at a known distance above a biosensor based on cytochrome c. Using a PLG polymer-modified carbon fiber ME, epithelial cells were expose to a controlled flux of ROS and a variety of morphological alterations of biological cells were observed. Additionally, $O_2^{\bullet-}$ was monitored in lithium-oxygen batteries during discharge using fluorescence microscopy in non-aqueous aprotic solvent containing a lithium salt. Moreover, the fluorescence detection was also used to demonstrate the spontaneous formation of H_2O_2 at the liquid|liquid interface containing a strong electron donor in the non-aqueous phase. We establish thereby the simple formation of H_2O_2 using liquid|liquid interface.

Zusammenfassung

Die Sauerstoffreduktionsreaktion (ORR, oxygen reduction reaction) ist zweifelsohne die häufigste Reaktion in unserer Umgebung, sowohl in biologischen als auch in technischen Systemen. Jedoch ergibt die Reduktion von molekularem Sauerstoff neben Wasser (Aufnahme von 4 Elektronen) und Wasserstoffperoxid (Aufnahme von 2 Elektronen) eine breite Palette von Sauerstoffverbindungen. Dies Produkte sind durch eine kurze Lebensdauer und eine hohe Reaktivität gekennzeichnet und werden zusammen mit Wasserstoffperoxid kollektiv als reaktive Sauerstoffspezies (ROS, reactive oxygen species) bezeichnet. Diese Dissertation beschreibt unterschiedliche Wege zur Herstellung und zur Detektion von ROS während der ORR. Die Reduktion von Sauerstoff ergab an einer Plumbagin (PLG) polymer-modifizierten auf Glaskohlenstoffelektroden (GCE) oder Mikroelektroden (ME) Superoxid-Radikale ($O_2^{\bullet-}$). Die modifizierte Elektrode weist neue Eigenschaften gegenüber herkömmlich abgeschiedenen Poly-PLG-Filmen auf. Bei pH 7 wird $O_2^{\bullet-}$ gebildet und zeigt die Existenz des 1-Elektrone-Reaktionspfades an. Die Bildung von $O_2^{\bullet-}$ und H_2O_2 wurde mit Fluoreszenzmikroskopie nachgewiesen. Eine selektiver und sensitiver Farbstoff wurde für jede ROS genutzt. Außerdem wurde die Diffusion von $O_2^{\bullet-}$ mit PLG polymer-modifizierten ME erzeugt. Diese wurde in einem bekannten Abstand über einem Biosensor auf der Basis von Cytochrom c positioniert. Unter Nutzung einer Kohlenstoff-Faser-ME mit einem PLG-Film wurden dann Epithel-Zellen einem definierten Fluss von ROS ausgesetzt. Die Zellen reagierten darauf mit unterschiedlichen morphologischen Veränderungen. Außerdem wurde $O_2^{\bullet-}$ in Lithium-Sauerstoff-Batterien während der Entladereaktion mit Fluoreszenz-Mikroskopie in lithium-ionenhaltigen, nicht-wässrigen Lösungsmitteln nachgewiesen. Fluoreszenzdetektion kam auch zum Einsatz, um die spontane Bildung von H_2O_2 an Flüssig-flüssig-Grenzflächen nachzuweisen, die einen starken Elektronendonor in der nichtwässrigen Phase und Sauerstoff in der wässrigen Phase enthielten. Damit konnte die einfache Bildung von H_2O_2 mit Hilfe von Flüssig-flüssig-Grenzflächen belegt werden.

Acknowledgement

First and foremost, I would like to express my deepest gratitude and special thanks to my supervisor Prof. Dr. Gunther Wittstock, for introducing me to the field of electrochemistry and scanning electrochemical microscopy. Beyond his enlightening discussions and advices, I have to thank Prof. Dr. Gunther Wittstock for dedicating his unlimited energy for shaping me as a scientist and to guide me in the exploration of the unknown by scientific research. This brought my imagination in a certain unexpected level and sowed the seeds of perfection. I would also like to offer my sincere gratitude to Prof. Dr. Rüdiger Beckhaus for his participation in the periodic evaluation by the DAAD and for accepting to be a second examiner for my PhD thesis.

Special thanks are due to Dr. Carsten Dosche for introducing me to the field of fluorescence microscopy and his invaluable comments. I must also express my deepest gratitude to Prof. Dr. Ulla Wollenberg and his graduate students, Thomas Dietz, at Potsdam University for valuable collaboration and their instruction on the preparation of biosensor based on cytochrome c. My sincere gratitude also goes to Prof. Dr. Christiane Richter-Landsberg and Janina Leyk of the Department of Neuroscience at the University of Oldenburg for valuable collaboration and joint work at the interface between electrochemistry and neurobiology. I am also thankful to Dr. Wojcieh Nogala and Justyna Jedraszko at the Institute of Physical Chemistry, Polish Academy of Sciences for our joint work. Many thanks go to Dr. Izabella Brand for her relevant contribution, and Dr. David Wipf who provided the carbon fiber.

I would like also to thank my fellow PhD student Julia Witt for her great contributions in this work.

I wish to express my thankful to all my former and current colleagues who have made the work in this thesis possible, especially Patrick Schwager, Heinz Bülter, Wiebke Schulte, Inka Plettenberg, Patrick Mösgen and Gerd Gertjegerdes.

I want to thank all my friends wherever in the world specially Floriant Doungmene and Roussin Lontio.

My sincere thanks go to my wife Eve Vanice and my son Erwin for their love and support during these years.

I would like to express my sincere thanks to German Academic Exchange Service (DAAD) for sponsoring this doctoral work.

Table of Contents

Abstract ..... **I**

Zusammenfassung ..... **II**

Acknowledgement ..... **III**

1 Introduction **1**

2 Reactive oxygen species **5**

2.1 Catalytic production of reactive oxygen species 6

2.2 Electrocatalytic production of reactive oxygen species 7

2.3 Oxidative and reductive stress 10

3 Detection of reactive oxygen species **13**

3.1 Fluorescence microscopy detection of reactive oxygen species 13

3.2 Electrochemical detection of reactive oxygen species 16

3.3 Controlled release of reactive nitrogen and oxygen species 19

3.3.1 Controlled release of reactive oxygen species 20

3.3.2 Controlled release of reactive nitrogen species 21

4 Theory and principle of scanning electrochemical microscopy **23**

4.1 Overview 23

4.2 Properties of microelectrodes 23

4.3 Different modes of SECM 26

4.3.1 Feedback mode 26

4.3.2 Generation-collection mode 28

4.3.3 Redox competition mode 28

4.4 SECM with modified microelectrodes 29

5 Experimental section **30**

5.1 Chemicals 30

5.2 Instrumentations 33
5.2.1 General electrochemical experiments 33
5.2.2 Atomic force microscopy (AFM) and scanning electron microscopy (SEM) characterizations 33
5.2.3 In-situ fluorescence microscopy 33
5.2.4 Bio-scanning electrochemical microscopy (Bio-SECM) for local oxidative stress investigation 34
5.3 Preparation of glassy carbon ME and carbon fiber ME 35
5.4 Preparation of quinone polymer-modified GC 38
5.5 Preparation of biosensor based on cytochrome c 38
5.6 Cell culture preparation 39

6 New approach for preparation of quinone polymers and electrocatalytic activity of oxygen reductions reactions 40
6.1 Grafting of PLG on GC 42
6.2 Electropolymerization of PLG on clean GC and passivation problem 49
6.3 Electropolymerization onto PLG/GC 52
6.4 Oxygen reduction reactions on quinone-modified GC electrodes 61

7 Selective detection of ROS using fluorescence microscopy 65
7.1 Detection of ROS in biphasic liquid systems 66
7.1.1 Electrochemistry at the liquid|liquid interfaces 67
7.1.2 Formation and detection of H_2O_2 in RTILs 69
7.1.3 Formation and detection of H_2O_2 in organic solvent 74
7.2 Detection of superoxide in lithium-oxygen batteries 75
7.3 Generation and Detection of ROS in cell culture media 79

8 Local generation and selective detection of ROS in biological system using electrochemical technique 87
8.1 Electrochemical detection using biosensor based on cytochrome c 87
8.2 Local oxidative stress on cultured retinal pigment epithelium cells 96

9 Summary and outlook 104

10 Appendix 108
10.1 Abbreviations 108
10.2 Symbols 110

11 Bibliography 112

12 Own publications and conference contributions 127
12.1 Publications 127
12.2 Oral presentations in national and international conferences 128
12.3 Posters in national and international conferences 129

13 Fellowship, Grant and Award 129

14 Curriculum vitae 130

1 Introduction

Oxygen appears as the second most abundant gas of the earth's atmosphere (21% of air atmosphere), and the third-most abundant element of the universe [1-3]. This chalcogen element was discovered by Joseph Priestley in 1774 who published the first paper on it [3, 4]. The name "oxygen" was coined by Antoine Lavoisier in 1777 [3, 4]. After fluorine, oxygen is the most active among all electronegative elements [3]. Its ground state allows accepting electrons leading to a reduction reaction of oxygen, which is the most widespread chemical or electrochemical process in many systems [4-6]. The reduction reaction of dioxygen (O_2) (oxygen reduction reaction, ORR) is of major importance in several energy converting systems or electrochemical technologies such as fuel cells, metal-air batteries, oxygen sensors [1, 4, 7-11]. However, the ORR produces side products or by-products considered as a double-edged sword [12-14]. These products can be useful or toxic for their environment [5, 12-17]. These intermediates are highly reactive and named collectively as reactive oxygen species (ROS) [13, 15-18]. Except hydrogen peroxide (H_2O_2), other ROS such as superoxide radical ($O_2^{\bullet -}$), hydroxyl radical ($HO^{\bullet}$) or hydroperoxyl radical ($HOO^{\bullet}$) are free radicals [14, 16-19].

ROS are also unavoidable products obtained during aerobic biological processes. They play multi-faceted and complex roles in biological systems [6, 14, 17, 19, 20]. In living cells, ROS are involved in respiratory mechanism [14, 17], photosynthesis [14, 16], defense mechanism termed as "oxidative burst" [6, 20] or agents of cellular signaling termed as "oxidative signaling" [14]. However, excessive release of ROS is more often damaging than beneficial due to uncontrolled side reactions of ROS with other compounds. The overproduction of ROS can be explained by many reasons such as decreases of concentrations of antioxidants, increasing level of endogenous or exogenous compound

involved in ROS productions, inactivation of antioxidant enzymes and combinations of those factors [17]. There are many regulators, which constitute a barrier and control the concentration of ROS by enzymatic reactions with enzymes such as catalase, peroxidase or superoxide dismutase. In biological systems, the excess of ROS leads to a situation named "oxidative stress" [6, 14, 19, 20]. This concept was founded by Helmut Sies, of Heinrich Heine University, Düsseldorf, Germany [14]. A new research proposed a classification of oxidative biological conditions based on the intensity of oxidative stress such as basal oxidative stress, low intensity oxidative stress, intermediate intensity oxidative stress and high intensity oxidative stress [14]. Another classification proposes three categories such as mild oxidative stress, temperate oxidative stress and severe oxidative stress [14]. Oxidative stress is suspected to be involved directly or indirectly in many pathologies such as aging cancers, Parkinson, Alzheimer, degenerative processes, syndromes (such as atherosclerosis, myocardial infarction, stroke, ischemia/reperfusion injury); central nervous system disorders (such as familiar forms of amyotrophic lateral sclerosis (ALS)). Due to this significance in the pathogenesis of several important pathological conditions, it has become an area of intensive scientific research [12, 14, 19, 20].

$O_2^{\bullet-}$ which is formed by a one electron transfer process to oxygen, is known as a main precursor of further formation of ROS [21-26]. For long time, free radicals like $O_2^{\bullet-}$ were ignored and their presence in biological systems was not considered due to many reasons such as low stability and high reactivity, high diversity of follow-up reactions, dependence on physiological state of the organism and more importantly absence of technical tools for reliable evaluation of their absolute and even relative concentration levels [17, 27]. Various molecules promote or catalyze the production of $O_2^{\bullet-}$. Quinone compounds are good candidates to obtain $O_2^{\bullet-}$. The role in the electron transport chains

and their capacity to form semiquinone radicals during electron transfers allow formation of $O_2^{\bullet-}$ by 1-electron transfer from semiquinone radicals to O_2 [19, 23, 25, 28-30]. Anthraquinone is used in industry for preparation of the H_2O_2, which has many technological applications such as bleaching, wastewater treatment and is considered as a green chemical because the final product of its decomposition is harmless water (H_2O) [31-35]. In living cells, quinones such as ubiquinone also promote the productions of ROS such as $O_2^{\bullet-}$ by formation of semiquinone radicals. Thereby, the quinone can be used as catalyst or electrocatalyst for $O_2^{\bullet-}$ formation [19, 22, 23, 28, 29, 36, 37]. Quinones also show good catalytic efficiency when they are immobilized on the surface such as carbon electrodes [38-41]. To date several investigations have been published to elucidate the mechanism of the oxygen reduction on quinone-modified electrodes. The $O_2^{\bullet-}$ seems to be the first oxygen-derived species generated at such electrodes [38-41].

Various analytical methods have been developed to detect and quantify the ROS using indirect method such as probe-assisted light spectroscopy technique (photometry, chemiluminescence, fluorescence microscopy) which involves the reactions with a molecular probe [42-46]. Electrochemical detection also provides powerful tools for real-time and non-invasive investigation of local generation of ROS [47-49]. Fluorescence microscopy offers a significant advantage compare to other optical spectroscopies such as the spatial and temporal resolution, the possibility of in-situ investigation, high selectivity and sensitivity since the emission of unique fluorescence wavelengths depends on each target species [43-46]. Electrochemical detection offers additional information on dynamics of formation and transport (diffusion) of target species especially when a microelectrode (ME) is used [50]. MEs allow local investigation when

combined with positioning equipment for instance in scanning electrochemical microscopy (SECM).

This thesis presents different results obtained during local formation and selective detection of ROS in different systems and preliminary investigation of local oxidative stress in cell environment. The local formation of ROS was performed using a polymer-modified ME and investigated by means of fluorescence microscopy and an electrochemical biosensor. The polymer was prepared by means of new approach of preparation on glassy carbon (GC) surface. The electrochemical detection involved a biosensor based on cytochrome c (cyt c). Optical inverted microscope combined with a SECM setup was used to expose healthy cells to a local flux of ROS. Then their morphological alterations were investigated. Formation of $O_2^{\bullet -}$ or H_2O_2 in technical systems such as lithium-oxygen battery and liquid|liquid interface was investigated using an adapted approach with fluorescence microscopy.

2 Reactive oxygen species

The importance of oxygen for biological systems and industrial applications is evident [10, 20]. Considering the molecular structure of oxygen, a reduction reaction is a typical process and lead to ROS [51]. ROS can be obtained by catalytic or electrocatalytic ORR. In biological cells, the production of ROS is observed after aerobic metabolism or after stimulation of defense mechanisms [6, 20]. ROS were also identified as intracellular messengers in the cell metabolism [16, 51]. Instead of singlet oxygen ($^1O_2$) where one e^- is elevated to a higher energy level, formation of ROS can be defined as sequential reduction of O_2 leading to $O_2^{\bullet-}$, hydroperoxyl radical ($HO_2^{\bullet}$), H_2O_2 and $HO^{\bullet}$ [6, 51]. Other derivatives such as peroxyl radical ($ROO^{\bullet}$), alkoxyl ($RO^{\bullet}$), and hypochlorous acid (HOCl) can be obtained after reaction with other components of biological systems [6, 51]. The final stage of ORR after the uptake of 4 electrons per O_2 molecule is H_2O or $HO^{\bullet}$ (Fig. 1).

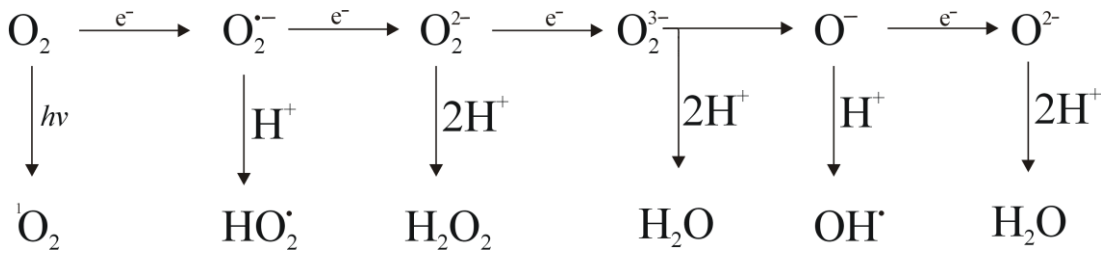

Figure 1: Proposed scheme of metabolic pathways of oxygen leading to different ROS. The scheme shows the overall stoichiometry but not the sequence of electron and proton transfer steps.

2.1 Catalytic production of reactive oxygen species

Different catalysts promote the ORR such as nanoparticles, metal complexes, metal oxides, enzymes, light, quinones and viologens [11, 22, 25, 28, 52]. The catalytic formation of ROS has been intensively investigated [11, 22, 28, 53]. In living cells, many processes contribute to the catalytic formation ROS during ORR [19, 28]. One typical example is the role of ubiquinones in the production of ROS such as $O_2^{\bullet-}$ or H_2O_2 during the respiratory process in mitochondria [19, 22]. The formation of $O_2^{\bullet-}$ requires the formation of the semiquinone radicals (Fig. 2) from quinone compounds which possess three main states such as quinone/semiquinone/hydroquinone ($Q/Q^{\bullet-}/QH_2$) [22, 25, 28, 54]. In aerobic cells, an electron donor such NADH reduces a quinone compound (e.g. ubiquinone) and forms the semiquinone radical, which then reacts with oxygen to yield $O_2^{\bullet-}$ [23, 29, 54, 55].

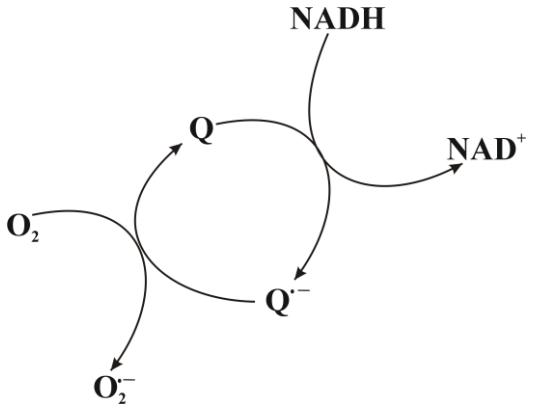

Figure 2: Formation of $O_2^{\bullet-}$ during an aerobic biological process.

Metals can also act as catalyst. In the presence of iron or copper metal, H_2O_2 produces $HO^{\bullet}$ during a Fenton reaction (Eq. (1)) [6, 13, 16]. $HO^{\bullet}$ which is an extremely harmful and reactive species. It is also produced during reaction between $O_2^{\bullet-}$ and H_2O_2 (Eq. (2)) [6, 13, 16].

$$H_2O_2 + Fe^{2+} \rightarrow HO^{\bullet} + HO^{-} + Fe^{3+} \quad (1)$$

$$H_2O_2 + O_2^{\bullet -} \rightarrow HO^{\bullet} + HO^{-} + O_2 \quad (2)$$

During a pulse radiolysis, radiation can catalyze the formation of ROS, from oxygen or from other ROS such as H_2O_2 [56]. Investigation of pulse radiolysis in seawater described first the generation of $HO^{\bullet}$ then, after reaction with oxygen, $O_2^{\bullet -}$ is produced [56].

A catalytic formation of ROS involving quinone compounds and Cu(II) ions was described [52, 57]. The kinetics of this reaction was investigated during autoxidation of quinone compounds in the absence of Cu(II) ions [52, 57]. The slow reaction turns to catalytic reactions in the presence of Cu(II) ions [52, 57].

2.2 Electrocatalytic production of reactive oxygen species

Electrocatalysis of ORR can be performed with various catalysts materials such Pt-based materials, other metals (e.g. gold, iridium, cobalt, nickel…), carbon materials, transition metal chalcogenides, quinone compounds and transition metal carbides [1]. For economical reason extensive research is currently conducted to discover alternative catalysts based on abundant and thus cheap elements.

The electrocatalytic ORR on gold nanoparticles was reported to lead to two products H_2O_2 and H_2O in strongly acidic medium (Eq. (3) and (4)) [58].

$$O_2 + 2H^{+} + 2e^{-} \rightarrow H_2O_2 \quad (3)$$

$$H_2O_2 + 2H^{+} + 2e^{-} \rightarrow 2H_2O \quad (4)$$

This indicates a reduction by a 2-step mechanism for an overall 4-electron reduction. On the other hand, mainly 2-electron reduction of oxygen is carried out on single crystal gold electrodes and leads to H_2O_2 also in acidic medium [58-61]. This illustrates the dependence of the mechanism of the ORR on the electrode material [58].

Electrocatalysis of ORR by Pt electrodes is well known. The reaction pathway leads to the H_2O with H_2O_2 as intermediate [1]. Recent investigations show the possibility of formation of $O_2^{\bullet-}$ and $HO^{\bullet}$. Mirkin and co-workers demonstrated the formation of $O_2^{\bullet-}$ during ORR on Pt surface by SECM, which suggest a 1-electron pathway (Eq. (5)) [62].

$$O_2 + e^- \rightarrow O_2^{\bullet-} \quad (5)$$

Hapiot and co-workers have also shown evidence for the production of $HO^{\bullet}$ during ORR in neutral and alkaline solutions. A footprint strategy based on the use of SECM was developed. ORR was carried out at the Pt ME localized near a GC substrate modified by an organic layer, then a local modification induced by $HO^{\bullet}$ was imaging using SECM. Different control experiments were implemented to eliminate the contribution of other ROS such as $O_2^{\bullet-}$ which behave differently in acidic and organic solvents [63]. This investigation suggests a 3-electron pathway and not the 2-step 4 electron mechanism as usually obtained (Eq. (6)) [63].

$$O_2 + 2H^+ + 3e^- \rightarrow HO^- + HO^{\bullet} \quad (6)$$

The formation of short-lived intermediate such as $O_2^{\bullet-}$ and $HO^{\bullet}$ was early undocumented or not considered since the lifetime of this species seems to be extremely short. With Pt, it is generally admitted that the ORR competes between two pathways which are 2-electron reduction (O_2 to H_2O_2) and 4-electron reduction (O_2 to H_2O) [1, 64]. However it is inadequate and there are additional pathways (O_2 to $O_2^{\bullet-}$, or O_2 to $HO^{\bullet}$) which are observable at neutral and basic pH in aqueous solution [63]. Investigations of mechanistic aspect of ORR involve transient species of ROS. Those measurements are complexes, which may explain the focus on the $2e^-$ and $4e^-$ pathways. The evidence for formation of $HO^{\bullet}$ during ORR on Pt was clearly demonstrated and calls for a re-evaluation of different experimental procedures for the study of ORR [63].

Quinone compounds are also a good candidate as mediator for electrocatalysis of ORR. The reduction of oxygen starts by the formation of semiquinone radicals (Eq. (7)) [38-41, 65]. Then the semquinone radicals react with oxygen yielding $O_2^{\bullet-}$ which is the rate-determining step (Eq. (8)). Table 1 presents some potential values required to form semiquinone radicals of different quinones. During the further disproportionation reactions, other ROS such as H_2O_2 are produced [38-41]. The mechanistic pathways of quinone compounds is not easy to elucidate because it depends on solution used and the pH [38-41]. However, the production of a variety of ROS using quinone compounds is possible.

$$Q + e^- \rightarrow Q^{\bullet-} \quad (7)$$

$$Q^{\bullet-} + O_2 \rightarrow O_2^{\bullet-} + Q \quad (8)$$

Table 1: Reductions potentials of some quinone compounds ($Q/Q^{\bullet-}$) at pH 7 versus (vs.) standard hydrogen electrode (SHE); $E°$ is a standard half-cell reduction potential at standard conditions [66-72].

Compounds	**Structure**	***E*°(Q/ $Q^{\bullet-}$)/ mV**	**Ref**
1,4-benquinone	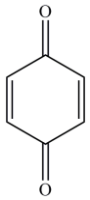	78	66
methyl-1,4-benzoquinone	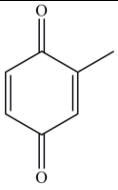	23	67

1,4-naphthoquinone	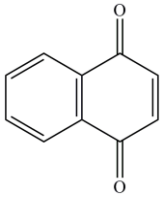	-104	69
5-hydroxy-1,4-naphthoquinone (juglone)	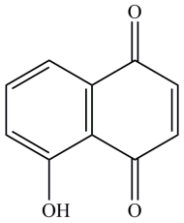	-95	69
2-hydroxy-1,4-naphthoquinone (lawsone)	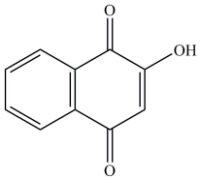	-415	70
5,8-hydroxy-1,4-naphthoquinone	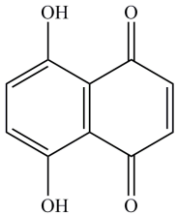	-110	71
2-hydroxy-1,4-naphthoquinone (menadione)	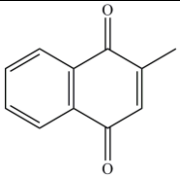	-335	72
5-hydroxy-2-methyl-1,4-naphthoquinone (plumbagin)	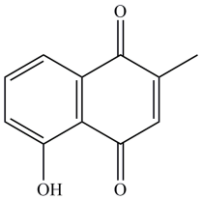	-156	73

2.3 Oxidative and reductive stress

Aerobic cells produce energy from the controlled oxidation of CH bonds using metalloenzymes. These reduced forms of the metalloenzymes are good reducing agents

and $O_2^{\bullet-}$ can be generated via oxygen reduction [19]. $O_2^{\bullet-}$ is considered as the precursor of other ROS, which are maintained at the nanomolar concentration range due to the action antioxidants or ROS scavengers [73-76]. Excess of ROS or reactive nitrogen species (RNS) induces cell damage and the chronic imbalance between the ROS/RNS generated and the antioxidant capacities is called oxidative/nitrosative stress (Fig. 3) [47, 75, 77, 78]. Surprisingly, the overproduction of antioxidants leads also to oxidative damage (Fig. 4). It is named reductive stress and is considered as a counterpart of oxidative stress. It can be defined as a drastic increase in reducing equivalents (GSH/GSSG, NADPH/$NADP^+$, NADH/NAD^+, etc…) [79-82]. This definition is somewhat confusing since it is known that NADH promotes the excessive ROS production (Fig. 2) leading to high level of ROS. During the reductive stress the electron acceptor are expected to be mostly reduced. In this case, other redox proteins generate ROS [80, 82]. In other words, during reductive stress paradoxically ROS production increases. This process was largely ignored and focus was placed only on oxidative stress [82].

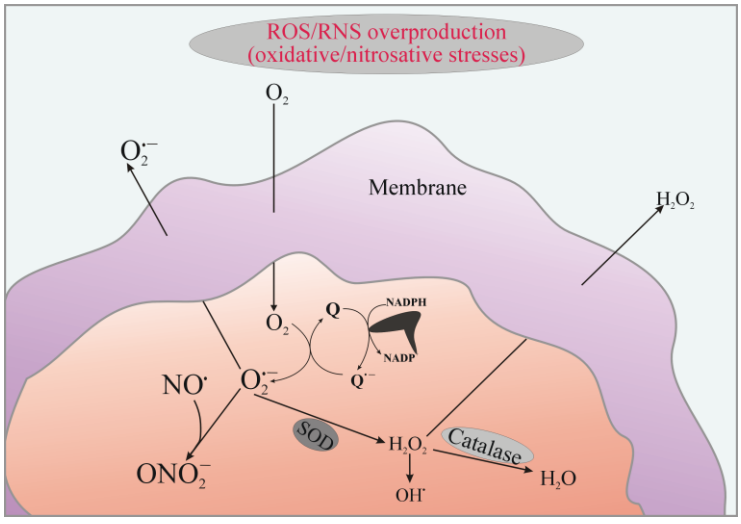

Figure 3: Generation of ROS during respiratory process in the cell.

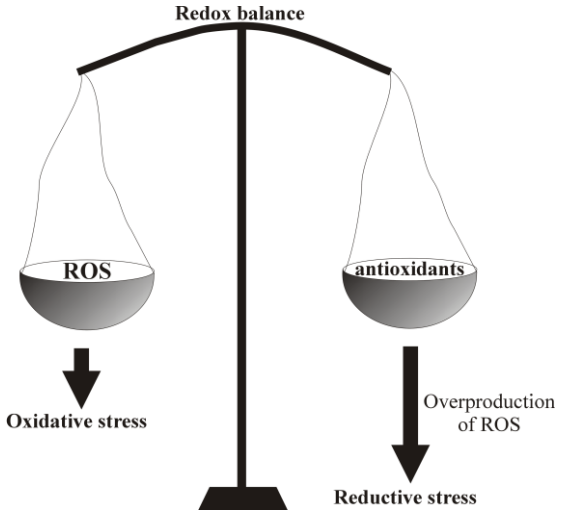

Figure 4: Balance between ROS and antioxidants. An abundance of ROS leads to oxidative stress, likewise overabundance of antioxidants increase paradoxically the production of ROS and again leads to oxidative damage initiated by reducing agents therefore called reductive stress (for details see text above).

3 Detection of reactive oxygen species

A particular attention was directed to the formation and detection of two ROS, $O_2^{\bullet-}$ and H_2O_2. The analysis of these species through selective detection remains a key experiment to understand the different interaction in biological and technical systems. Except for H_2O_2, the detection of ROS ex-situ is usually not possible and requires an in-situ investigation. Due to the short lifetimes and typically low concentration of ROS, the direct investigation of these transient species is only possible on sub-millisecond timescales and does not reflect the exact concentration profile of the target species [42]. Indirect detection involves the use of chemical probes, which react selectively with the target species and yield a derived long-lived analyte. This can be analyzed ex-situ or in-situ using another technique [42]. Important features of the ROS detection method are sensitivity, selectivity, non-invasive nature and fast response time [42, 47, 83]. Therefore, techniques such as spectroscopy and electrochemical techniques were used for this purpose. In this chapter, we will focus on two techniques, which are fluorescence microscopy and electrochemical techniques.

3.1 Fluorescence microscopy detection of reactive oxygen species

Among different techniques, fluorescence microscopy is a promising method to investigate a selected ROS and to provide spatial and temporal information of the target species [83]. ROS probes designed to detect a selected ROS aimed to understand the physiological roles of ROS since it is now clear that each ROS has its own unique physiological activity [83]. It is therefore essential to develop accurate and sensitive methods for their detection. Fluorescent probe molecules have received much attention

because of their sensitivity and their non-invasive nature. Good fluorescent probe molecules should be easy to synthesize, have a dark initial state (i.e., non-fluorescent), be fully compatible with the target media and very importantly, completely photostable [44]. For biological application, compatibility must include absorbance in a convenient spectral region and minimal overlap of their fluorescence with autofluorescence [44]. In this instance different dyes were prepared for the detection of $O_2^{\bullet -}$ and H_2O_2 as summarize in Fig. 5 and 6 [42, 45, 46, 53, 84]. The dyes react with H_2O_2 in a reaction catalyzed by horseradish peroxidase (HRP). For $O_2^{\bullet -}$, probes are oxidized. The selection of dyes depends on the system under study and the equipment used for detection and the monitoring of the emission wavelength.

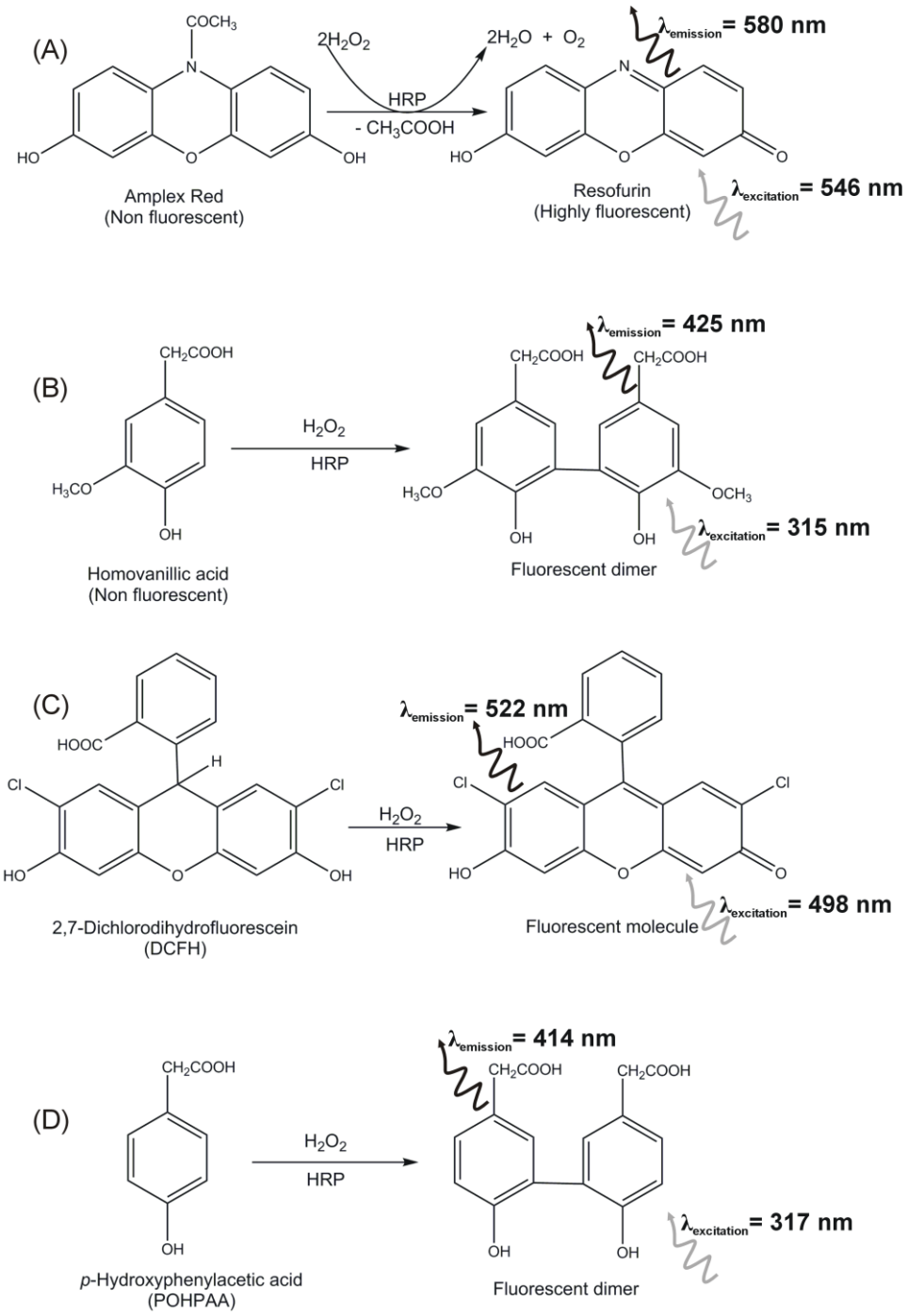

Figure 5: Dyes for H_2O_2 detections.

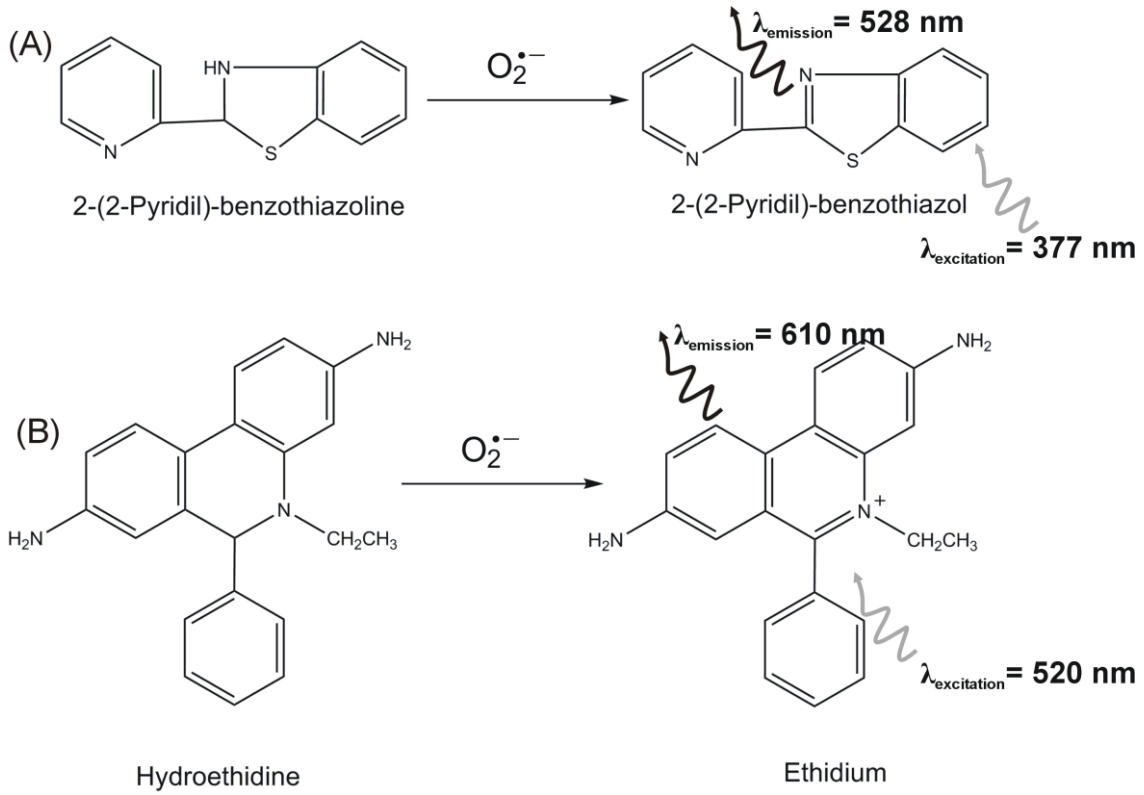

Figure 6: Dyes for $O_2^{\bullet-}$detections.

3.2 Electrochemical detection of reactive oxygen species

Intensive research has been conducted to develop real-time electrochemical detection methods for ROS for many medical relevant conditions [26]. The electrochemical detection was performed initially directly on unmodified metal or carbon electrodes. Based on the standard redox potential of the $O_2/O_2^{\bullet-}$ redox couple (which is quoted between -330 mV and -140 mV vs. NHE), an electrochemical detection of $O_2^{\bullet-}$ generated by human neutrophils was performed in 1984 by Hill using pyrolytic graphic electrode modified with human immunoglobulins [19, 85-87]. In 1985, Hill and co-worker reported the direct detection of $O_2^{\bullet-}$ from isolated human neutrophil on a 10 µm diameter gold microelectrode (ME). Recently Pt MEs or carbon fibers were used to

assess the oxidative burst [77, 87-90]. However, this direct detection suffers from poor sensitivity and selectivity. Therefore, substantial investigations were made in developing of more selective biosensors involving biology recognition elements to react with the targeted ROS [87, 91].

Beside high selectivity and short response time, the analytical tools for detection of $O_2^{\bullet-}$ and H_2O_2 must also be small enough to be placed in the close proximity of the investigated source [92, 93]. In this way, small amounts of $O_2^{\bullet-}$ and H_2O_2 released by a biological cells can lead to a large concentration change, enough to be detected when the volume between sensor and cell is small [91, 94]. Several different electrochemical methods have the required temporal resolution, selectivity, and sensitivity [91]. The electrochemical method for ROS is amperometry. In this electrochemical method, the sensor is polarized at a constant potential and the current is recorded vs. time. The temporal resolution of the measurement can be in milliseconds interval (i.e. excellent) [91]. Differential pulse amperometry can also be used for detection, the sensor is polarized at a constant potential but some potential pulses are superimposed at regular intervals [91]. The current signal will be the difference between the current prior to the pulse and the current measured during the pulse [91]. This difference will be recorded as a function of time. The temporal resolution of this method is not as good as in the case of constant potential amperometry. By the careful selection of the pulse parameters, some additional sensitivity is gained because contributions from baseline drift, interferences and capacitive currents are eliminated to some extent [91]. Research group headed by Christian Amatore is one of the group which uses electrochemical microsensors to observe ROS and RNS produced by single cells [91]. Due to the extreme reactivity of $O_2^{\bullet-}$, many research groups do not target a direct detection of $O_2^{\bullet-}$, but detect species

resulting from the disproportionation of $O_2^{\bullet-}$ or from the reaction of $O_2^{\bullet-}$ with nitric oxide.

Mediated electrochemical sensors or biosensors were used for the detection of superoxide [26, 87]. The detection of $O_2^{\bullet-}$ was performed using a biosensor based on cyt c or superoxide dismutase (SOD) essentially during direct or indirect electron transfer (Fig. 7) [26]. In the literature there are essentially 3 types of electrochemical biosensors for the detection of $O_2^{\bullet-}$ using SOD [26, 87]. $O_2^{\bullet-}$ biosensors based on SOD involve the dismutation of the $O_2^{\bullet-}$ to H_2O_2 and oxygen. In the first generation SOD-based sensor for $O_2^{\bullet-}$, the generated H_2O_2 is detected at the electrode (Fig. 7B1) [26, 87, 95]. The second generation is based on the use of electron transfer mediators to enhance the signal (Fig. 7A2 and 7B2). The third generation involves direct electron transfer between redox active centers and the electrode (Fig. 7A3 & 7B3) [26, 87]. Another biosensor for $O_2^{\bullet-}$ was prepared using cyt c (Fig. 7A1). It was immobilized on a self-assembled monolayer (SAM). Long chain or short chain also was tested. Instead of a SAM, cyt c could also be also immobilized between electroactive polymers [26, 87]. Cyt c and HRP were also used to detect H_2O_2 [26, 87].

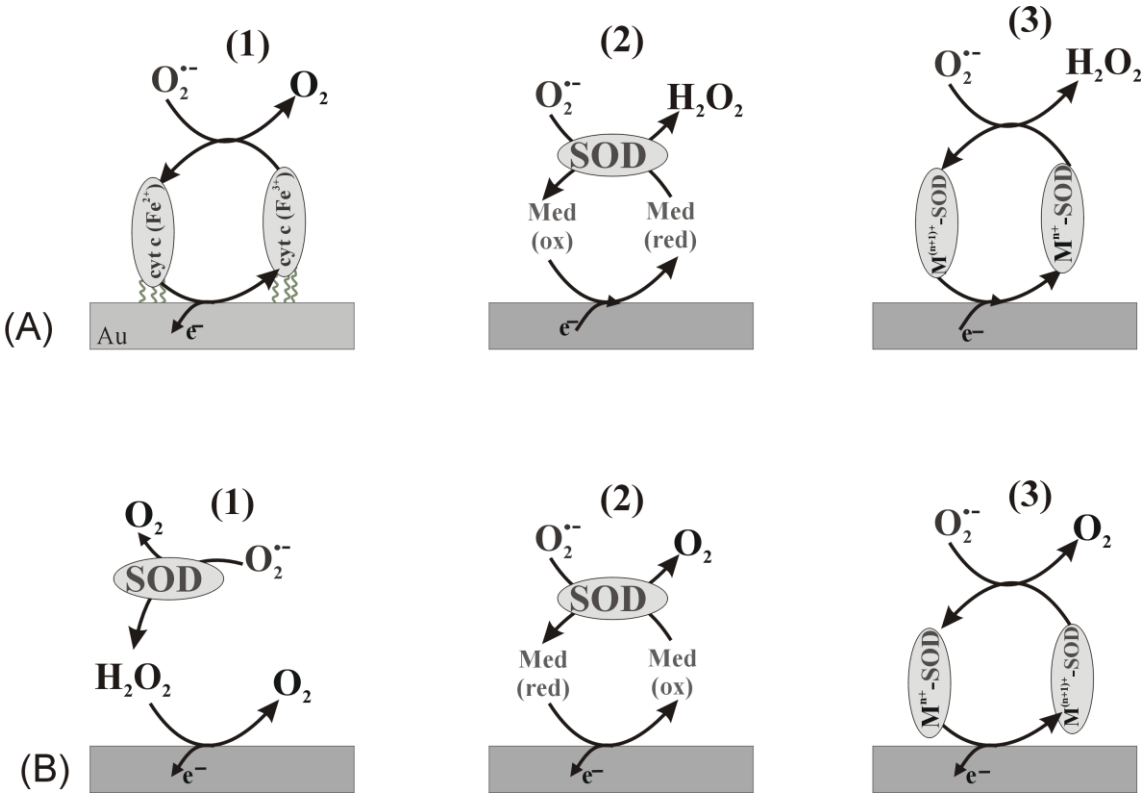

Figure 7: Different biosensors use for $O_2^{\bullet-}$ detection; A1) biosensor based on cyt c immobilize on gold-modified SAM; B1) first generation SOD based biosensor; A2 & B2) second generation SOD based biosensor; A3 & B3) third generation SOD based biosensor.

3.3 Controlled release of reactive nitrogen and oxygen species

The release of RNS and ROS or neurotransmitter agents is a part of the metabolic process of cells. The release serves different purposes and contributes to defense mechanisms or simple respiratory processes of cells. Two main aspects can be considered, the controlled release from cells and detection at the ME, or the generation of ROS at the ME and exposure of the cells. In this chapter, these two aspects are described.

3.3.1 Controlled release of reactive oxygen species

As previously mentioned, ROS are products of oxygen reduction. When the ROS are produced by the cell, they can diffuse out of the cell and interact with other molecules present in the cell media. However, this ROS release by the cell is well controlled by the presence of scavengers or antioxidants, which maintain suitable concentrations of these species [19, 77]. On other hand, the controlled release of ROS can be provoked [96]. Cells can be specifically stimulated and release ROS. Alternatively, controlled flux of ROS can be generated at an electrode in the cell environment as described in this thesis. Amatore and co-workers reported controlled release of ROS after stimulation of living cells such as macrophages. The ROS were detected by a nanoelectrode or ME (Fig. 8) [19, 77, 96]. It was used to investigate the theory about the generation of the ROS from the cells [19, 77, 96]. In this instance, macrophage cells are considered as the key cell of the immune system. They release ROS during the phagocytosis of foreign bacteria, viruses and particles [19]. A platinized nanoelectrode can be placed carefully inside the macrophage cells to detect the ROS generated [19, 77]. Pt or carbon MEs can be used to detect the release ROS above the cells [19, 77]. The macrophage cells were stimulate either using a stimulus micropipette or by reproducing the conditions which initiate the generation of ROS as digestion of external species or cells [19, 47, 77]. The ROS detected inside and outside of macrophages prove that this powerful technique can be used to investigate the concept of oxidative stress. Release of ROS such as H_2O_2 from mitochondria activated by addition of antimycin, was also investigated. Low concentration of H_2O_2 generated was related to picoampere current recorded during chronoamperometry (CA) [47, 94]. Many other techniques, such as SECM, were also used to investigate oxygen consumption and ROS [97]. However, the electrochemical

generation of ROS using modified nanoelectrodes or MEs in cell culture environment has not been reported so far. In this thesis, the first attempts in this direction are reported.

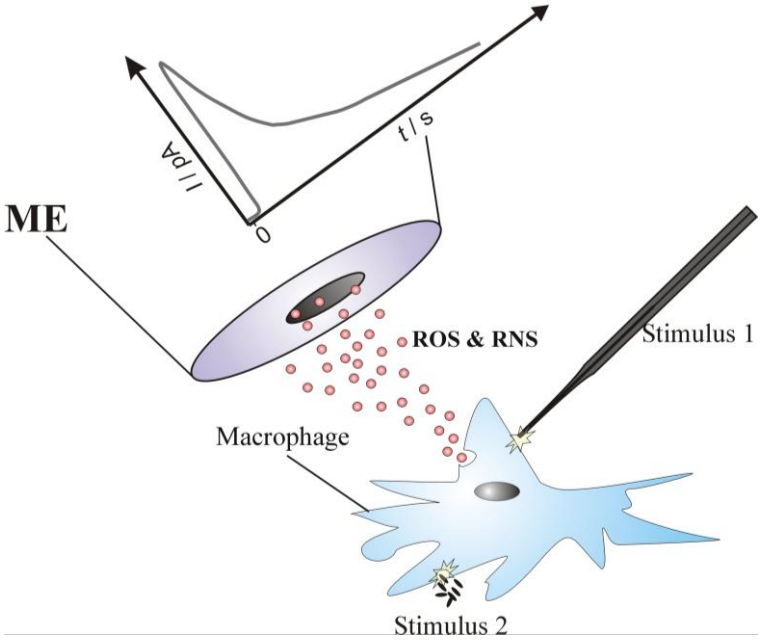

Figure 8: Schematic representation of controlled release and detection of ROS using a macrophage cell and micropipette (stimulus 1) or external particles (stimulus 2) as stimuli.

3.3.2 Controlled release of reactive nitrogen species

NO is one of the RNS frequently investigated in biological context. It plays a key role during cell-to-cell communication as messenger. It can also prevent thrombosis and bacterial infections [98-101]. NO release by cells was investigated using a nanoelectrode or modified ME [102]. Electromodulation of release of NO known as good vasodilator was performed on a copper wire in a nitrite (NO_2^-) reservoir. During an anodic pulse in presence of low concentrations of Cu(I) ions, NO is produced locally at the electrode surface (Fig. 9) [98-101]. Cu(I) ions react directly with NO_2^- to form NO (Eq. (9)) [98-101].

This technique of electrochemical NO generation can be used to design NO generating catheters or other biomedical devices [98-101].

$$Cu(I) + NO_2^- + 2H^+ \rightarrow Cu(II) + NO + H_2O \quad (9)$$

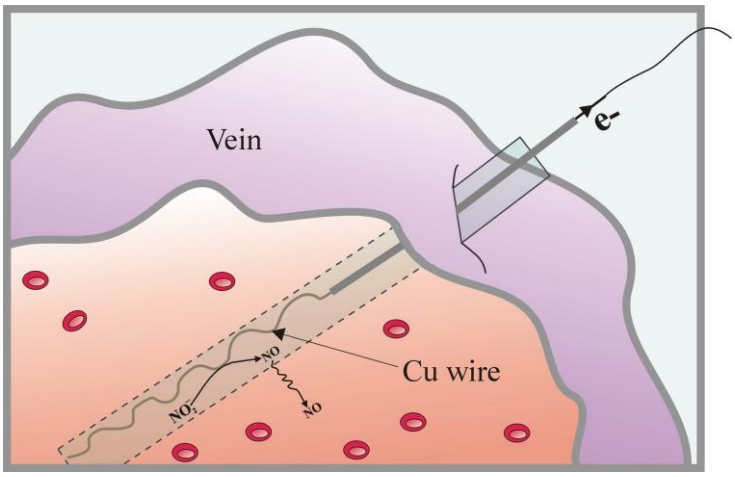

Figure 9: Schematic representation of controlled release of NO to prevent infection or thrombosis.

4 Theory and principle of scanning electrochemical microscopy

4.1 Overview

SECM is a scanning probe technique and electrochemical tool where the MEs can induce local electrochemical changes and probe the electrochemical reactivity or topography of a wide range of surfaces of interest [103-105]. In 1986, Engstrom and co-workers implemented the first SECM-type experiment where a ME was used as a sensor recording concentration profiles of short-lived intermediates. The term SECM was used for the first time in 1989 by Bard et al. who also developed the theoretical foundation [103, 105-107].

During the SECM investigation, the ME moves near to the surface in *x*, *y* or *z* directions. It collects the flux of redox species from the substrate using high precision positioning devices. The MEs are the most important part of electrochemical microscope and influence the results of scanning. The properties of MEs and the classic SECM working modes will be discussed in this chapter.

4.2 Properties of microelectrodes

The development of MEs has completely revolutionized the approaches in electrochemistry and has pushed the boundaries of this area into small scales, which allow the explorations of new environments. Many definition of MEs or ultramicroelectrode (UME) were presented since the discovery of the unusual properties of MEs [108]. MEs can be defined as the electrodes with the characteristic dimensions on the micrometer or sub-micrometer scale [108]. Fast double-layer charging, reduced ohmic

loss and high mass-transport efficiency describe the electrochemical features of the MEs [104, 108]. In order to compare MEs to conventional electrodes the concept of mass transport will be used and involves different processes, namely diffusion, convection (natural and forced convections) and migration. We focus on the diffusion process assuming that the electrochemical experiment is designed to eliminate the contributions of electrostatic potential (migration) and of the hydrodynamic velocity on the overall flux of redox active species. Thereby mass transport is limited by the contribution from diffusion (diffusion-controlled current). In practice, this can be achieved when the experiment is conducted in quiescent solution in the presence of an excess of supporting electrolyte to exclude the undesired effects.

Cyclic voltammetry (CV) can be used to demonstrate easily the difference between MEs and the conventional electrodes in term of mass transport during a diffusion-controlled process. At a large electrode, planar diffusion is observed in which the mass transport occurred perpendicular to the interface of the electrode (Fig. 10A). For a reversible process, a typical peak-shaped voltammogram is obtained and the peak current follows the Randles-Sevick equation (Eq. (10)) [109]:

$$i_p = (2.69\times10^5)n^{3/2}AD^{1/2}c^*v^{1/2} \quad (10)$$

Where i_p is peak current [A], n is the electron stoichiometry, A is the electrode area [cm^2], D is the diffusion coefficient [$cm^2\ s^{-1}$], c^* is the bulk concentration of redox active substance [mol cm^{-3}], and v is scan rate [$V\ s^{-1}$] [109].

By contrast, the voltammogram at MEs differs markedly. A hemispherical concentration profile is observed for the mass transport through radial diffusion (Fig. 10B). A steady-state diffusion-limited current $i_{T,\infty}$ is rapidly established and given by :

$$i_{T,\infty} = gnFDc^*r_T \quad (11)$$

where g is a geometry-dependant factor related to electrode shape of the electrode housing. For infinitely large insulators around the active area g equals 4. n is the number of transferred electrons, F is the faraday constant [A S mol^{-1}], D is the diffusion coefficient [cm^2 s^{-1}], c^* the bulk concentration of the redox active substance [mol cm^{-3}] and r_T the radius of the active electrode area [cm] [104].

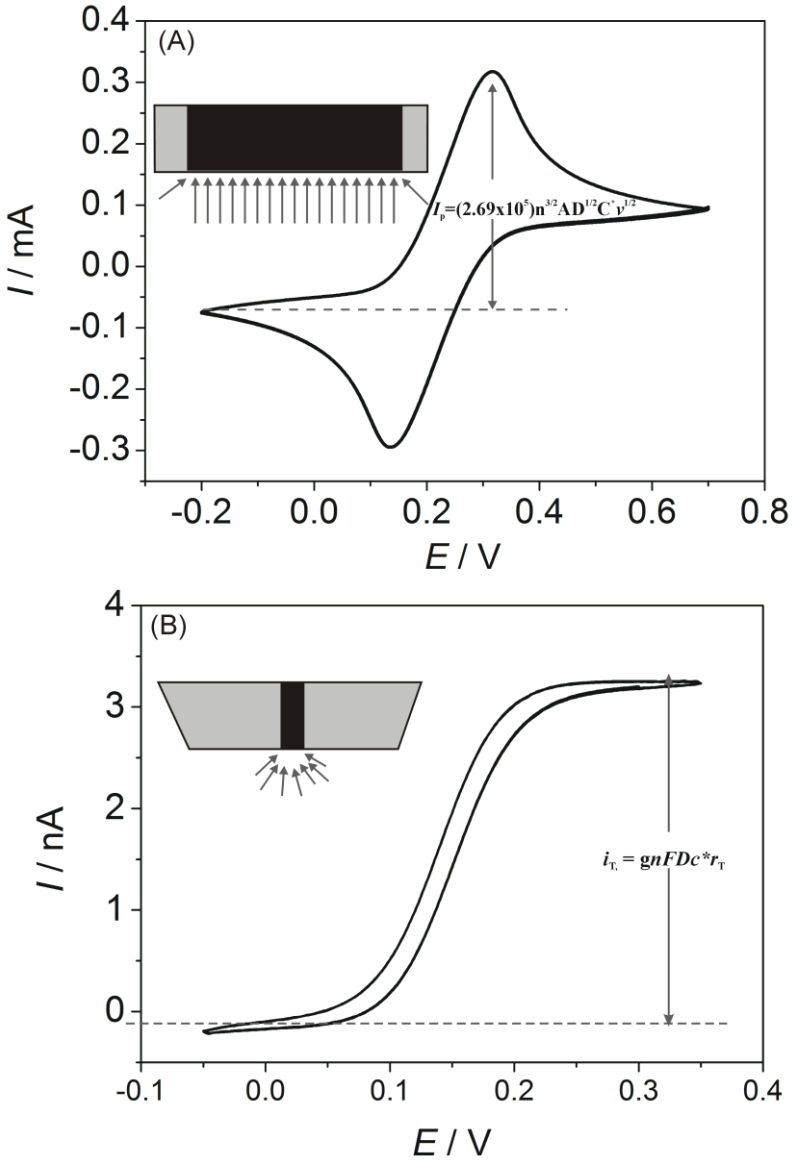

Figure 10: Properties of a macroelectrode and a ME. (A) CV of conventionally-sized electrode with planar diffusion (GC, 3 mm diameter, in 5 mM FcMeOH vs. Ag/AgCl) and (B) ME with radial diffusion (Pt, 25 µm diameter, 1 mM FcMeOH vs. Ag/AgCl).

4.3 Different modes of SECM

For diverse electrochemical applications, there are different SECM modes and variants of SECM suitable for a specific investigation. The details here will be restricted to the feedback (FB) mode, generation-collection (GC) mode and the redox competition (RC) mode. In most cases, the MEs are placed at a known distance close to the substrate by recording an approach curve. An approach curve is a change of the ME current with the distance between a substrate and the ME. More details on the theoretical description of approach curves can be found in the following references [107, 110-116].

4.3.1 Feedback mode

The SECM is based on the faradaic current changes at the ME during its movement above a substrate immersed in a solution containing appropriate species in the oxidized (Ox) or reduced (Red) state. The compound is sometimes called mediator [109]. In the SECM feedback mode, Ox is reduced at the tip to give Red.

$$\mathrm{Ox} + n\mathrm{e}^- \rightarrow \mathrm{Red} \qquad (12)$$

If the tip is far from the surface, a steady state current ($i_{T,\infty}$) is given by Eq. (11) with g = 4. Red can be oxidized at the sample. Therefore, a constant flow of redox mediator results that includes a contribution from the sample. This contribution depends on the kinetics of the reaction at the sample. When the tip is close enough to the conductive surface of the substrate (a distance of few tip radii), the species Ox can be regenerated by electrochemical conversion via reaction:

$$\mathrm{Red} \rightarrow \mathrm{Ox} + n\mathrm{e}^- \qquad (13)$$

The additional flux of Ox species increases the flux of Ox at the ME and increase the ME current i_T ($i_T > i_{T,\infty}$). This is called positive feedback (Fig. 11A). If the ME is

brought close to an insulating substrate, the species Ox cannot be regenerated. Therefore, the surface hinders the diffusions of Ox from the solution bulk to the ME and the ME current i_T decreases ($i_T < i_{T,\infty}$). This is called negative feedback (Fig. 11B). The closer the ME is placed to the insulating surface, the smaller is the measured ME current.

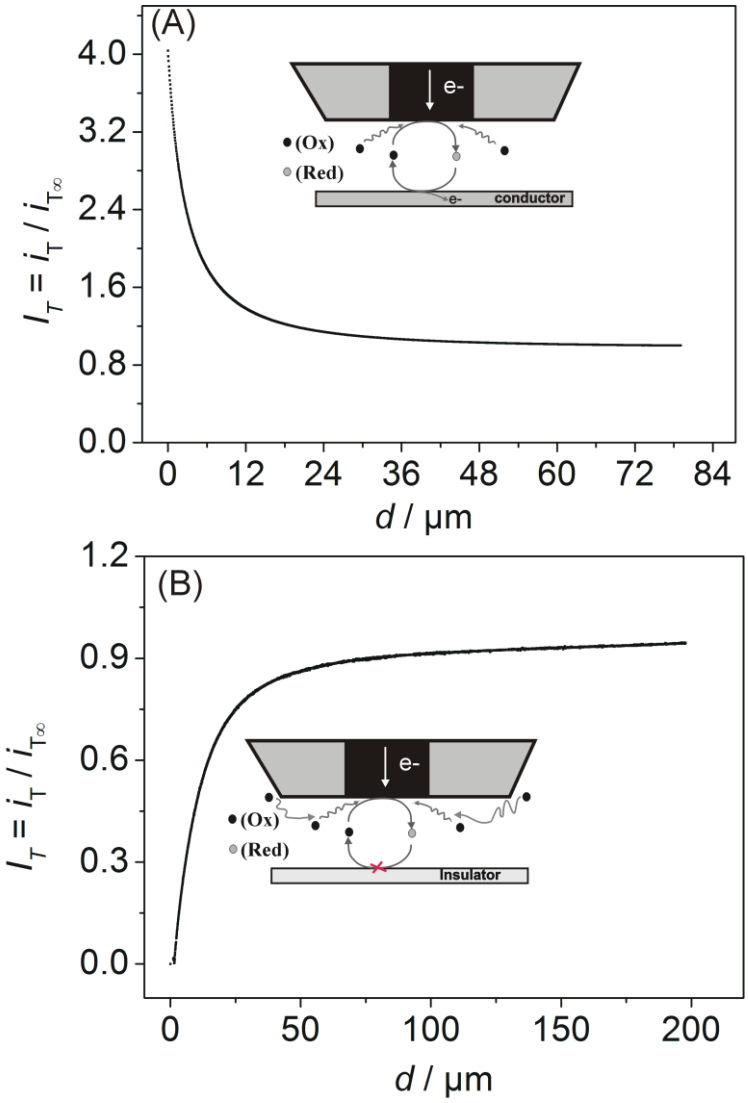

Figure 11: Principle of SECM feedback mode: (A) diffusion-controlled feedback and corresponding approach curve and (B) hindered diffusion and corresponding approach curve; *d* is a tip-substrate separation.

4.3.2 Generation-collection mode

Unlike feedback mode, no mediators are required in the generation-collection mode. A redox active species can be generated at the ME, diffuses to the substrate and is collected or detected there. This is called tip-generation/substrate-collection (TG/SC) mode. The current is measured at the ME and at the substrate (Fig. 12A). The collection efficiency close to 100% is observed at the substrate if the distance between the ME and substrate is less than $2r_T$. The species generated at the tip diffuse to the large substrate rather than diffuse away to the surface [117]. On the other hand, the roles can be reversed and a redox species generated at the sample is collected at the ME. This is called substrate generation/tip collection (SG/TC) mode (Fig. 12B). Typical applications of the generation-collection mode are the investigation of the activity of immobilized enzymes, the study of diffusion of metabolites released from living cells and the study of ORR in fuel cells, biofuel cells and metal-air batteries [104, 118-120].

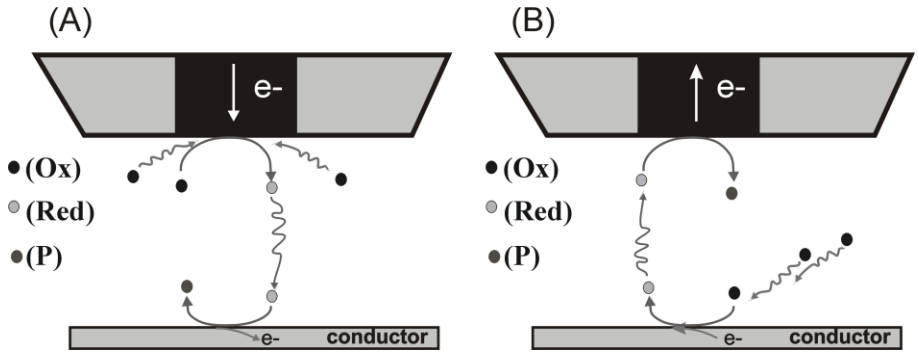

Figure 12: Principle of generation-collection mode; (A) TG/SC and (B) SG/TC.

4.3.3 Redox competition mode

In the SECM redox competition (RC) mode, the ME and substrate compete to collect the same redox species in the electrolyte (Fig. 13). The advantage of the RC mode is the absence of limitation with respect to the sample size. It has been used to study

electrocatalysis at various substrates. The RC mode was first introduced in a double potential step experiment, by Schumann and co-workers [121, 122].

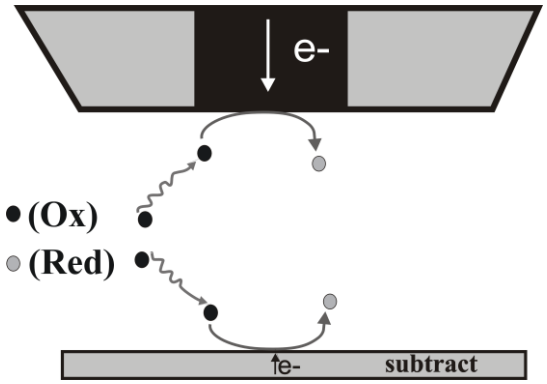

Figure 13: Principle of redox competition mode.

4.4 SECM with modified microelectrodes

Modification of electrode aimed to enhance specific features of electrode such as sensitivity during detection or electrocatalytic reactions, which are normally unfavorable on bare electrodes. However, accuracy in SECM investigation using modified MEs remains a big challenge. A major problem is due to the immobilized layer on the ME, which affects the diffusion process towards the ME. Consequently, the approach curves are different compare to bare electrodes. The diffusion-control observed at the bare ME using a mediator is not established in this case and unpredictable current results. It was therefore concluded that it is not realistic to place a modified ME close to a substrate in a reproducible and accurate way. Only under certain conditions, when the layer is thin enough and porous a diffusion controlled current can be obtained and SECM approach curves are suitable to handle the ME with a good accuracy close to the surface [123-125]. The problems become even more complicated when the substrate is also modified. Here, SECM was combined to optical technique to accurately place the modified GC ME.

5 Experimental section

In this chapter, all chemicals and materials are listed in section 5.1. In section 5.2, the different procedures of samples preparation and the important instrumental descriptions are detailed.

5.1 Chemicals

All chemicals listed in Table 2 were used without further purification, and were of analytical grade. Aqueous solutions were prepared using deionized water (Seralpur PRO 90 C, Ransbach, Germany) with a resistance of 18.2 MΩ cm at room temperature.

Argon was used for deaeration of the solution. Stock solution of plumbagin (PLG) (10 mM) and amplex ultra red (AUR) (10 mM) was prepared in acetone and dimethylsulfoxide (DMSO) respectively and store at -20˚C. 4-Chloro-7-nitrobenzo-2-oxa-1,3-diazole (NBD-Cl) 10 mM stock solution was prepared freshly before each measurement in acetonitrile and stored in the dark.

Table 2: List of Chemicals.

Product	Formula	Supplier	Grade
5-Hydroxy-2-methyl-1,4-naphthoquinone (plumbagin/PLG)	$C_{11}H_8O_3$	Sigma Aldrich	−
5-Hydroxy-1,4-naphthoquinone (juglone/JUG)	$C_{10}H_6O_3$	Sigma Aldrich	≥97.0 %
Sodium bicarbonate	$NaHCO_3$	Sigma Aldrich	≥99.5 %
Sodium phosphate monobasic dihydrate	$NaH_2PO_4 \cdot 2H_2O$	Merk	≥99.0 %
Sodium phosphate dibasic dihydrate	$Na_2HPO_4 \cdot 2H_2O$	Merk	≥99.5 %

Hydrogen peroxide 30 %	H_2O_2	Fluka	≥30 %
Potassium phosphate monobasic	KH_2PO_4	Sigma Aldrich	≥98.0 %
Potassium phosphate dibasic	K_2HPO_4	Sigma Aldrich	≥99.0 %
Horseradish peroxidase, Type II (150-250 units/mg)	–	Sigma Aldrich	–
11-Mercapto-1-undecanoic acid (MUA)	$C_{11}H_{22}O_2S$	Sigma Aldrich	≥95 %
11-Mercapto-1-undecanol (MU)	$C_{11}H_{24}OS$	Sigma Aldrich	≥97 %
L-Glutathione reduced (GSH)	$C_{10}H_{17}N_3O_6S$	Sigma Aldrich	≥98 %
Potassium dioxide	KO_2	Sigma Aldrich	–
Hypoxanthine	$C_5H_4N_4O$	Sigma Aldrich	≥99 %
Cytochrome c (cyt c)	–	Sigma Aldrich	–
Xanthine oxidase from bovine milk, Grade III (1.0-2.0 units/mg protein)	–	Sigma Aldrich	≥95 %
Superoxide dismutase (SOD)	–	Sigma Aldrich	–
1-Ethyl-3(3-dimethylaminopropyl)	$C_8H_{17}N_3$	Sigma	–

carbodiimide (EDC)		Aldrich	
4-Chloro-7-nitrobenzo-2-oxa-1,3-diazole (NBD-Cl)	$C_6H_2ClN_3O_3$	Sigma Aldrich	≥97 %
L-Glutamine solution	$C_5H_{10}N_2O_3$	Sigma Aldrich	−
Decamethylferrocenne (DMFc)	$C_{20}H_{30}Fe$	ABCR	≥97 %
α,α,α-Trifluorotoluene (TFT)	$C_6H_5CF_3$	Acros Organics	≥99 %
Ferrocene methanol (FcMeOH)	$C_{11}H_{12}FeO$	Alfa Aesar	≥97 %
Amplex ultra red (AUR)	−	Life Technologies	−
Penicillin-streptomycin	−	Life Technologies	−
Fetal bovine serum (FBS)	−	Life Technologies	−
Dulbecco's modified Eagle's medium (DMEM)	−	Invitrogen	−
1-Butyl-3-methylimidazolium bis(trifluoro-methylsulfonyl)imide (C_4mimN(Tf)$_2$)	$C_{10}H_{15}F_6N_3O_4S_2$	Iolitec	99%
1-Decyl-3-methylimidazolium bis(trifluoro-methylsulfonyl)imide C_{10}mimN(Tf)$_2$	$C_{12}H_{19}F_6N_3O_4S_2$	Iolitec	98%

5.2 Instrumentations

5.2.1 General electrochemical experiments

Electrochemical measurement were performed at room temperature using potentiostats CHI 660 A, 620 A (CH Instruments, Electrochemical Analyser, Austin, TX, USA) and bi-potentiostat Ivium Compactstat (Ivium Technologies, Eindhoven, The Netherlands) in a three or four-electrode configuration. The working electrode was a glassy carbon (GC) with a diameter of 3 mm (BAS Technicol, UK), home-made GC microelectrode (ME), carbon fiber ME or a gold surface. A platinum wire and Ag/AgCl/3 M NaCl electrode served as auxiliary and reference electrodes, respectively.

5.2.2 Atomic force microscopy (AFM) and scanning electron microscopy (SEM) characterizations

AFM thickness determinations were carried out by Julia Witt under ambient conditions with a Nanoscope IIIA controller and an Enviroscope stage (Veeco Instruments Inc, Santa Barbara, CA, USA). The contact mode was applied with Au-coated Si_3N_4-cantilever (Bruker, MSCT tip) of a nominal spring constant of 0.6 N/m. The analysis of film thickness was made using the software Analysis 1.4. Morphology of the film was elucidated by SEM using Helios Nanolab 600i system (FEI Company, Eindhoven, The Netherlands) and EDAX detector at acceleration voltages of 15 to 25 kV. A detailed procedure of AFM and SEM characterization is described in the Ref. [126].

5.2.3 In-situ fluorescence microscopy

Fluorescence microscopy detection was carried out using DMIRE2 microscope in inverted configuration (Leica Microsystems GmbH, Wetzlar, Germany) using a HC PL

Fluotar objective with 5 x or 10 x magnifications (numerical aperture NA = 0.5, Leica). Samples were excited with a tungsten lamp with a dichroic filter set for NBD-Cl (470 nm excitation/540 nm emission) or AUR (546 nm excitation/580 nm emission). The signals were recorded at a rate of 1 s per frame by a camera (DC152QC-FI scientific CMOS with Solis control software, Andor Technology, Belfast, UK) attached to the third optical port of the microscope setting. The recorded intensities were converted to a false colour image.

5.2.4 Bio-scanning electrochemical microscopy (Bio-SECM) for local oxidative stress investigation

The Bio-SECM device is composed of the fluorescence microscopy setup (section 5.2.3) and a piezo motor mounted on the adaptor, which allows positioning of ME above a living cell and objective lens. This positioning part is connected to the SECM device developed in-house. This SECM device consisted of a bi-potentiostat (Ivium Compactstat, section 5.2.1), a high-resolution positioning system, and a computer. The computer controls the positioning system, the data acquisition system and displays the electrochemical data. The bi-potentiostat is connected to the computer using a USB connection and the piezo motor is controlled with an analog signal from the conversion of the digital signal coming from computer using a digital-to-analog converter (AD/DA board PCI-DAS 1602/16, Plug-In Electronic GmbH, Eichenau, Germany). The electrochemical cell, which can be a cell culture dish or a cell containing a lateral window and allows monitoring of the movement of ME using camera. It included the ME as working electrode, a platinum wire as auxiliary and Ag/AgCl/3 M NaCl electrode served as reference electrodes placed above the inverted optical microscope (Fig. 14).

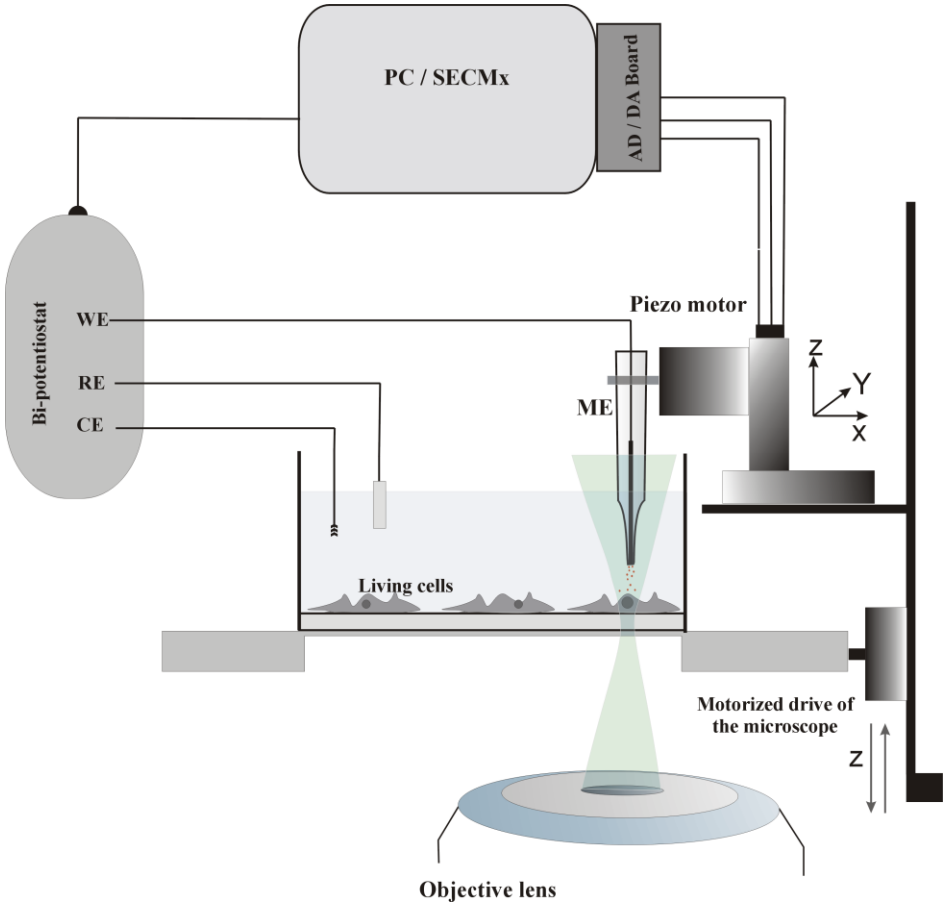

Figure 14: Bio-SECM setup for local oxidative stress investigation in the environment of living cells.

5.3 Preparation of glassy carbon ME and carbon fiber ME

GC MEs were prepared using a similar procedure as previously reported [127]. A GC rod (Type 2, 1 cm length, 1 mm diameter, Alfa Aesar, Karlsruhe, Germany) was immersed in 4 M KOH solution, where a DC voltage of 5 V was applied for 20 min between GC rod and a large graphite electrode as a cathode. In order to etch the top end of the rod, the same voltage was applied again for 20 min. The etching process in the strong basic solution leads to the formation of oxygen gas bubbles from anodic electrolysis of H_2O and detachment of carbon particles from the GC [128]. The following equations were proposed to explain the etching process:

$$C_{(s)} + OH^-_{(aq)} \rightarrow C_{(s)}(OH)_{ads} + e^- \quad (14)$$

$$4C_{(s)}(OH)_{ads} \rightarrow 4\,C + 2H_2O + O_2 \quad (15)$$

Where $C_{(s)}$ is a intact carbon lattice of GC, $C_{(s)}(OH)_{ads}$ is the OH group chemisorbed on the GC surface and C is the carbon material or particle removes from the surface of GC. Then after rinsing with water, the carbon needle was inserted into one end of a borosilicate capillary (1.5 mm O.D, 1.17 mm I.D), connected to the Cu wire using Ag epoxy resin. The exposed end of the GC needle was dipped in nitrocellulose solutions containing plasticizers. The coating is obtained in the contact with air during few minutes. This procedure was repeated 4 times. Finally, the tip of the electrode was covered with epoxy resin to protect the coating layer from scratches (Fig. 15). Before each experiment the ME was polished with sand paper and alumina suspension and characterized by CV and confocal laser scanning microscopy (CLSM).

The carbon fiber (CF) with 30 µm diameter (provided by Prof. Dr. David Wipf of Mississippi State University) was used to prepare the ME. A borosilicate glass capillary 10 cm long, 1.5 mm outside diameter and 0.375 mm wall thickness (Hilgenberg GmbH, Malsfeld, Germany) and the CF were rinsed with water, ethanol and dried prior to use. Then, the capillary was cut into half by heat puller (Model PP-830, Narshige, Japan). The tip was sealed by burning with a portable torch. A 5 cm piece of the 30 µm CF was inserted at the end of the glass capillary. The assembly was put back in the heat puller setup with its terminal tips positioned in the centre of a tungsten coil. The open end of the capillary was connected to a vacuum pump by a thin silicon tube to prevent formation of air bubbles between the CF and the glass. The tungsten coil was heated for 5 minutes to melt the glass around the CF and obtain a good sealing of the tip. After the sealing and cooling step, the electrode was inspected under the optical microscope to

check that the fiber is completely sealed at the tip and that there are no air bubbles inside. The Cu wire was fixed at the upper part of the capillary with silver epoxy glue (EPO-TEK® H24 part A & B) and dried in an oven at 65° C over the night. The resulting ME was polished with 0.3 and 0.05 µm alumina powder and characterized by CV and CLSM before each experiment.

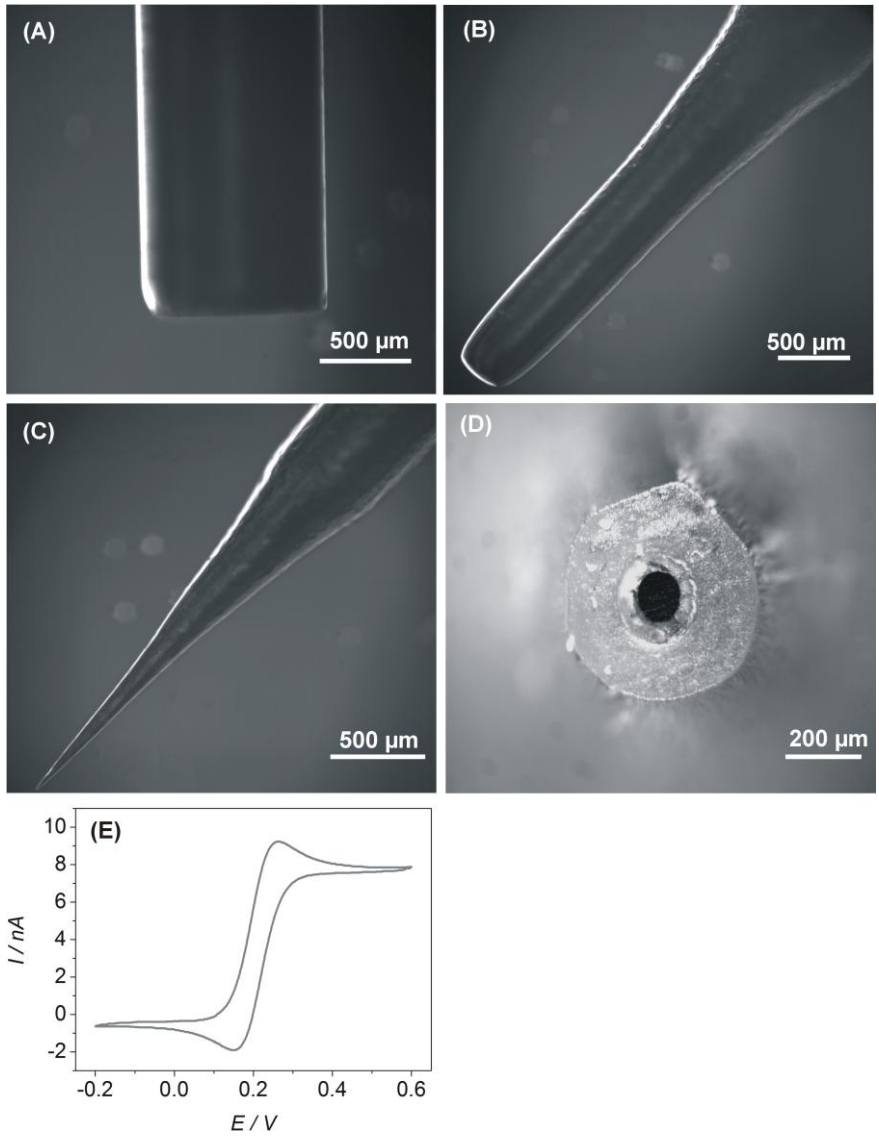

Figure 15: Optical image of (A) initial GC rod; (B) after etching of 20 min; (C) after etching the tip of GC rod; (D) 110 µm diameter ME obtained and (E) the CV of GC ME in 0.25 mM FcMeOH in phosphate buffer, pH 7 at 0.025 V s^{-1} vs. Ag/AgCl/3 M NaCl.

5.4 Preparation of quinone polymer-modified GC

PLG-modified electrodes were prepared as described by Ardakani et al. [129]. The GC electrode surface was polished with 0.3 and 0.05 µm alumina powder followed by sonicating and rinsing with deionized water after each polishing step for 15 min to remove the alumina and abraded particles. Subsequently, the pre-cleaned GC electrodes were activated electrochemically in 0.1 M $NaHCO_3$ by performing 40 cycles between -1.1 and 1.8 V (vs. Ag/AgCl/3 M NaCl) at a scan rate ν = 0.1 V s^{-1}. After rinsing with water, grafting of the PLG on the electrode surface was done by immersing the activated GC in 0.1 M phosphate solution pH 4, containing 0.2 mM PLG and performing 30 potential cycles between 0.1 and -0.3 V at ν = 0.01 V s^{-1}. Then, the PLG-modified electrode, abbreviated as PLG/GC was immersed in phosphate buffer pH 7 containing 0.2 mM PLG and the potential was again cycled between -0.8 to 1.2 V at 0.05 V s^{-1} for 25 cycles causing the formation of phenoxy radicals and formation of the polymer. After rinsing with water, electrode was stored in phosphate buffer solution pH 7.

5.5 Preparation of biosensor based on cytochrome c

A biosensor for $O_2^{\bullet-}$ was prepared as described previously [93]. Clean Au wires (1 mm diameter, Goodfellow Cambrige, limited, Huntingdon, England) were incubated in a mixture of 5 mM 11-mercapto-1-undecanoic acid (MUA) and 5 mM 11-mercapto-1-undecanol (MU) (ratio 1:3) in ethanol (96%) for 1 day at room temperature followed by rinsing with ethanol. The MU/MUA-modified electrodes were rinsed with ethanol and 5 mM potassium buffer saline (K-PBS) pH 7. The modified surface was incubated in a solution containing 30 µM cyt c in 5 mM K-PBS pH 7 for 2 h. Covalent bonding was promote by addition of 2.5 mM 1-ethyl-3(3-dimethylaminopropyl) carbodiimide (EDC).

After 30 min of reaction, the electrodes were rinsed with 5 mM K-PBS pH 7 and dried. The biosensor was checked using CV before (Fig. 16) and after each measurement to test the stability of the protein on the modified gold surface, and the interaction with $O_2^{\bullet-}$ using xanthine oxidase/hypoxanthine or KO_2 as source of $O_2^{\bullet-}$. By choosing a suitable potential value such as -0.05 V, the reduced cyt c (Fe^{2+}) is formed and H_2O_2 can be detected (Fig. 16(3)). At a potential of -0.13 V oxidized cyt c (Fe^{3+}) is formed and $O_2^{\bullet-}$ is detected (Fig. 16(4)) without interference of H_2O_2 [93, 130, 131].

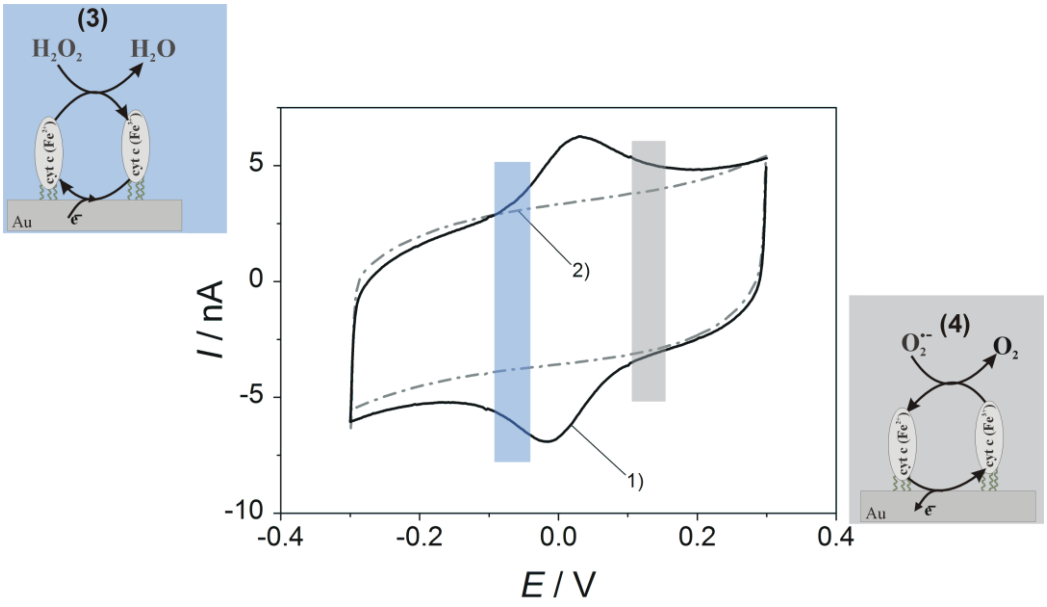

Figure 16: CV of (1) cyt/MUA-MU/Gold and (2) MUA-MU/gold in oxygen-free 0.1 M phosphate buffer pH 7, v = 0.05 Vs^{-1} vs. Ag/AgCl/3 M NaCl; potential window of selective detection of (3) H_2O_2, (4) $O_2^{\bullet-}$.

5.6 Cell culture preparation

Cell culture and passage were conducted by Janina Leyk (Department of Neuroscience, Molecular Neurobiology, and Research Center Neurosensory Science) as described by Chen et al. [132]. Briefly, mouse derived retinal pigment epithelium cells (B6-RPE07 cell

line) were kept in Dulbecco's modified Eagle's medium (DMEM) supplemented with 2 mM glutamine, 50 U/ml penicillin, 50 mg/ml streptomycin and 10% fetal bovine serum (FBS) at 37 °C and 10% CO_2-atmosphere and passaged twice a week. 60.000 cells were seeded on 35 mm cell culture dishes (μ-dish 35 mm Grid-500, ibidi, Munich, Germany) and cultured for 24 hours in DMEM with 10% FBS. Cells were then washed twice with PBS and cultured for further 24 h in DMEM serum-free solution or DMEM without FBS (Fig. 17). The entire electrochemical investigation was performed in serum-free solution. The viability of the cells was carefully verifying by Janina Leyk. The data interpretations were done by Janina and me.

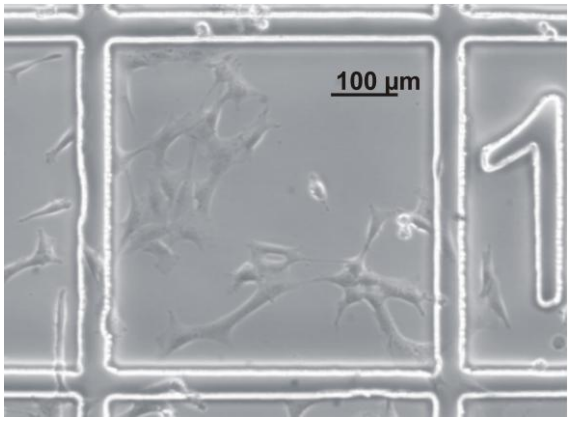

Figure 17: Optical image of the mammalian B6-RPE07 cells on μ-dish containing cultured medium serum-free. The lines and labels allowed precise relocation of specific cells under ME.

6 New approach for preparation of quinone polymers and electrocatalytic activity of oxygen reductions reactions

This chapter describes a new approach of electropolymerization of quinone compounds on GC and the unexpected effect observed during formation of the non-conducting film

compared to the classical electropolymerization. I performed the preparations and the entire electrochemical investigation of the polymer. The characterization using AFM and SEM was carried out by Julia Witt (Wittstock group). Finally this part of the work led to a publication, for which the draft was prepared by Julia Witt and me [126].

Quinone compounds have been chosen because of their capacity to generate $O_2^{\bullet-}$ or H_2O_2 as described in chapter 2. Different strategies of electrode modifications using quinone compounds were investigated with the aim to obtain a stable film on the surface of the electrode. Regarding the stability of active films on electrodes, new strategies are continuously developed. Quinone-coated electrodes obtained by electrografting, chemical grafting, adsorption or electropolymerization have been used intensively in the past, however their instability remained one of the major problem [133-135]. Furthermore, most protocols lead to inactivity of the major part of the film, i.e. the signal of the quinone redox reaction is very small compared to the total amount of deposited polymer. This means that the quinone moieties were transformed or, more likely, that they are present, but cannot be addressed by the electrode. This is prevented by the electronically insulating nature of the obtained films.

The electrochemical activity of quinone moieties on the electrode is an important aspect of quinone-modified electrode and was investigated intensively [136]. The blocking properties affect the electron transfer kinectics to the quinone groups and depend on many parameters. Since the films formed on the surface electrodes are insulating, but redox active films, the redox signals of the film depend on its structure and thickness [136-138]. When the film is not compact, the electron transfer can be easily performed and the redox species remains in contact with the electrode surface via the ion mobility in the films [136]. In contrast, when the film or the monolayer is compact, the electron transfer

may occur from quinone group to quinone through the film. In this case, the film thickness influences the electron transfer. The thicker is the film the lower is the activitiy of the film [136]. Hydrophobic/hydrophilic properties also influence the redox film. Hydrophobic layers inhibit the electron transfer compared to hydrophilic layers in aqueous solutions [139].

In this thesis, we described another preparation strategy using a combination of chemical grafting and electropolymerization of quinone compounds.

6.1 Grafting of PLG on GC

GC has become an interesting electrode material for various electrochemical investigations. It possesses a low oxidation rate, high chemical inertness with small pores. These properties make GC a convenient inert electrode [140]. However, the electrochemical performance of GC depends on its surface treatment, which can be a mechanical, physical, chemical or electrochemical treatment and leads to good reproducibility of results [140-145]. Commonly, electrochemical treatment or activation is used to increase the concentration of oxygen function on the GC and to improve the condition for further surface modifications [146-148].

Surface modification with quinone can be made using various techniques to obtain a thin or thick layer [126]. Quinone or napthoquinone such as PLG or juglone (JUG) can undergo a 1,4-addition with nucleophiles [149]. This ability opens many possibilities for attachment of 5-hydroxy-1,4-naphthoquinone on the gold surface where the quinones react with the aminothiols terminal tail and form a compound able to form a SAM on the surface [150]. On GC, electrochemical grafting is possible using diazonium derivative of the molecule to graft [126]. Recently, the chemical grafting of PLG on GC was reported [129]. As described in chapter 5.4, GC was activated by electrochemical

oxidation using bicarbonate solution. The CV before and after activation attested the increased surface concentration of redox-active groups, which cause the signal at around -0.1 V in Fig. 18B. The CV of GC before the activation in Fig. 18A only shows capacitive currents. It can be concluded that the redox active oxygen-containing groups are introduced during the activation process.

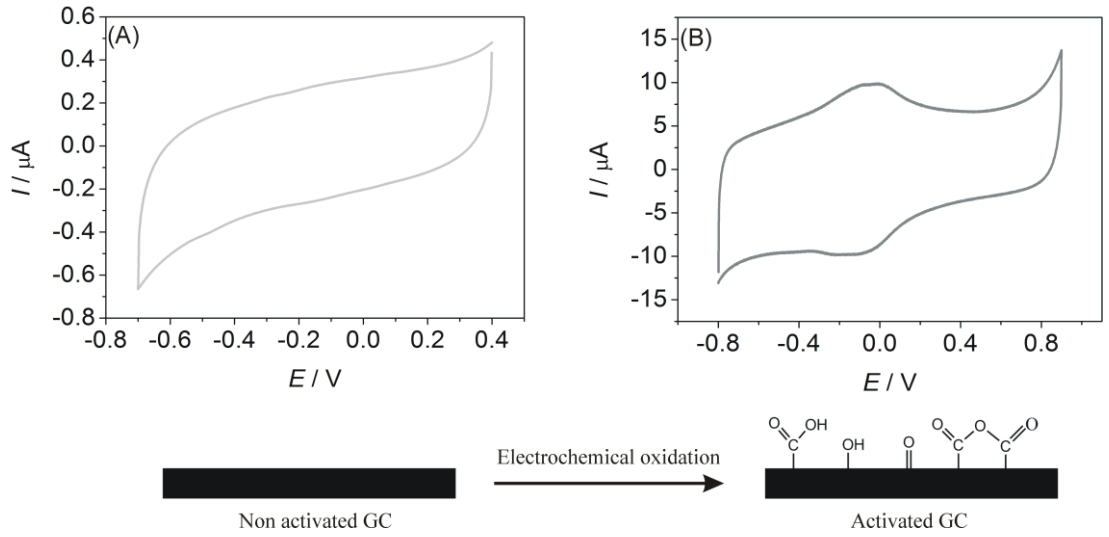

Figure 18: CV of GC (A) before electrochemical activation and (B) after activation, v = 0.05 Vs^{-1} vs. Ag/AgCl/3 M NaCl.

After the formation of oxygen-containing functional groups such as carboxyl, hydroxyl or ketone groups, the GC provides a suitable surface for nucleophile attack of the PLG through Michael 1,4-addition. The modified GC or PLG/GC exhibits a perfect CV of the adsorbed species (Fig. 19). A prominent wave is obtained at -0.28 V due to the strong binding of PLG on the GC surface. A further potential scan has shown a very stable CV in which the current was proportional to the sweep rate which proofs that the redox active group is a surface-bound species [151]. For an ideal film, the peak current is given by:

$$i_p = \frac{n^2 F^2}{4RT} \nu A \Gamma^* \qquad (16)$$

where $A\Gamma^*$ is the amount of bound molecules.

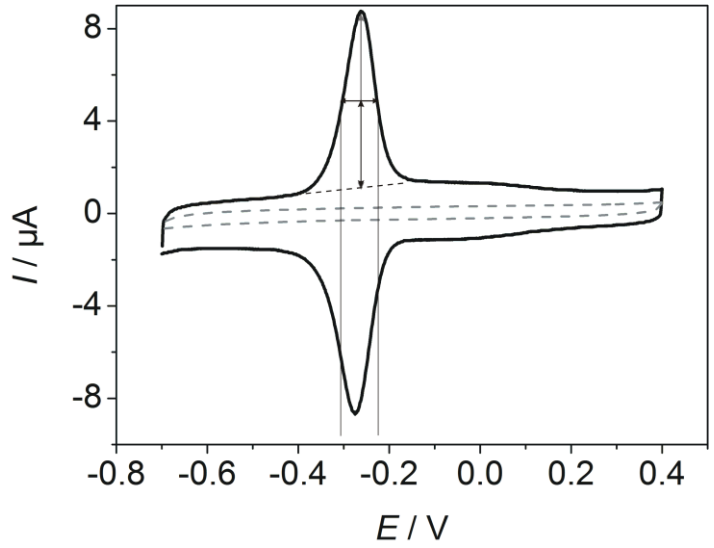

Figure 19: CV of clean GC (dashed line) and PLG/GC (bold line) in buffer phosphate pH 7, oxygen free, ν = 0.05 Vs^{-1} vs. Ag/AgCl/3 M NaCl.

However, a non-ideal film is obtained as exhibited by the asymmetrical wave (Fig. 19), since the total width at half-height of either the cathodic or anodic wave (83.3 mV) is not equal to 90.6/*n* where *n* is the number of electrons exchanged during the redox reactions. This non-ideal behavior can be ascribed to the irreversible attachment of the reactant to the GC surface. To obtain a good approximation it is necessary to consider activity coefficients, which depend on the surface concentration. Such investigation was well described by Alan and co-workers [151, 152], where the behavior of 9,10-phenanthrenequinone was investigated experimentally and theoretically taking into account the non-ideal behavior.

A mechanism was proposed to illustrate the chemical reaction of the PLG with activated GC. Considering the shape of the CV signals, the redox active groups are bound to activated GC and PLG (Scheme 1).

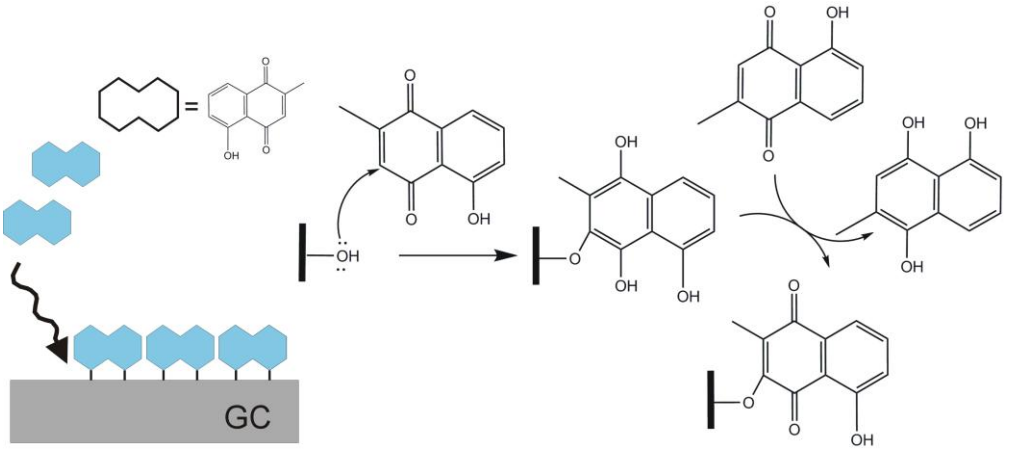

Scheme 1: Proposed reaction mechanism for grafting of PLG onto GC.

A simple electrochemical strategy was developed to demonstrate the proposed mechanism of chemical grafting. In fact, JUG; a similar molecule, was used to explain this chemical bonding. It binds to the activated GC in a similar way as PLG (Fig. 20D). After the grafting step, JUG still possesses an available electrophilic position for a further 1,4-addition with a strong nucleophile such as glutathione (GSH) (Fig. 20D). This is in contrast with PLG, where this position is occupied by a methyl group (Fig. 20B). Thereby, the exposure of the JUG-grafted layers to the GSH during CV in deaerated solution will cause another 1,4-addition evidenced by a shift of the redox potential of the surface bound species from -0.22 V for JUG/GC to -0.3 V for GSH-JUG/GC (Fig. 20B). In contrast, such a shift in peak potential is not observed when conducting a CV of PLG/GC in GSH (Fig. 20A). This feature after the 1,4-addition was reported by many authors where the quinone compound was used to design an electroanalytical method for detection of thiol groups [153-155]. However, this experiment

described in Fig. 20 illustrates a preliminary investigation and at this early stage, more experiments need to be conducted for a good interpretation of this strategy such as XPS characterization.

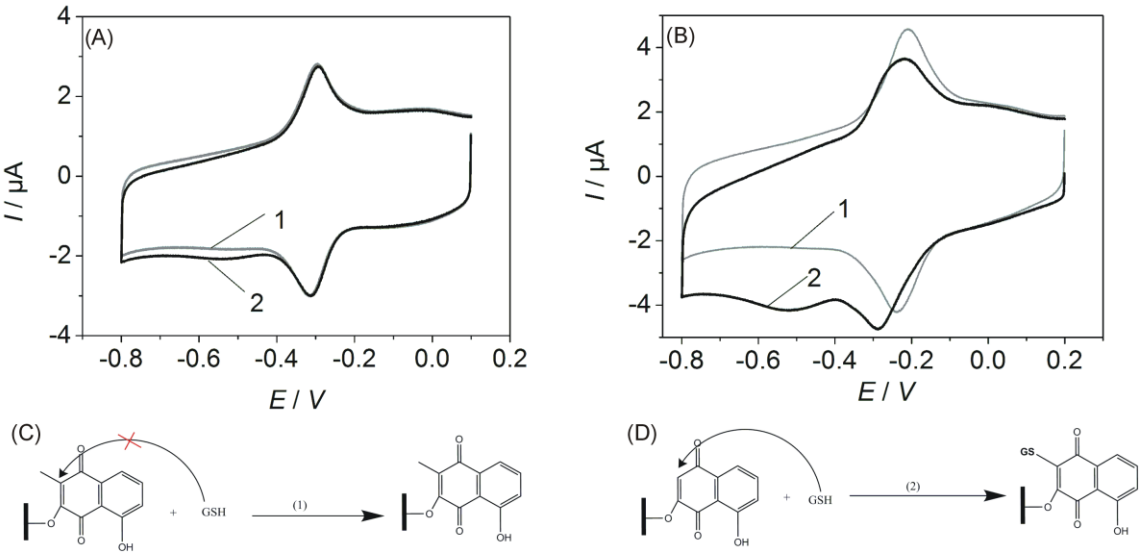

Figure 20: CV of (A) PLG/GC before (1) and after (2) interaction with GSH; (B) JUG/GC before (1) and after (2) interaction with GSH, in phosphate buffer pH 7. oxygen-free v = 0.05 Vs^{-1} vs. Ag/AgCl/3 M NaCl; proposed mechanism of chemical reaction of GSH with (C) PLG and (D) JUG.

Another feature of the PLG-grafted film is the capacity to generate a phenoxy radical from the free hydroxyl function. The grafted layer was subjected to the potential sweep up to +1.3 V where the electrooxidation of the hydroxyl functional group is observed as in other phenolic compounds [156, 157]. The CV recorded exhibits an irreversible oxidation of the phenol group at +1.1 V (Fig. 21). During the first scan the reduction and oxidation of the couple Q/QH_2 is depicted at -0.11 V in oxygen-free phosphate buffer pH 4. After the oxidation of the phenol group, the signals from Q/QH_2

are strongly disturbed and decreased until complete disappearance. However, a new signal appears at around +0.59 V which can be assigned to a new Q/QH_2 system generated during the possible formation of different products due to the mesomerism of the phenoxy radical (Scheme 2). More details will be developed in the next section. The ratio of evaluated charge of Q/QH_2 system and the charge of phenoxy group (Ph) was $Q(Q/QH_2)$: Q (Ph) = 2 in agreement with processes described as 2-electron reactions for the Q/QH_2 system, and one-electron reaction for the Ph system (Fig. 22). This observation proves also that the 5-hydroxyl functions are still accessible and preserved after chemical grafting of PLG on activated GC. Consequently, an idea emerged from this investigation and lead to the control of generation of phenoxy radical at the PLG/GC, which competes with phenoxy radicals of PLG in the bulk solution.

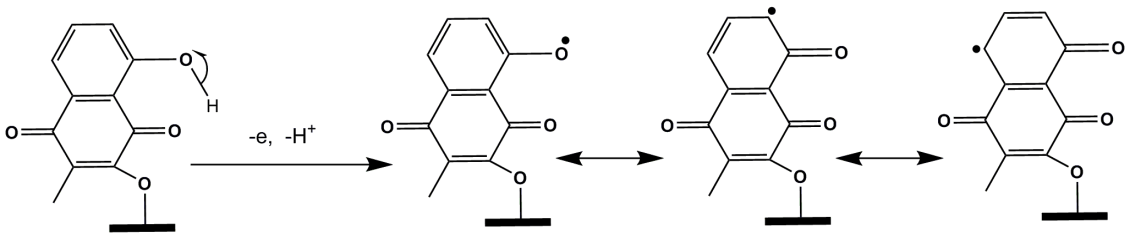

Scheme 2: Electrooxidation of PLG/GC in deaerated 0.1 M phosphate solution pH 4 at +1.1 V.

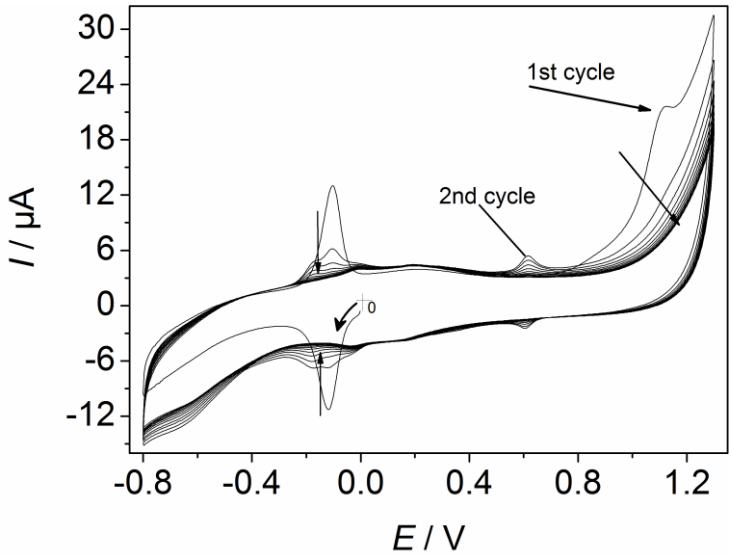

Figure 21: CV detailing the electropolymerization of PLG/GC in oxygen-free 0.1 M phosphate solution pH 4, v = 0.05 Vs^{-1} vs. Ag/AgCl/3 M NaCl.

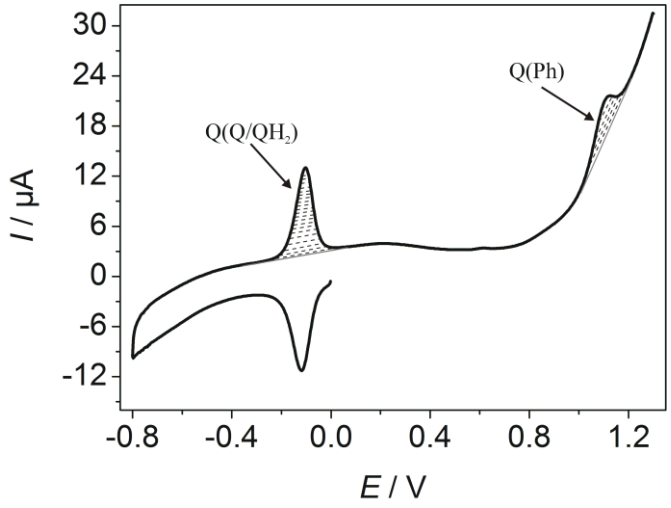

Figure 22: Evaluation of charges required for redox reactions of Q/QH_2 system and phenoxy radicals formation ($Q = \frac{1}{v}\int_{E_1}^{E_2} I(E)dE$). The diagonal stripes represent the integration of the peak used for calculating the charge density.

6.2 Electropolymerization of PLG on clean GC and passivation problem

Electrochemistry provides many advantages during the preparation of polymer films such as selectivity of reaction of one functional group and preservation of other functional groups [135]. Furthermore, electrochemical approaches offer a good control of thickness of polymer films during the electropolymerization [135].

Electrooxidation or electropolymerization of 5-hydroxynaphthoquine in aqueous solutions leads to a redox active polymer in contrast to the other films such as pyrrole-based anthraquinone which is not redox active in aqueous solutions[133, 134]. However, the film obtained from 5-hydroxynaphthoquinone is not conductive and the film thickness is difficult to control [158].

The electrooxidation of phenolic compounds leads to the passivation of the electrode surface [133, 134, 156-160]. In fact, a decrease of the current is observed during formation of a polymeric film on the electrode surface [156, 159]. Following electrooxidation, phenol compounds generate phenoxy radicals that enter to complex pathways of further reactions. They can yield different dimeric products. These dimers can be further used to produce a radical and then interact with all other products around to produce a polymer (Scheme 3) [156, 157, 161]. The oxidation of PLG was described to lead to an insulating layer electropolymerization resulting from the formation of phenoxy radicals. A similar observation was noted for JUG [133, 159]. A complex process and different pathways may affect the final product as observed with the phenol (Ph) compound [156, 157]. A similar interaction and reaction could be observed with the PLG.

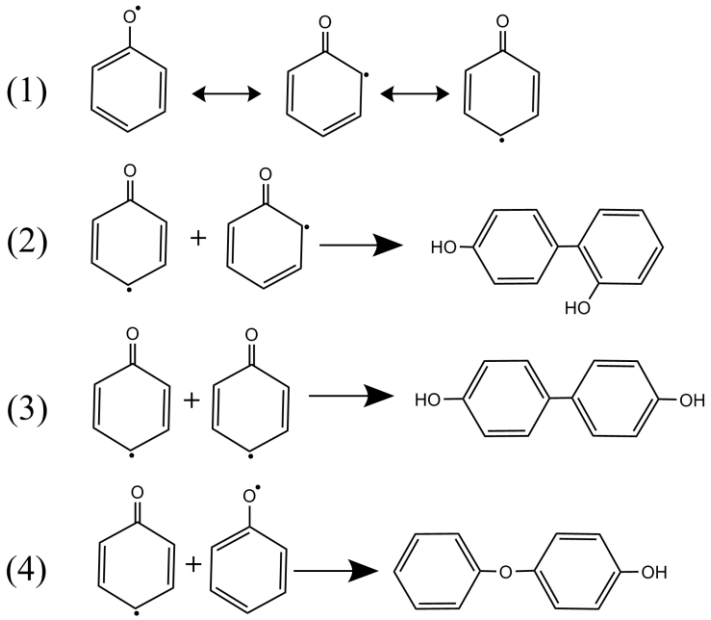

Scheme 3: Some reaction pathways after electrochemical oxidation of phenol [156].

A film was prepared on a graphite substrate using JUG and the structure was determined [133, 134]. Similarly to the case of phenol the chemical bond between two monomers was established between the 5-hydroxy function and the position 8 of another JUG monomer (Scheme 4) [133]. This mechanism is likely also valid for PLG, which is a similar compound.

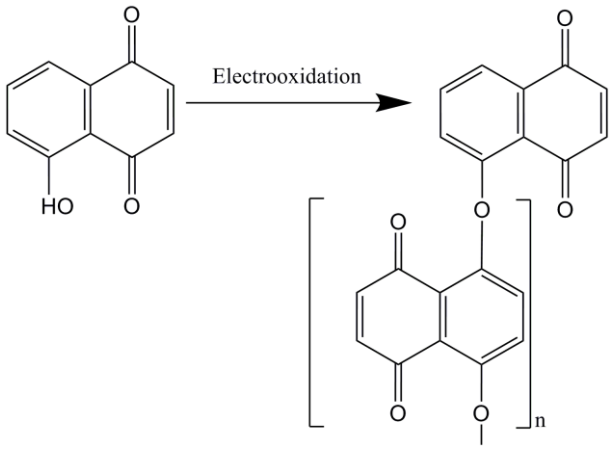

Scheme 4: Structure of polymer film obtained after electropolymerization of JUG [133].

The electropolymerization of PLG on clean GC shows a decrease of the irreversible peak current of the phenoxy radical formation at around -1 V during the potential cycles (Fig. 23) and a self-limiting growth of the polymer. The maximun thickness of the film is 12 nm as measured by AFM (Fig. 25, curve 2). The polymeric products block the surface and stop the access of further monomers to the interface (Scheme 5). The voltammetric signal of Q/QH_2 also changed during the voltage sweep. After the first scan, a shift of the quinone peak is observed to a more negative value. This reflects the chemical changes of the GC surface after the first scan due to the immobilization of the products of the reactions of the radicals. The concentration of monomers, pH of the solution and the temperature affect the formation rate of the films [161, 162]. For example, the monomer radicals are more stable in basic solution and non-aqueous solution and can react with similar molecules rather than with protons. This increases the quantity of deposited material [159, 161].

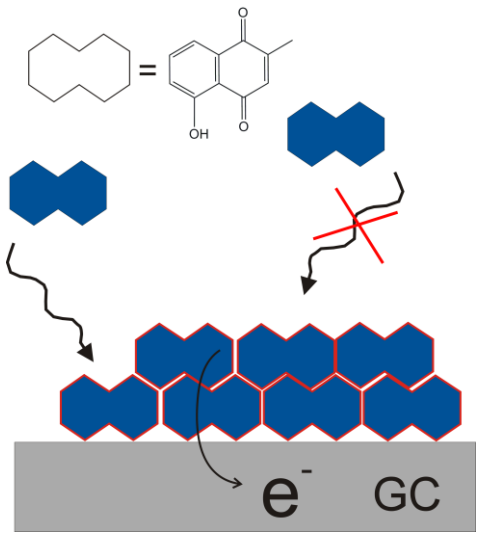

Scheme 5: Self-limiting growth of the polymer film during electropolymerization of PLG onto bare GC.

The surface deactivation and degree of polymerization seem to be influenced by the permeability of the polymer film [156]. The electroactivity of the polymer afterwards is explained by the stability and preservation of the quinone functions which cause a clear wave during redox reaction of Q/QH_2 system [159].

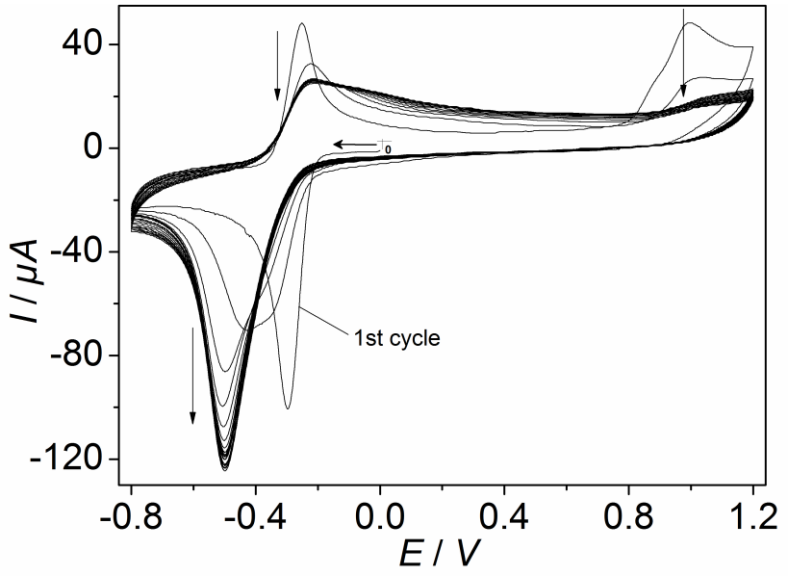

Figure 23: CV of electropolymerization of PLG on cleaned GC in oxygen-free 0.2 mM PLG solution pH 7, v = 0.05 Vs^{-1} vs. Ag/AgCl/3 M NaCl.

6.3 Electropolymerization onto PLG/GC

A new approach of electropolymerization is described here. The PLG contained in the buffer solution is not directly electropolymerized on the clean GC but onto a monolayer of grafted PLG on a GC electrode (PLG/GC). PLG as well as PLG/GC are able to produce a phenoxy radical when a high positive potential is applied as presented in the Fig. 21 and 23. Surprisingly, a new behavior was observed when the polymeric film is prepared on PLG/GC. The electropolymerization onto PLG/GC seemed to avoid the

passivation of the surface usually observed with phenolic compound or hydroxynaphthoquinones.

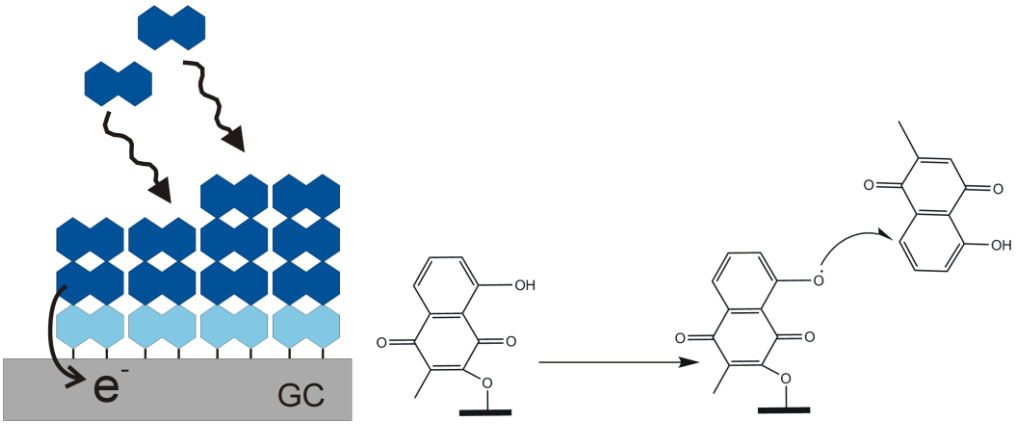

Scheme 6: Continuous growth of the film during electropolymerization of PLG on PLG/GC.

During the electropolymerization a slight decrease in the current is observed during the formation of phenoxy radicals (Fig. 24). This reflects the easy accessibility of the interface for the new monomer during the potential cycles despite the existence of a film. This causes a continuous growth of the polymer as it has been reported for the conductive polymers (Scheme 6) [158]. The film thickness was determined as function of CV cycles (Fig. 25B, curve 1) and shows a film thickness of up to 70 nm, i.e. about 6 times thicker than for PLG polymerization on bare GC. This new process promotes the formation of pits or small holes (Fig. 25A, white arrows) during the formation of the redox polymer and preserves a good permeability of the film. Therefore, the counter ions can still transport charge through the film and enable the formation of phenoxy radicals at the GC-film interface. This is proved by the constant potential values for the Q/QH_2 couple and the oxidation of phenol. The comparison of the capacitive current at 0.2 V between the polyPLG/PLG/GC and polyPLG/GC shows a current 40 times higher value

for polyPLG/PLG/GC than for polyPLG/GC in accordance with the permeability of both polymers.

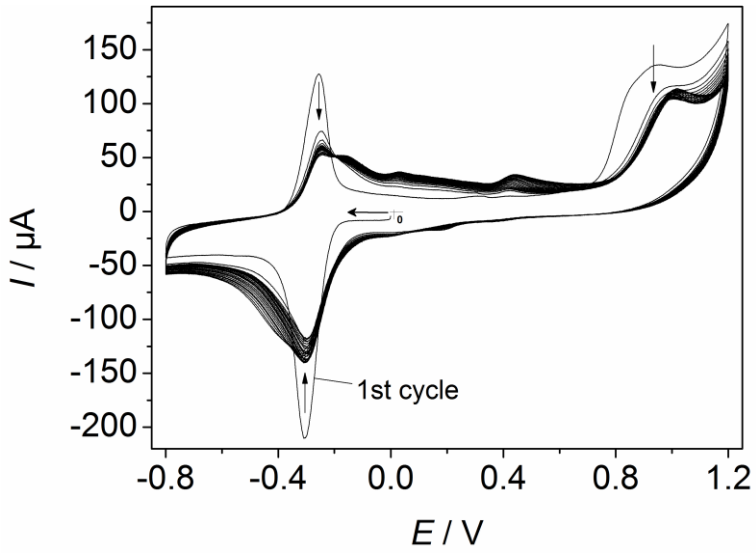

Figure 24: CV of electropolymerization of PLG on PLG/GC in oxygen-free 0.2 mM PLG pH 7 at v = 0.05 Vs^{-1} vs. Ag/AgCl/3 M NaCl.

The growing polymer chains on PLG/GC seem unrestricted. The film thickness (evaluated using AFM) shows a fast increase of the film thickness up to 50 cycles followed by a slower further growth upon continuous cycling. In contrast, a self-limiting growth of the film is observed for polyPLG/GC reaching 12 nm after 25 cycles (Fig 25B, curve 2). With the same cycle number a film thickness of 25 nm is obtained for poly/PLG/PLG/GC. The SEM image shows a homogeneous and smooth distribution of globular structure on the surface affected by many pits (Fig. 25A, white arrows) that contribute to the permeability of the polymer. The grafted PLG layer has a strong influence on the morphology of the subsequently electropolymerized film. This assertion was confirmed when electropolymerization of PLG was performed on activated GC in the potential regions excluding the redox reactions of Q/QH_2 (Fig. 26). Clearly, the

decrease of the current is observed when the activated GC is not modified with PLG and proves the key role of the grafted PLG layer on GC. Furthermore, a CV of electropolymerization of phenol on bare GC (Fig. 27A) changes completely when phenol is electropolymerized on PLG/GC (Fig. 27B). The passivation effect observed during formation of polyphenol on bare GC does not occur when the film is prepared on PLG/GC. AFM topography of polyPh/PLG/GC also shows globular structures as observed in the case of the polyPLG/PLG/GC and underlines the important role of PLG grafted on GC (Fig. 28).

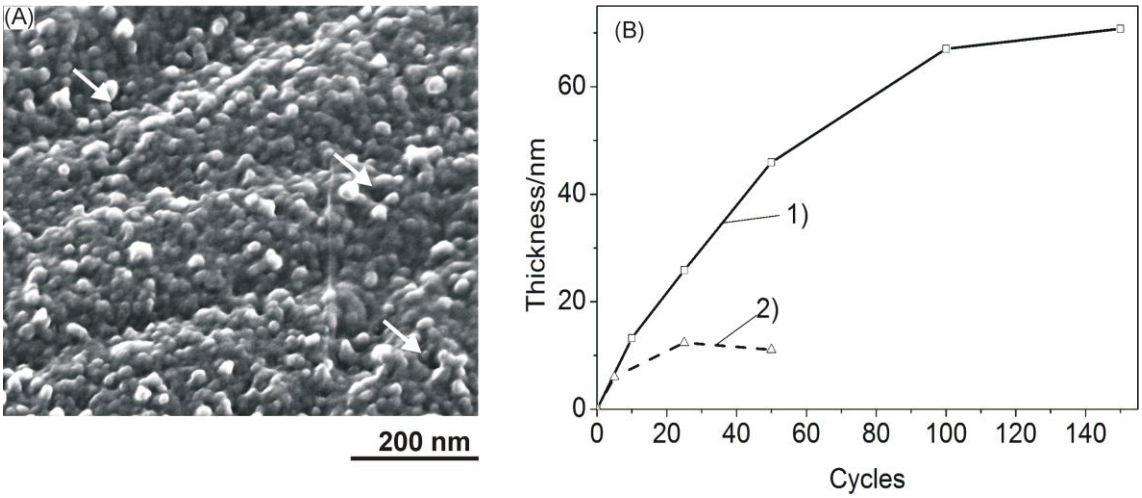

Figure 25: (A) SEM image of poly/PLG/PLG/GC after 25 cycles and (B) AFM thickness of (1) polyPLG/PLG/GC after 10, 25, 50, 100, 150 potential cycles and (2) polyPLG/GC after 5, 25 and 50 potentials cycles.

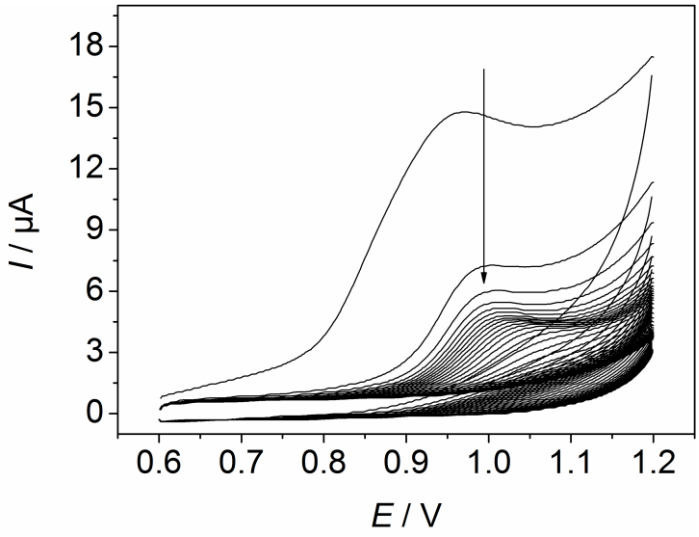

Figure 26: CV of electropolymerization of PLG on activated GC in the potential range excluding the redox reaction of Q/QH_2 system, in oxygen-free 0.2 mM PLG pH 7, v = 0.05 Vs^{-1} vs. Ag/AgCl/3 M NaCl.

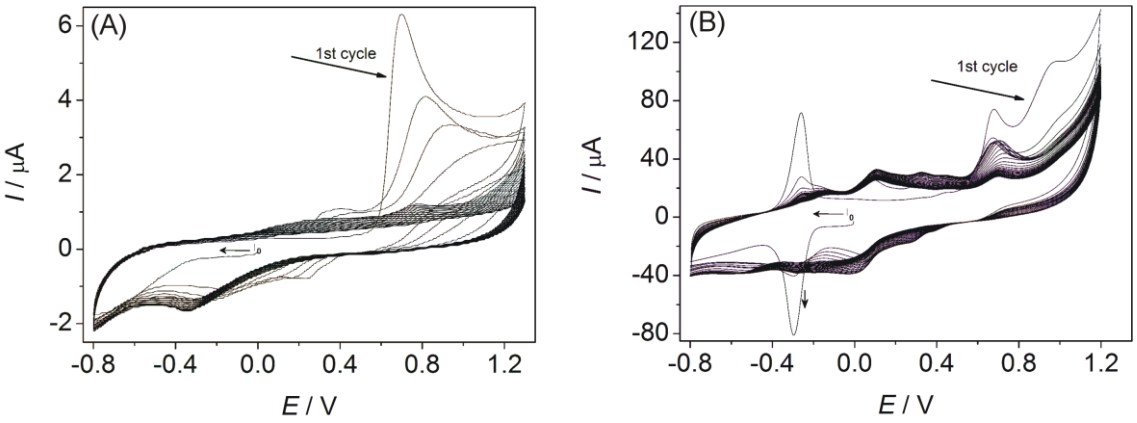

Figure 27: CVs detailing the electropolymerization of 0.2 mM phenol in deaerated phosphate buffer pH 7 on bare GC (A) and on PLG/GC (B). v = 0.05 Vs^{-1} vs. Ag/AgCl/3 M NaCl.

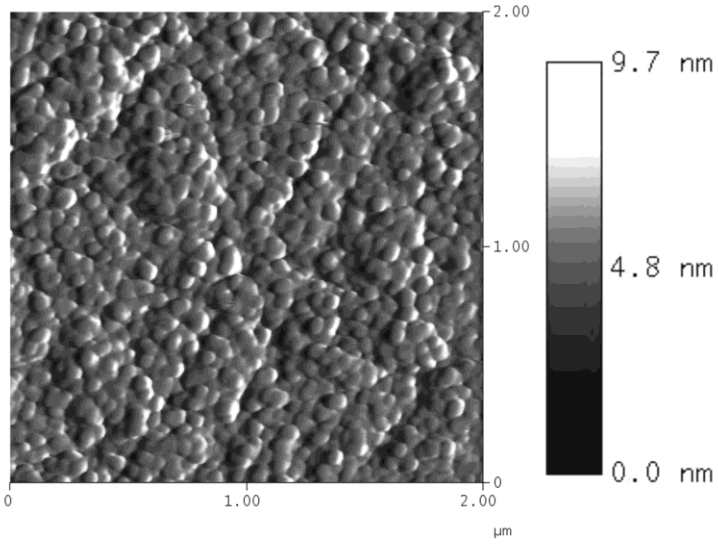

Figure 28: AFM topography (scan area 2 µm x 2 µm) of polyPPh/PLG/GC.

The CV of poly/PLG/PLG/GC demonstrated that the quinone function was obviously retained, and exhibited a voltammetric wave related to the redox reaction of the Q/QH_2 system (Fig. 29). The surface coverage or quinone concentration on the surface was evaluated for 25 electropolymerization cycles. The polyPLG/PLG/GC film showed a 5 times higher concentration of redox active quinone groups than polyPLG/GC. The apparent coverage or surface concentration of quinone groups appears to be pH-dependent with a value between 0.7 and 3.0×10^{-9} mol cm^{-2} with a minimum at pH 4 (Fig. 29B).

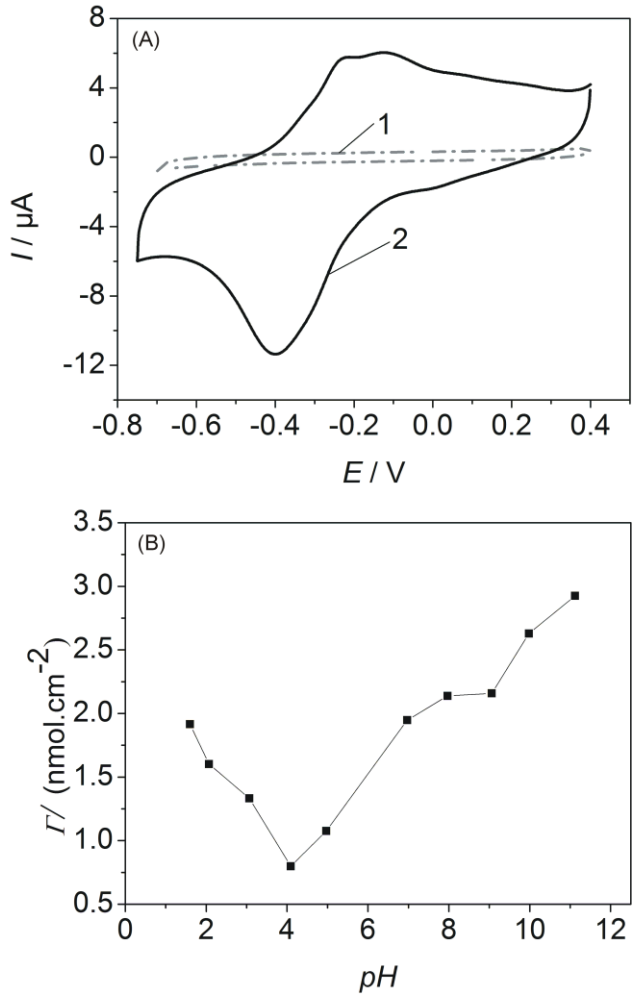

Figure 29: (A) CVs of (1) cleaned GC, (2) polyPLG/PLG/GC (obtained after 25 cycles electropolymerization) in oxygen-free 0.1 M phosphate buffer pH 7 at v = 0.05 V s^{-1} vs. Ag/AgCl/3 M NaCl, and (B) influence of pH on active site of polyPLG/PLG/GC films.

The pH-dependence of redox process, which takes place in the film during potential cycling, was investigated. The plot of formal potential vs. the pH shows a straight line with a slope of -57 mV/pH in the range of pH from 2 to 8 and a second straight line with a slope of -28 mV/pH (Fig. 30). Both values are close to Nernstian value of -59.2 mV for a two-electron/two-proton process and -29.6 mV for a two-electron/one proton process.

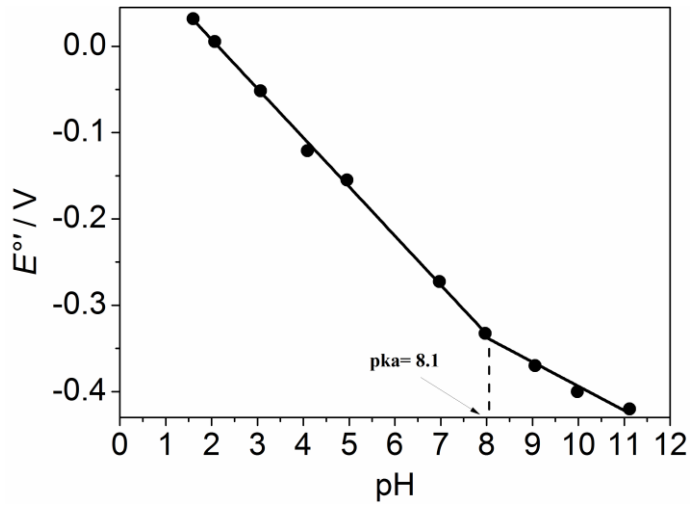

Figure 30: pH dependence of formal potential for polyPLG/PLG/GC obtained after 25 cycles in oxygen-free 0.1 M phosphate solution.

As expected, the chemistry inside the polymer is complicate and depends of the thickness. For 25 electropolymerization cycles (thickness of 15 nm), a two-electron/two-proton process is observed and a well-defined dependence of the current with the scan rate is found. However, with increasing thickness, this trend does not hold. Investigation of redox activity of polyPLG/PLG/GC shows a preservation of quinone moieties during CV in oxygen-free phosphate buffer solution pH 7 (Fig. 29A). The concentration of active quinone moieties of polyPLG/PLG/GC is pH dependent which exhibit a high activity for high pH values and low activity at pH 4 (Fig. 29B).

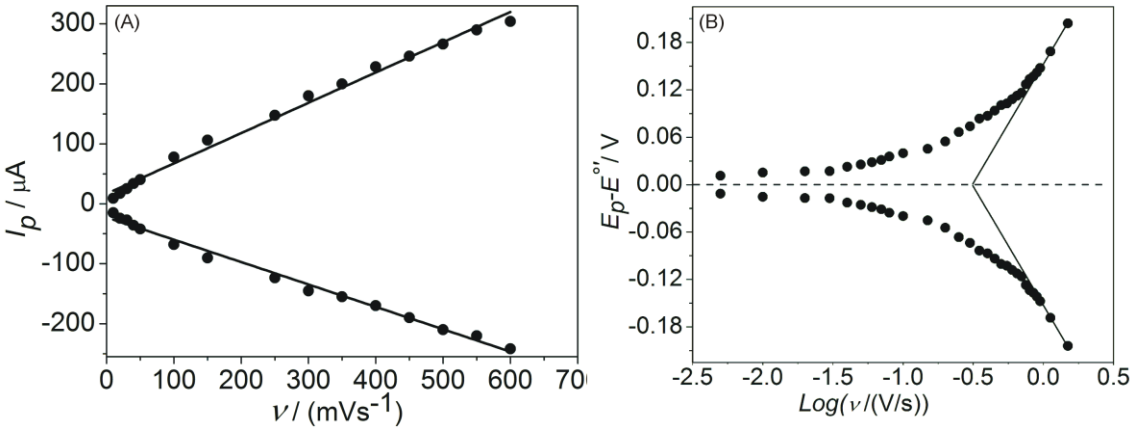

Figure 31: (A) The influence of scan rate on the anodic and cathodic peak currents of polyPLG/PLG/GC and (B) Laviron plot for polyPLG/PLG/GC.

The scan rate dependence of the peak current of the Q/QH_2 system within the polyPLG/PLG/GC film nicely conforms to the expectation for a surface-confined redoxactive species (Fig. 31A). Among the theories developed to describe the kinetics of this process, Laviron's theory [163] was chosen to evaluate the electron-transfer rate constant or apparent charge transfer rate constant and the transfer coefficient between the GC and the quinone moieties. In the plot of $\Delta E = E_p - E^{\circ\prime}$ vs. log v, the transfer coefficient $\alpha = 0.5$ was obtained according to Eq. (17) from the crossing points of a linear fit to the anodic ($v_a = 0.319$ V s^{-1}) and cathodic ($v_c = 0.319$ V s^{-1}) branches where E_{pa}-$E_{pc} > 200$ mV/n (Fig. 31B) [163]. $E^{\circ\prime}$ is the formal potential taken as the average of the anodic (E_{pa}) and cathodic (E_{pc}) peak potentials and E_p stand for either E_{pa} or E_{pc}.

$$\alpha/(1 - \alpha)) = v_a/v_c \quad (17)$$

The heterogeneous standard rate constant $k_s^\circ = 12.5$ s^{-1} of the surface-confined system was obtained from the same plot by Eq. (18)

$$k_s^\circ = nF\alpha\, v_c /(RT) = (1 - \alpha)nF\, v_a/(RT) \quad (18)$$

The relative low values of k_s° can be explained by the coupled electron-proton transfer reactions and a possible hydrophobic nature of the film which increases with the thickness [163]. This deeply affects the mobility of the protons between active site. It is worth to note that k_s° illustrate the electrocatalytic activity of the polymer. This prediction is in correlation with a relatively high peak separation (ΔE_p) value obtained between anodic and cathodic peaks at low scan rate.

This new polymer-modified electrode was further used as a source of the ROS selectively produced by electrocatalysis of ORR at quinone film.

6.4 Oxygen reduction reactions on quinone-modified GC electrodes

The CV of polymer in oxygen-free phosphate buffer and aerated solution illustrated a clear evidence of electrocatalytic activity of polyPLG/PLG/GC during ORR (Fig. 32). The magnitude of the reduction peak is significantly increased in aerated solution compare to the current obtained in oxygen-free solution.

PLG/GC and polyPLG/GC were used for electrocatalysis of ORR and lead to the formation of ROS. Electrocatalytic activity of different PLG-derived films was compared using CV and chronoamperometric measurements. A CV of PLG/GC (Fig. 33, curve 1) in aerated phosphate buffer solution shows a well developed peak of quinone reduction followed by a wave for ORR at lower potential. The ORR at bare GC occurs at more negative potentials (Fig. 33, curve 4). The polyPLG/GC (Fig. 33, curve 2) also exhibits the same ORR catalysis activity, however, there is no separate signal of quinone groups which can be explained by the fact that the disordered films provide different environments to the quinone system and the ionic mobility inside the film is hindered. This leads to a broadening and shifting of the peak. PolyPLG/PLG/GC (Fig. 33, curve 3)

film shows a peak for the reduction of quinone groups shifted by 0.13 V to more negative potentials compared to PLG/GC. The hindered ionic transport in the film for a charge compensation can explain this result. Compare to the polyPLG/GC, this hindrance is not strong although the film is thinner than the polyPLG/PLG/GC film prepared with the same number of electropolymerization CVs. The peak of the wave of ORR at the polyPLG/PLG/GC film is about 20% higher than the peak of the PLG/GC monolayer. This could be a result of partitioning of oxygen between the aqueous phase and the polymer phase. Furthermore, the response of PLG/GC shows that the first monolayer makes the largest contribution to the overall signal. The usual inhibitions of the response know for polyPLG/GC is not observed when the polymerization is made after grafting a PLG monolayer.

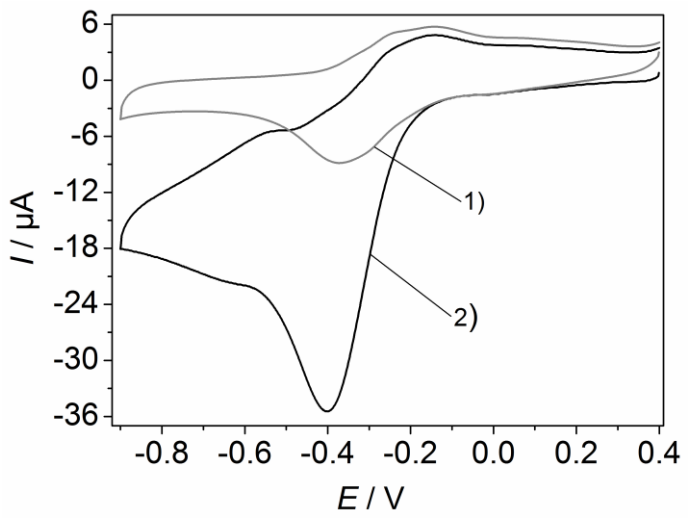

Figure 32: CVs of polyPLG/PLG/GC in 0.1 M phosphate buffer solution pH 7 in (1) oxygen-free solution, (2) aerated solution. ν = 0.05 V s^{-1} vs. Ag/AgCl/3 M NaCl.

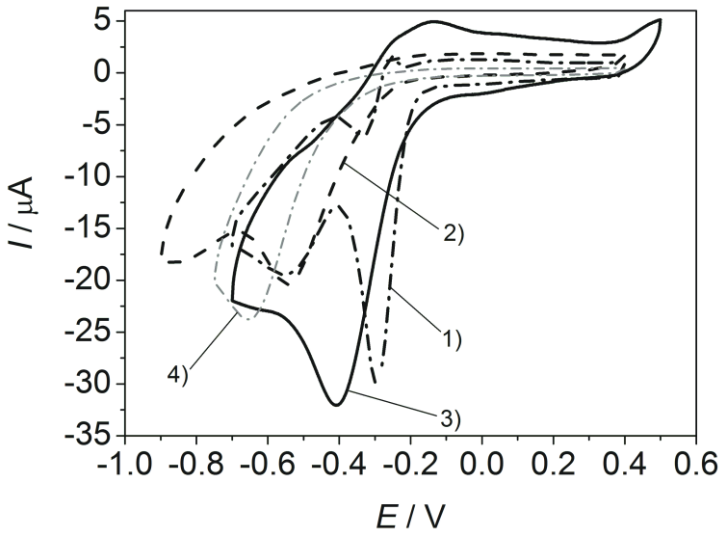

Figure 33: Electrocatalysis of plumbagin-derived layers in aerated 0.1 M phosphate buffer, pH 7 at v = 0.05 V s^{-1} vs. Ag/AgCl/3 M NaCl; (A) for (1) PLG/GC, (2) polyPLG/GC (prepared in 25 cycles), (3) polyPLG/PLG/GC (prepared in 25 cycles), (4) bare glassy carbon for comparison.

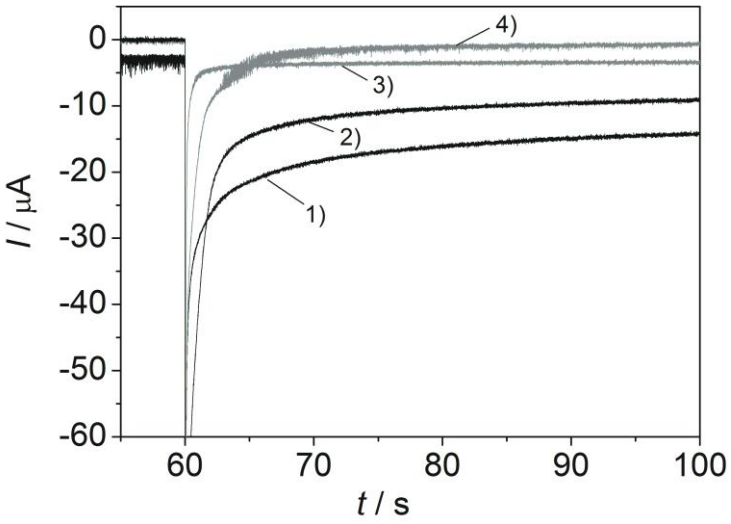

Figure 34: Chronoamperometric responses of (1) PLG/GC, (2) polyPLG/PLG/GC. For comparison the response of (3) PLG/GC and (4) polyPLG/PLG/GC in oxygen-free phosphate buffer is also shown.

For CA experiments the potential program consisted of a step at t = 60 s from E = 0 V where no reaction was observed in oxygen-saturated solution to E = -0.45 V where ORR set in. The experiment was conducted for PLG/GC and polyPLG/PLG/GC in oxygen-free solution and in oxygen-saturated solution. The response in deaerated solution provided the currents due to the conversion of the film itself and the charging of double layer. The difference of the currents in oxygen-saturated solution compared to the deaerated solution was due to the ORR (Fig. 34, curve 3 and 4). The CA response of the polyPLG/PLG/GC layer in the presence of oxygen (Fig. 34, curve 2) was initially higher than that of the PLG/GC electrode (Fig. 34, curve 1), but quickly felt below the currents at the PLG/GC. Again partitioning of oxygen from the aqueous phase into the polymer phase can explain the initially higher current. It seems that the initially grafted PLG layer retains its catalytic activity even if a thicker polyPLG film is electropolymerized on top of the monolayer (Fig. 34, curves 1 and 3). However, the PLG/GC electrode is more effective than the polyPLG/PLG/GC electrode. This would be consistent with the notion that the first monolayer is especially active and the thicker film slightly hinders the access of oxygen to this layer. Both films were more effective than a directly polymerized polyPLG film where the number of accessible quinone groups was much lower. A potential advantage of the polyPLG/PLG/GC layer over a monolayer system is the enhanced mechanical stability of a polymer film vs. a monolayer [134].

7 Selective detection of ROS using fluorescence microscopy

In this chapter attention is given on the detection of two different ROS ($O_2^{\bullet-}$ and H_2O_2) using fluorescence microscopy in different systems. One is related to a technical application, one to biological systems. The reactions involve in the ORR and productions of particular side-products. The experiment in chapter 7.1 was conducted in collaboration with the groups of Prof. Dr. Marcin Opallo (Institute of, Physical Chemistry, Polish Academy of Sciences, Warsaw, Poland) and Prof. Dr. Hubert Girault (Ecole Polytechnique de Lausanne (EPFL), Switzerland). I carried out the investigation using fluorescence microscopy and Justyna Jedraszko (Opallo group) made the preparation of samples. This led to joint publications [164, 165]. The in-situ detection of spontaneous formation of H_2O_2 in organic and ionic liquid phases was achieved by Amplex Ultra Red. The in-situ detection was also realized in lithium-oxygen batteries during ORR on gas diffusion-electrode (GDE) and described in chapter 7.2. These experiments were conducted in cooperation with of Patrick Schwager (Wittstock group). In this cooperation we used of a selective dye to probe the formation of $O_2^{\bullet-}$ as side product during ORR process in a lithium-oxygen battery. My contribution was the detection the $O_2^{\bullet-}$. The results were a subject of a joint publication [166]. Chapter 7.3 presents the detection of two ROS ($O_2^{\bullet-}$ and H_2O_2) obtained during ORR on poly/PLG/PLG/GC. This experiment was conducted by me and the results obtained were published [167] and showed how the poly/PLG/PLG/GC electrode can be used as a generator of ROS and to define a flux of ROS to expose a living cell to small concentration of ROS.

7.1 Detection of ROS in biphasic liquid systems

The biphasic liquid system consisted of two immiscible electrolyte solutions. It can exhibit charge transfer processes at the liquid|liquid interface such as electron and ion transfer [168, 169]. These charge transfer processes at the liquid|liquid interface are subject of great interest because those biomimetic features of these processes are considered as key processes in biology system [168, 169].

In this work, formation of H_2O_2 will be described in two systems, room temperature ionic liquids (RTILs)|aqueous solutions and trifluorotoluene (TFT)|aqueous solutions.

RTILs have found many applications in various industrial processes or in advanced materials [164, 165]. RTILs are salts which are liquid at low temperatures (< 100 °C) and consist of ions [170]. The first development of ionic liquids was in 1914. Ethylamonium nitrate was synthesized and liquid at room temperature but usually contained a small amount of water [170]. RTILs possess high conductivity, good solubility for a wide number of organic and inorganic substances, good chemical stability, low flammability and negligible volatility [171].

The major advantage of RTILs is the large number of possible combinations of anions and cations that give liquids for specific purposes. Moreover, simply by adding an additional functional group to the cation or anion a huge number of feasible ions are possible [172]. In addition, physical and chemical properties of RTILs are also easily tuned by a selection of cation and anion [173]. Ionic liquids have attractive properties such as high viscosity, high densities, high intrinsic conductivities, high thermal stabilities, high polarities and good solvating properties [170]. These attractive properties, highly increase the use of RTILs in many technology area such as green synthesis, and catalysis

[174], biosensing [175-180], and energy conversion [180-185]. Therefore, RTILs offers huge and new possibilities to replace a conventional solvent in different areas.

In this chapter, investigations of catalytic formation of H_2O_2 are described in two similar RTILs and in organic solution and the different advantages in each case are identified.

7.1.1 Electrochemistry at the liquid|liquid interfaces

In 1902, Nernst and Reisenfeld study for the first time a charge transfer processes across interfaces between immiscible solutions by describing the transfer of potassium iodide between two aqueous phases separated by a phenol phase [186-188].

We consider two immiscible solvents, oil "o" and aqueous "w" containing the same ionic species "*i*", the difference between the potential of the bulk aqueous phase ϕ^{w} and the potential of the bulk oil phase ϕ^{o} is called the Galvani potential difference $\Delta_{o}^{w}\phi = \phi^{w} - \phi^{o}$.

The standard transfer Gibbs energy of a species from one phase (water) to another phase (organic) is by definition equal to the difference between the Gibbs energy of solvation, $\mu^{o,o}$ and the standard Gibbs energy of hydration, $\mu^{o,w}$ which is expressed by [189] :

$$\Delta G_{tr}^{o,w\to o} = \mu^{o,o} - \mu^{o,w} \tag{19}$$

In case of an ionic species *i*, after developing Eq. (19) at equilibrium, the equation can written as:

$$\mu_i^{0,w} + RTlna_i^{w} + z_i F\phi^{w} = \mu_i^{0,o} + RTlna_i^{o} + z_i F\phi^{o} \tag{20}$$

Where, z_i is the charge of the ion *i*, ϕ^{α} is the Galvani potential of the phase α and $\mu_i^{0,\alpha} + RTlna_i^{\alpha}$ is a chemical potential of *i* in phase α

Then $\Delta_{o}^{w}\phi = \phi^{w} - \phi^{o}$ can be written as [189, 190]:

$$\Delta_{\mathrm{o}}^{\mathrm{w}}\phi = \frac{\Delta G_{\mathrm{tr,i}}^{0,\mathrm{w}\to\mathrm{o}}}{z_i F} + RTln\left(\frac{a_i^{\mathrm{o}}}{a_i^{\mathrm{w}}}\right) \tag{21}$$

Where $\Delta G_{\mathrm{tr,i}}^{0,\mathrm{w}\to\mathrm{o}}$ is the standard molar Gibbs energy of ion transfer from phase "w" to phase "o" and $\frac{\Delta G_{\mathrm{tr,i}}^{0,\mathrm{w}\to\mathrm{o}}}{z_i F}$ represents the standard potential of transfer for *i*, so $\Delta_{\mathrm{o}}^{\mathrm{w}}\phi_i^0 = \frac{\Delta G_{\mathrm{tr,i}}^{0,\mathrm{w}\to\mathrm{o}}}{z_i F}$.

Therefore, the Nernst equation for ions transfer across an interface between two immiscible electrolyte solutions (ITIES) is:

$$\Delta_{\mathrm{o}}^{\mathrm{w}}\phi = \Delta_{\mathrm{o}}^{\mathrm{w}}\phi_i^0 + RTln\left(\frac{a_i^{\mathrm{o}}}{a_i^{\mathrm{w}}}\right) \tag{22}$$

Eq. (22) can be written using concentrations instead of a_{i}, then the standard ion transfer potential can be replaced by a formal ion transfer potential $\Delta_{\mathrm{o}}^{\mathrm{w}}\phi_i^{0'}$, which includes the ratio of the activity coefficient (γ):

$$\Delta_{\mathrm{o}}^{\mathrm{w}}\phi = \Delta_{\mathrm{o}}^{\mathrm{w}}\phi_i^{0'} + RTln\left(\frac{c_i^{\mathrm{o}}}{c_i^{\mathrm{w}}}\right) \tag{23}$$

with $\Delta_{\mathrm{o}}^{\mathrm{w}}\phi_i^{0'} = \Delta_{\mathrm{o}}^{\mathrm{w}}\phi_i^0 + RTln\left(\frac{\gamma_i^{\mathrm{o}}}{\gamma_i^{\mathrm{w}}}\right)$.

If we take the case of heterogeneous electron transfer between redox couples across the liquid|liquid interface, the reactions can be express as:

$$\mathrm{O}_1^{\mathrm{w}} + n_1 e^- \rightleftarrows \mathrm{R}_1^{\mathrm{w}} \tag{24}$$

$$\mathrm{R}_2^{\mathrm{o}} \rightleftarrows \mathrm{O}_2^{\mathrm{o}} + n_2 e^- \tag{25}$$

$$n_2\mathrm{O}_1^{\mathrm{w}} + n_1\mathrm{R}_2^{\mathrm{o}} \rightleftarrows n_2\mathrm{R}_1^{\mathrm{w}} + n_1\mathrm{O}_2^{\mathrm{o}} \tag{26}$$

At equilibrium, the electrochemical potentials of reactants and products are equal [191]:

$$n_2\mu^{w}_{O_1} + n_2\mu^{o}_{R_2} = n_2\mu^{w}_{R_1} + n_2\mu^{o}_{O_2} \tag{27}$$

With Eq. (27) can be derived and written as:

$$\Delta^{w}_{o}\phi = \Delta^{w}_{o}\phi^{0}_{et} + \frac{RT}{n_1 n_2 F} ln\left(\left(\frac{a^{w}_{R_1}}{a^{w}_{O_1}}\right)^{n_2}\left(\frac{a^{o}_{O_2}}{a^{o}_{R_2}}\right)^{n_2}\right) \tag{28}$$

With $\Delta^{w}_{o}\phi^{0}_{et} = \frac{n_2(\mu^{0,w}_{R_1} - \mu^{0,w}_{O_1}) + n_2(\mu^{0,o}_{O_2} - \mu^{0,o}_{R_2})}{n_1 n_2 F}$

This Nernst equation can be expressed in terms of concentrations:

$$\Delta^{w}_{o}\phi = \Delta^{w}_{o}\phi^{0'}_{et} + \frac{RT}{n_1 n_2 F} ln\left(\left(\frac{c^{w}_{R_1}}{c^{w}_{O_1}}\right)^{n_2}\left(\frac{c^{o}_{O_2}}{c^{o}_{R_2}}\right)^{n_2}\right) \tag{29}$$

Analogous to reactions at the metals or solid electrodes involving redox couples in a solution, the reactions between redox couple at the interface can be theoretically determined and the current from Galvani potential difference calculated.

7.1.2 Formation and detection of H_2O_2 in RTILs

H_2O_2 production is still a subject of much attention. However, its industrial production using quinone compounds is a source of many wastes and also very energy-consuming [165]. RTILs represent an encouraging alternative for the production of H_2O_2 by its simplicity and attractive possibility of a single-step process during the formation of H_2O_2 avoiding the generation of other ROS [165].

Here thermodynamic favorable redox reactions using a strong electron donor such as decamethylferrocene (DMFc, Fig. 35) and generation of H_2O_2 were investigated at different liquid|liquid interfaces. The reactions take place between O_2 in the acidic aqueous solution and DMFc in RTILs. The efficiency and the pathway of interfacial processes involving charged reactants depend on the Galvani potential difference across

the interface. The reactions were followed by the generation of H_2O_2 at the interface of the biphasic system as described by the following reactions.

$$2DMFc + O_2 + 2H^+ \rightarrow 2DMFc^+ + H_2O_2 \quad (30)$$

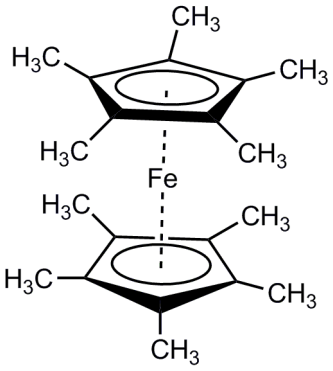

Figure 35: Chemical structure of DMFc.

In presence of an oxidant such as oxygen or protons, H_2O_2 or hydrogen can be produced by oxidation of DMFc in RTILs phase. The partition of fluorescent molecule can be observed during the in-situ detection (Fig. 36). The spatial and temporal generation of H_2O_2 were followed using in-situ fluorescence microscopy. A high-resolution camera was used for this purpose, which allows an appropriate background correction.

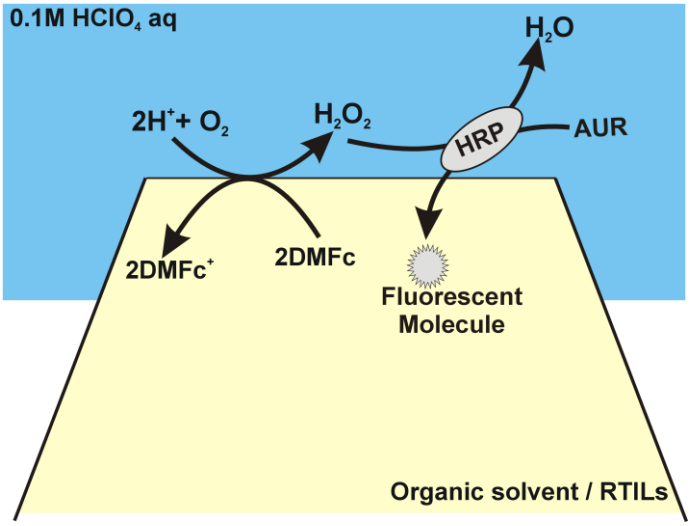

Figure 36: Principle of detection of H_2O_2 generated at the liquid|liquid interface.

Fluorescence detection of H_2O_2 in a biphasic system using two different RTILs was performed. 5 mM DMFc was dissolved in the hydrophibic RTILs (Fig. 37) such as C_4mimN(Tf)$_2$ (1-butyl-3-methylimidazoliumbis(trifluoro-methyl-sulfonyl)imide) or C_{10}mimN(Tf)$_2$ (1-decyl-3-methylimidazoliumbis(trifluoro-methyl-sulfonyl)imide) and brought in contact with aqueous perchloric acid.

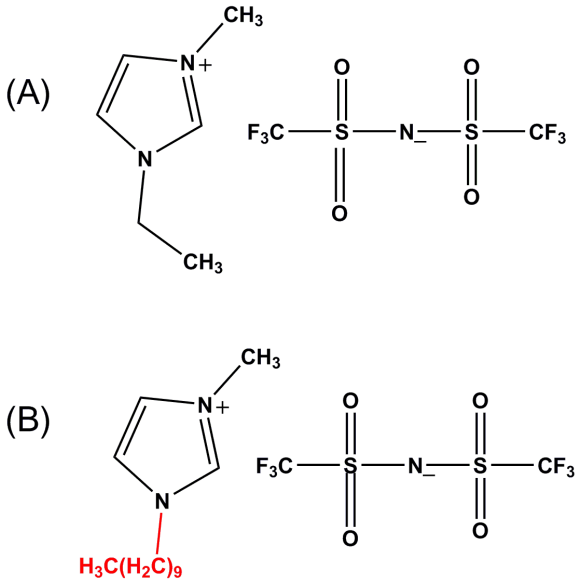

Figure 37: Chemical structure of (A) C_4mimN(Tf)$_2$ and (B) C_{10}mimN(Tf)$_2$.

These two RTILs differ by the number of carbon atoms in the side chain of the cations, which influence the viscosity of ionic liquid. The viscosity is an important property for many applications since high viscosity slows down the rate of diffusion-controlled chemical reactions. The viscosity of these ionic liquids is determined by van der Waals forces. Therefore, a high viscosity of $C_{10}mimN(Tf)_2$ can be observed compare to $C_4mimN(Tf)_2$ because the increasing of the length of the carbon chain on the imidazolium cation also increases van der Waals interactions.

The redox reaction at the interface involves an electron transfer and an ion transfer (reaction (31)).

$$DMFc_{(RTIL)} + C_4mim^+_{(RTIL)} + N(Tf)_2^-{}_{(RTIL)} \rightleftharpoons DMFc^+_{(RTIL)} + e^- + C_4mim^+_{(aq)} + N(Tf)_2^-{}_{(RTIL)} \quad (31)$$

It was shown that the peak potential of the couple $DMFc/DMFc^+$ is independent of the different anions present in the aqueous phase. This indicates the transfer of a cation across the RTIL|water interface to maintain the electroneutrality. This ions transfer can lead to significant changes in composition of both phases in the long term and would result in liquid interface instabilities. The generation of H_2O_2 is observed only in the presence of DMFc. If HRP and Amplex Ultra Red (AUR) are present, the fluorescence emission of the resofurin derivative formed by AUR and H_2O_2 increases with time (Fig. 38). Most of the light was emitted close to the pipette orifice in the RTIL phase. This does not mean that there are no fluorescent molecule in the aqueous phase. In fact, rescaling intensity and background reveals how fluorescent molecules diffuse into the RTIL phase. A reason for the low fluorescence intensity in the aqueous phase could be the protonation of the fluorescent molecules, which decreases their fluorescent yield. Futhermore, the fluorescent molecules may be extracted to the organic phase.

Compared to C_{10}mimN$(Tf)_2$ (Fig. 38B), the size of the fluorescence zone was found to be large in the case of C_4mimN$(Tf)_2$ which possess a lower viscosity. This causes a faster diffusion of the fluorescent molecule (Fig. 38A). Both, the fluorescence intensity and expansion rate of the fluorescent zone towards the pipette bulk was larger for C_4mimN$(Tf)_2$ than that for more viscous C_{10}mimN$(Tf)_2$.

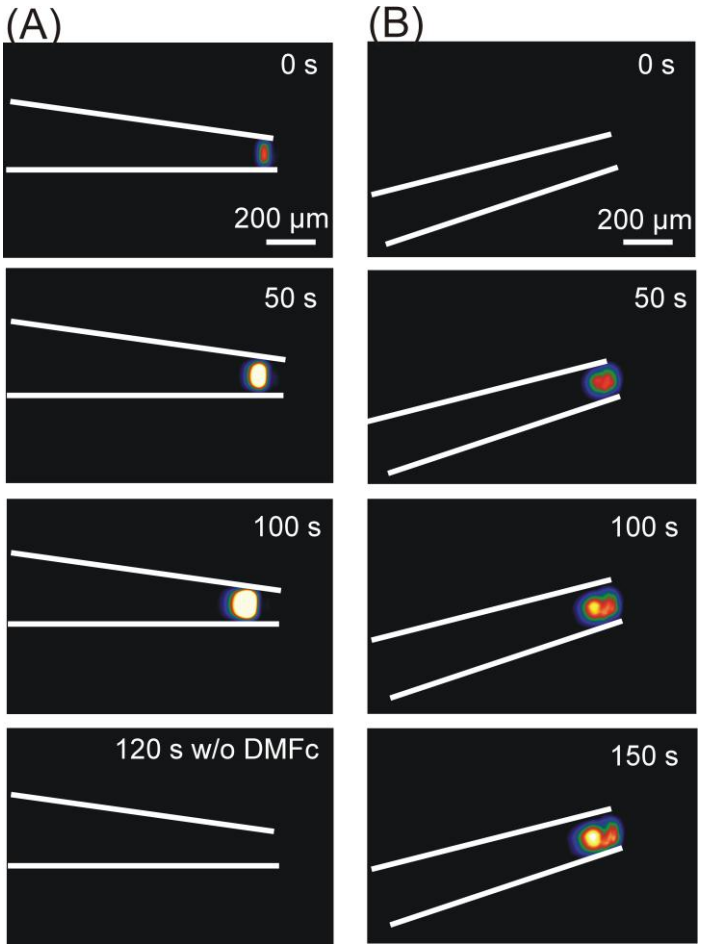

Figure 38: Fluorescence detection of H_2O_2 generated at the interface between 5 mM DMFc in (A) C_4mimN$(Tf)_2$ or (B) C_{10}mimN$(Tf)_2$ and oxygen in 0.1 M aqueous $HClO_4$ containing 0.1 mg ml^{-1} HRP and 30 µM AUR.

7.1.3 Formation and detection of H_2O_2 in organic solvent

H_2O_2 can also be formed during ORR at TFT|H_2O interface. In TFT, the molecules are electrically neutral. There is no ion transfer as in the case of ionic liquid. Here the ionic liquid was replaced by the TFT solvent and contained the same strong electron donor DMFc. Again, a strong fluorescence was observed at the end of capillary few seconds after the pipette was immersed into the aqueous phase (Fig. 39) indicating the H_2O_2 formation. In absence of DMFc, fluorescence was not observed. As previously described, the fluorescence was observed only in the organic phase at the tip of the capillary. Deliberately added H_2O_2 caused fluorescence only in the organic phase. It proofed that the fluorescence is emitted by the deprotonated form of the dye only. This form is not likely to exist in the strongly acidic aqueous phase and can emit only after transfer to the organic phase. To maintain the electroneutrality of the organic phase the anion ClO_4^- crosses the liquid|liquid interface as describe by the following equation:

$$2DMFc_{(o)} + 2H^+_{(w)} + 2ClO_4^-{}_{(w)} + O_{2(o)} \rightarrow 2DMFc^+_{(o)} + H_2O_{2(w)} + 2ClO_4^-{}_{(o)} \quad (32)$$

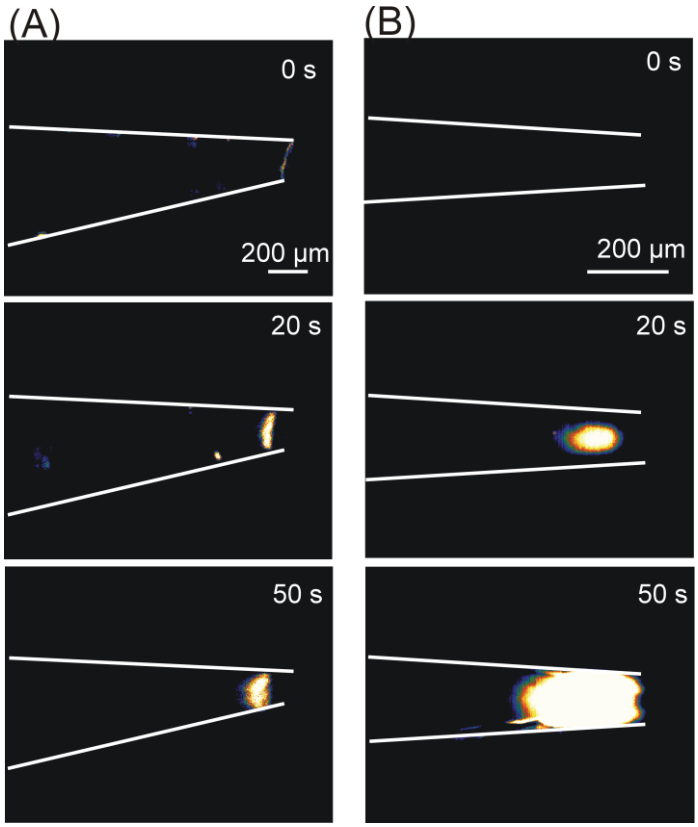

Figure 39: Fluorescence detection of H_2O_2 generated at the interface between 5 mM DMFc in TFT and oxygen in 0.1 M aqueous $HClO_4$ containing 0.1 mg ml^{-1} HRP and 30 µM AUR (A) in-situ generation of H_2O_2 and (B) deliberate addition of H_2O_2 into aqueous phase.

7.2 Detection of superoxide in lithium-oxygen batteries

The storage of energy is one of a big challenge of this and the next century [166, 192]. There is a broad investigation and development to improve the storage capacity [166, 192]. Lithium is the lightest metal element. Electrodes produced from it could produce a theoretical energy density of 11680 Wh kg^{-1}. This is close to gasoline [193]. Therefore, interest is increasing to use it in lithium-air batteries. The Li-oxygen batteries is an attractive technology which involve the chemistry of multiphase processes (solid, gas and liquid) and were proposed as early as in 1970s for automobiles. Currently, it

receives an increasing attention [194-197]. They are four types of lithium-oxygen batteries based on the types of electrolytes. It involves a lithium metal anode and a porous oxygen diffusion cathode. A lithium salt is dissolved in either aprotic (non-aqueous), aqueous, hybrid (aqueous and aprotic) or solid-state electrolyte [198]. The lithium-oxygen battery with organic electrolytes could be a future main technology for energy storage. One challenge are the side reactions, which take place during discharge and charging processes at the oxygen electrode of this battery [166, 192]. ROS are produced during the side reaction. The exact nature and quantity depends on the electrolytes used. It was claimed that during the charging process in a lithium-air battery, $O_2^{\bullet-}$ is released during oxidation of Li_2O_2 [199, 200].

Here, we prove that also during discharging process $O_2^{\bullet-}$ is released as intermediate [166]. The overall reactions of discharging can be described as follows.

$$2Li \rightleftharpoons 2Li^+ + 2e^- \quad (33)$$

$$O_2 + 2e^- + 2Li^+ \rightleftharpoons Li_2O_2 \quad (34)$$

The ORR is performed on gas-diffusion electrode (GDE) in DMSO and the electrogeneration of $O_2^{\bullet-}$ is observed using the 4-Chloro-7-nitrobenzo-2-oxa-1,3-diazole (NBD-Cl) dye as illustrated below (Fig. 40). A mechanism reaction of NBD-Cl will be described in chapter 7.3.

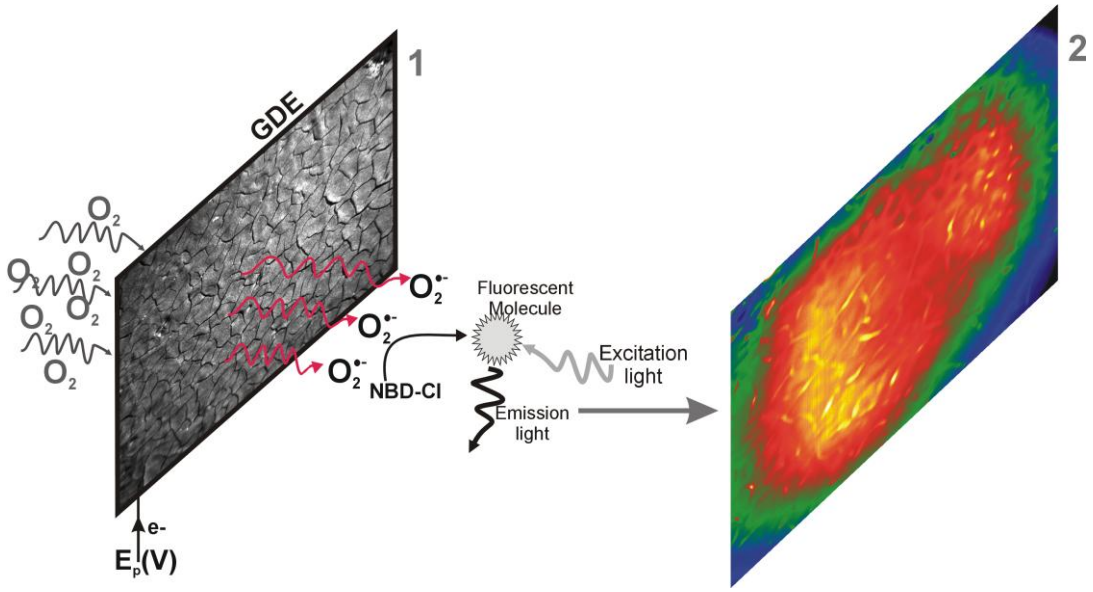

Figure 40: Selective detection of $O_2^{\bullet-}$ in oxygen saturated solution (1 M $LiClO_4$, 0.5 mM NBD-Cl in DMSO) during ORR on GDE.

The detection was performed in combination with a chronoamperometric pulse program applied to the GDE and the spatial and temporally resolved detection of fluorescence using the CMOS camera described in section 5.2.3. A background correction was applied to eliminate the background fluorescence from the GDE. In order to remove this contribution, the GDE was biased at E_{GDE} = 0 V for 60 s, where no ORR current can be detected. The image taken at t = 60 s was used as reliable background and was subtracted from all subsequent recordings taken at more negative potentials. During the ORR reaction at E_{GDE} = -0.7 V for 60 s, the production of $O_2^{\bullet-}$ was evident from the increasing fluorescence intensity recorded between t = 4 s and 40 s. A control measurement proved that no fluorescent product was formed at E_{GDE} = -0.7 V in oxygen-free solution and the absence of a reduction of dye precursor and the GDE system. During drying, the slurry of the active carbon materials form cracks as commonly see in GDE processed according to similar protocols [166]. At E_{GDE} = -0.7 V, the highest

fluorescence intensity is observed in the cracks after 4 s reaction time (Fig. 41). Afterward, the intensity decreases with the time due to the diffusion of the fluorescent molecules into the solution bulk. The high fluorescence intensity in the cracks can be explained by many factors. Firstly, the solution layer probed by the fluorescence measurement is thicker in the cracks compared to the optically opaque mesoporous carbon material of the GDE. Secondly, oxygen transport may be a limiting factor for the solution-filled pores that leads to higher production of $O_2^{\bullet-}$ in the regions of the GDE facing the outer solution volume. Finally, the $O_2^{\bullet-}$ formed in the inner of the pore volume may consume all the NBD-Cl without contributing to measured intensities due to the opaque nature of the carbon GDE. The formation of $O_2^{\bullet-}$ during discharge is in accordance with the recent results reported by Bruce and co-workers, where they used a spectroscopic method to directly identify the reaction products and intermediates. The following mechanism was proposed [201]:

$$O_2 + e^- \rightarrow O_2^{\bullet-} \quad (35)$$

$$O_2^{\bullet-} + Li^+ \rightarrow LiO_2 \quad (36)$$

$$2LiO_2 \rightarrow Li_2O_2 + O_2 \quad (37)$$

The oxygen firstly reduced to $O_2^{\bullet-}$ and reacts then with Li^+ to form the instable product LiO_2 which disproportionates to give a stable product Li_2O_2.

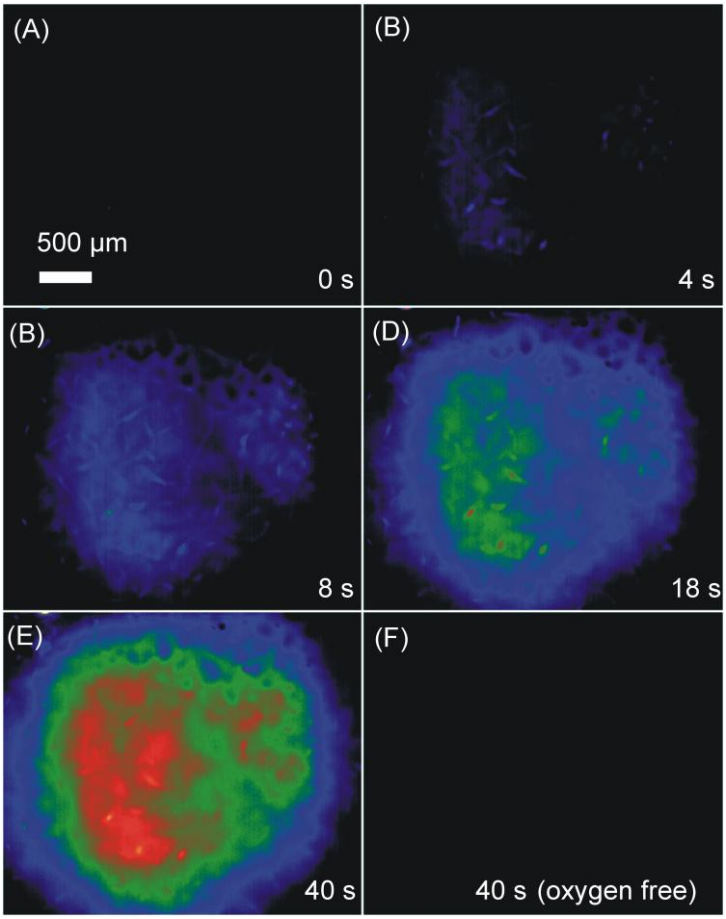

Figure 41: In-situ fluorescence detection of $O_2^{\bullet-}$ generated at GDE

7.3 Generation and Detection of ROS in cell culture media

Formation of ROS using quinone compounds during ORR or a catalyzed chemical reaction between quinone and oxygen is well know and intensively documented [126]. The quinone is widely known as a source of H_2O_2 [39, 41]. Typically quinones act as catalysts for ORR producing H_2O_2 and for some quinones $O_2^{\bullet-}$ in neutral or basic media [28, 126, 167]. In neutral solution, some quinones such as naphtoquinone produces $O_2^{\bullet-}$ and this species could be consider as the first step of the reactions. The electrochemical behaviour of quinones in buffered aqueous solutions is complex and can be explain by the scheme 7:

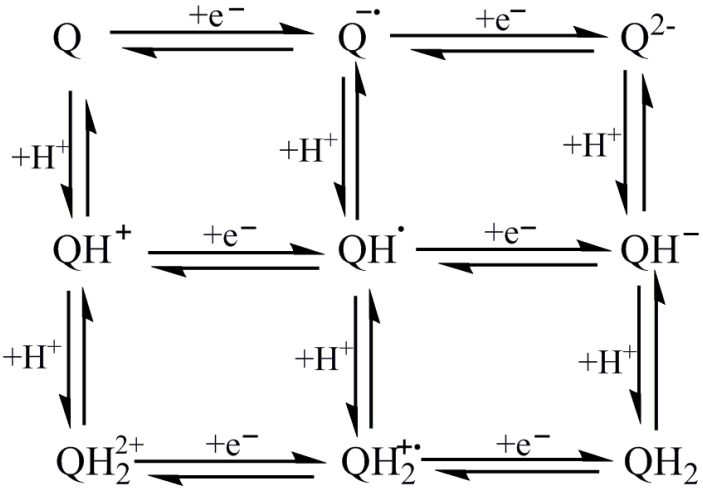

Scheme 7: Square scheme of electrochemical behavior of quinone (Q) and hydroquinone (QH_2) in buffered aqueous solutions [150, 202].

The dianion state should require extreme pH conditions. Other species plays a more important role, depending on the pH and electrode material.

Formation of ROS and particularly H_2O_2 using quinone-modified electrode has been widely investigated using rotating disc electrode (RDE) or rotating ring disc electrode (RRDE) measurement. Recently, Newton et al. [159], described a technique using a chemical probe or scavenger of ROS such as ascorbic acid where the formation of ROS was monitored by a decrease of voltammetric peak for ascorbic acid. Here we use fluorescence microscopy for in-situ detection using selective and sensitive dyes during ORR (Fig. 42).

The generation of $O_2^{\bullet-}$ has been monitored using NBD-Cl. H_2O_2 was observed with AUR. Detection of $O_2^{\bullet-}$ poses many questions concerning the sensitivity and very importantly by the selectivity of the dye used. In certain cases dyes as NBD-Cl can be used to detect $O_2^{\bullet-}$. This dyes has been tested intensively for the detection of thiols, primary and secondary amines [203]. However, recently NBD-Cl is also an efficiency dye

for the detection of $O_2^{\bullet-}$, if the measurement is performed in solutions free of thiols or amine [53, 56, 203]. The large rate constant for the reaction between NBD-Cl and $O_2^{\bullet-}$ (2×10^5 M^{-1} s^{-1}) suggest that NBD-Cl can rapidly react without significant interference from other competitive reactions such as disproportionation reaction of $O_2^{\bullet-}$ which possess a rate constant of 2.3×10^5 M^{-1} s^{-1} in neutral pH solution [91, 93, 203]. Reaction between NBD-Cl and nucleophile yields Meisenheimer adduct (Scheme 8) [56]. A stable Meisenheimer complex adduct is a product of reaction between arene carrying an electron withdrawing groups and a nucleophile [204, 205]. These adducts could possess fluorescence properties [83, 206, 207].

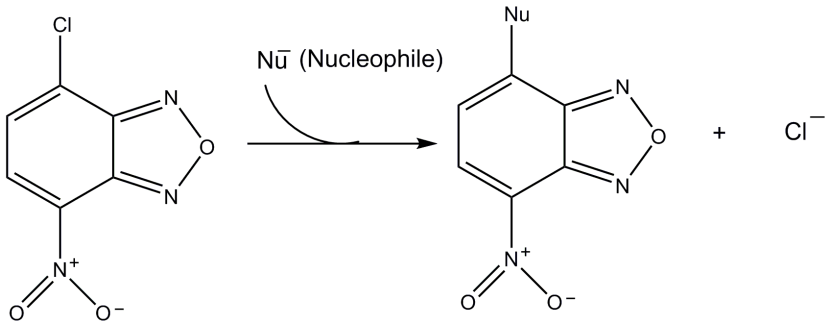

Scheme 8: Proposed reaction mechanism between NBD-Cl and nucleophile.

Assuming that the prominent quinone species formed in the first step are semiquinone radicals the following reactions can take place [167].

superoxide formation: $O_2 + Q^{\bullet-} \rightarrow O_2^{\bullet-} + Q$ (38)

The $O_2^{\bullet-}$ enters different parallel reaction.

$$O_2^{\bullet-} + O_2^{\bullet-} + 2\ H_2O \rightarrow O_2 + H_2O_2 + 2\ OH^- \quad (39)$$

$$O_2^{\bullet-} + R \rightarrow O_2\text{-}R^{\bullet-} \quad (40)$$

$$O_2^{\bullet-} + \text{NBD-Cl} \rightarrow O_2\text{-NBD-Cl} \quad (41)$$

The relative weight of the reaction channels depends on the $O_2^{\bullet-}$concentration and the concentration and efficiency of the different compounds R which contributes to the scavenging of $O_2^{\bullet-}$. The disproportionation reaction (39) is second order with respect to $O_2^{\bullet-}$. The reaction with the constituents of the buffer is represented by reaction (40). In the serum-containing culture media, this reaction may reduce the initial amount of detectable $O_2^{\bullet-}$. Reaction (41) illustrates the reaction with superoxide selective dye and acts in this system as a particular efficient scavenger. As previously described a suitable background correction was made and the $O_2^{\bullet-}$ formation is switched on by a controllable trigger i.e the CA of ORR. Concerning the detection of H_2O_2 generated by polyPLG/PLG/GC which is known, the auto-fluorescence intensity of AUR was eliminated by background correction during CV. The remaining signal is related to the formation H_2O_2 during ORR or chemical follow-up reactions such as disproportionation of $O_2^{\bullet-}$.

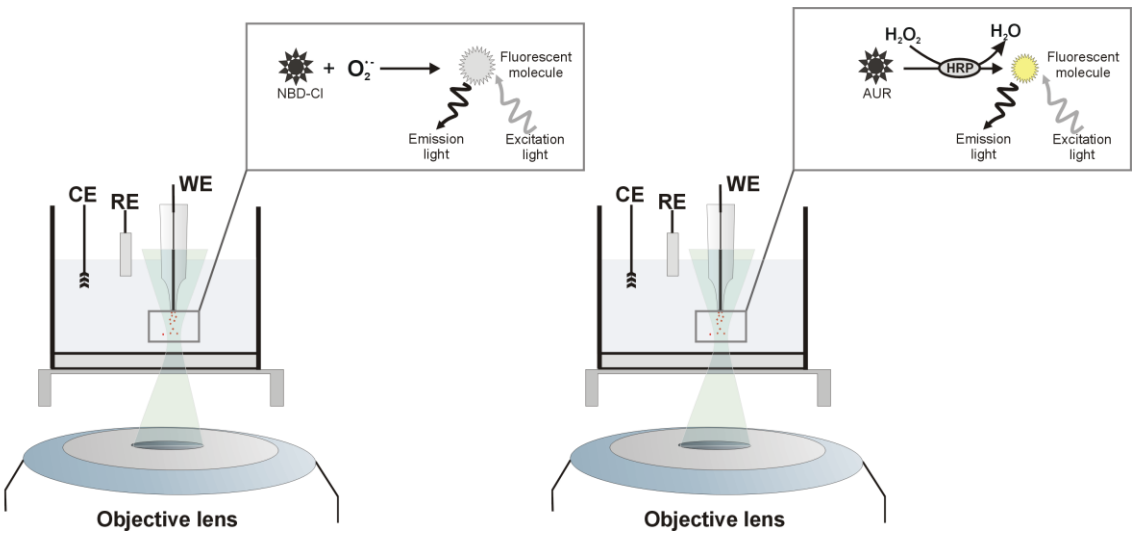

Figure 42: In-situ detection of ROS generated by polyPLG/PLG/GC using fluorescence microscopy.

During detection of $O_2^{\bullet-}$, the interaction between the AUR dye and poly/PLG/PLG/GC was investigated. We found that there is no chemical interaction as shown in Fig. 43A. The CVs obtained in presence and absence of AUR in oxygen-free solution are similar. A chronoamperogram with two potential pulses 0 V and -0.8 V were performed for a precise investigation. A clear difference of the electrochemical signal is seen during experiment in oxygen-free buffer or aerated buffer (Fig. 43B).

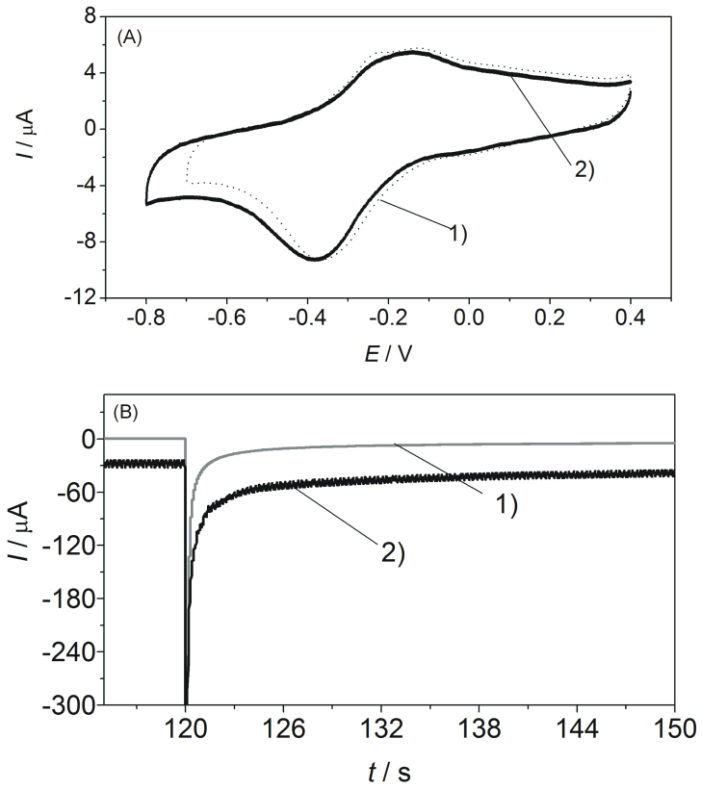

Figure 43: (A) CVs (2nd cycle, v = 0.05 Vs^{-1}) of poly/PLG/PLG/GC (3 mm diameter) (1) in oxygen-free 0.1 M phosphate buffer pH 7 and (2) after addition of AUR; (B) CA during of polyPLG/PLG/GC (3 mm diameter) in phosphate buffer pH 7; (1) oxygen-free and (2) aerated.

The electrogeneration in the cell culture environment was performed using a polyPLG/PLG/GC electrode. The generation was investigated firstly in phosphate buffer solution pH 7.4. During the detection of H_2O_2 with the CMOS camera, a background correction was set and used to remove the auto-fluorescence of AUR. The remaining signal in Fig. 44 is related to H_2O_2 generation during the ORR or to H_2O_2 formation during chemical follow-up reactions such as disproportionation of $O_2^{\bullet-}$. It is clearly observed that the formation rate of H_2O_2 shows strong variations over the electrode surface (Fig. 44b to f). The reason for this variation is not clear, but could be related to the heterogeneous distribution of active quinone moieties in the film. The H_2O_2 can be the product of the disproportionation reactions of $O_2^{\bullet-}$ (reaction (39)) or may be due to the $2e^-$, $2H^+$ mechanism as observed generally with quinone catalysts. As the fluorescent resorufin derivative is accumulating during the CV, the overall intensity is increasing within the sequence.

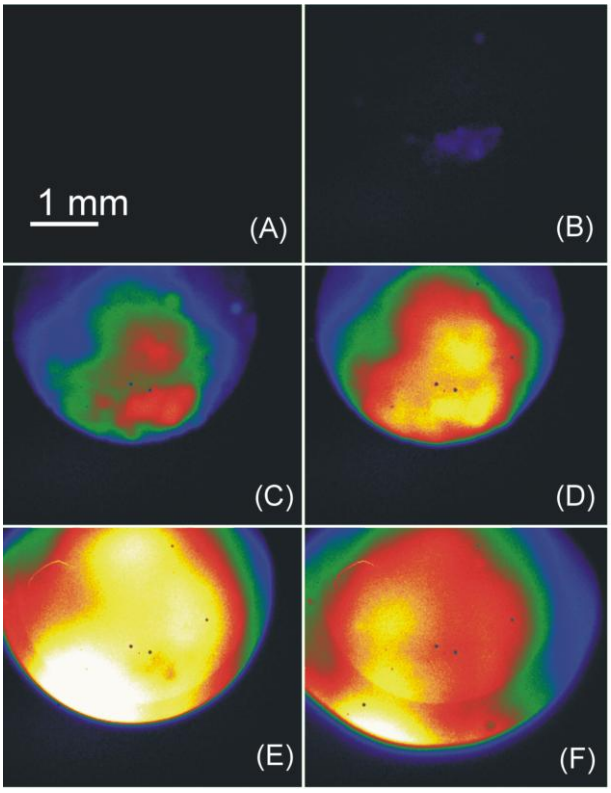

Figure 44: Time series of selected images of H_2O_2 detection during a CV on polyPLG/PLG/GC (3 mm diameter) in aerated solution, v = 0.05 V s^{-1} in 0.1 M phosphate buffer pH 7 containing 10 µM AUR and 0.1 mg mL^{-1} HRP, image (a) is a control experiment in oxygen free buffer.

A time resolved investigation during detection of $O_2^{\bullet-}$ was performed (Fig. 45). The background correction was made using images recorded at a potential of 0 V in oxygen-free solution containing NBD-Cl. The images at -0.8 V after background subtraction show the generation of $O_2^{\bullet-}$. The NBD-Cl-$O_2^{\bullet-}$ adduct accumulates as the reaction progresses because the formed adduct is stable. Therefore momentary concentration of $O_2^{\bullet-}$ cannot be derived because the adduct forms before $O_2^{\bullet-}$ can enter into other decomposition pathways. Nevertheless, the fluorescence image recorded here

proves the chemical identity of the ROS as $O_2^{\bullet-}$. The presence of $O_2^{\bullet-}$ point out the formation of semiquinone radical of PLG. This promotes the production of $O_2^{\bullet-}$.

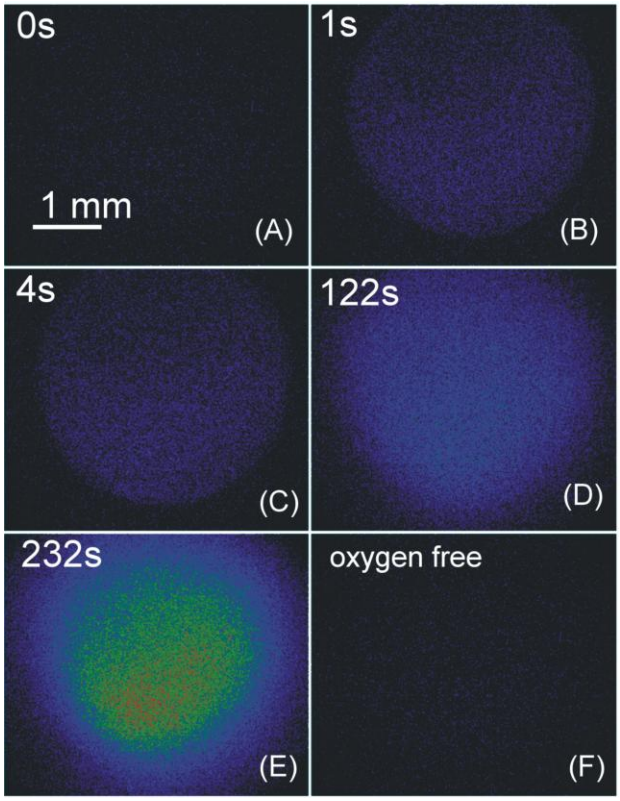

Figure 45: Time series of selected images of $O_2^{\bullet-}$ detection during a CA at polyPLG/PLG/GC (3 mm diameter) using NBD-Cl in aerated 0.1 M phosphate buffer solution pH 7 containing 0.5 mM NBD-Cl.

8 Local generation and selective detection of ROS in biological system using electrochemical technique

In this chapter a selective detection of $O_2^{\bullet-}$ generated by polyPLG/PLG/GC ME and the exposure of biological cells to a local flux of ROS are described. The detection of local generation $O_2^{\bullet-}$ was performed with a biosensor based on cyt c. I made the preparation of biosensor after instruction and advices received from Prof. Dr. Wollenberger. Janina Leyk (PhD student in Christine Richter-Landsberg group, University of Oldenburg) and me performed the local oxidative stress using retinal cells. The cells were prepared and cultured by Janina Leyk and I conducted the oxidative stress investigation. This project led to the joint publication [167].

8.1 Electrochemical detection using biosensor based on cytochrome c

Here we described the electrochemical detection of local formation of $O_2^{\bullet-}$, which is a controversial topic. There are open questions about its significance in biological systems. For instance, it is unclear how it can be transported despite its short lifetime in aqueous solution [91, 102]? How $O_2^{\bullet-}$ can be efficiency electroanalyzed in the aim to obtain an absolute value of the $O_2^{\bullet-}$ flux [91]?

The distance of diffusion of $O_2^{\bullet-}$ from its source is subject of many discussion and depends clearly on the chemical environment or microenvironment in which the $O_2^{\bullet-}$ diffuses [91]. The lifetime of $O_2^{\bullet-}$ depending of the composition of the solutions [48, 208-211]. In biological systems or solution with physiological pH (pH 7.4) diffusion distances between 45 nm to 1 mm were reported with a variable half-life time [48, 208-211]. Dismutation is one of the main reactions determining the lifetime of $O_2^{\bullet-}$ [16].

Dismutation of $O_2^{\bullet-}$ is very slow in alkaline pH (0.3 M^{-1} s^{-1}) and reaches a maximum at pH 4.8 (10^8 M^{-1} s^{-1}) [16]. Therefore, the lifetime is longer than in acidic pH. In fact in alkaline pH $O_2^{\bullet-}$ is mainly deprotonated [16]. Furthermore, low concentration of $O_2^{\bullet-}$ increase the lifetime of superoxide by affecting the dismuations reactions rate which is second order [16]. In water, lifetimes of 0.005 s and 14 h were reported for the concentrations of 0.1 mM and 0.1 nM respectively. Therefore, lower formation rates of $O_2^{\bullet-}$ yield long lifetime. In seewater, half-life times of 10-100 s were evaluated for 87-1120 pM of $O_2^{\bullet-}$ [16]. Thus, regarding wide span of reported half-life times it is not ruled out that $O_2^{\bullet-}$ can diffuse even over mm distances.

A cyt c-based electrochemical sensor was used to detect $O_2^{\bullet-}$. Its selective detection with $O_2^{\bullet-}$ is widely reported [91, 93, 130]. Cyt c is immobilized on a modified gold electrode as described in the chapter 5.5. Additionally to the sensitivity which the sensor offers based on cyt c, a selected potential value can be applied and a selective detection of either of $O_2^{\bullet-}$ or H_2O_2 can be performed. In this manner, the oxidized or reduced form of cyt c can be regenerated on the electrode after reaction with the target species (Fig. 7 A1) [130].

The preparation of polyPLG/PLG/GC ME was made as described in the chapter 5.3 and the preservation of the quinone on modified GC ME was proven using CV in oxygen-free phosphate buffer (Fig. 46). The polyPLG/PLG/GC ME was used further to generate $O_2^{\bullet-}$ locally.

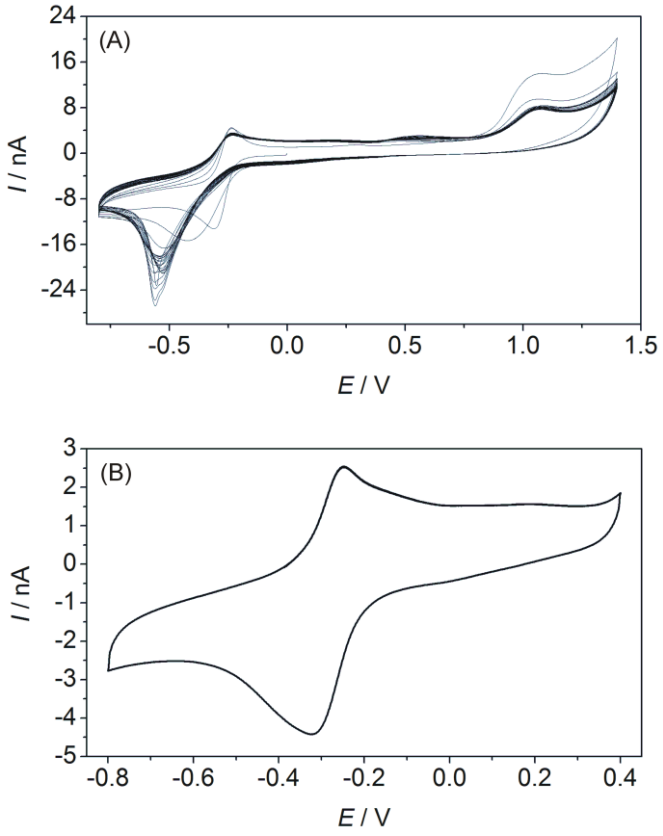

Figure 46: CV of (A) electropolymerization of PLG during 25 cycles on GC ME (90 µm diameter) and (B) polyPLG/PLG/GC ME (90 µm diameter) in oxygen-free 0.1 M phosphate buffer pH 7, v = 0.05 Vs^{-1} vs. Ag/AgCl/3 M NaCl.

A non-conventional procedure was used to place the poly/PLG/PLG/GC ME relatively close to the biosensor with acceptable accuracy. Initially the poly/PLG/PLG/GC ME was placed above the insulating sheath of the biosensor and approached under the control of an optical microscope until they just touched (Fig. 47). Then the poly/PLG/PLG/GC ME was retracted by 4 mm. PBS pH 7.4 was filled into the electrochemical cell and the approach was repeated. After touching of the insulating sheath, the poly/PLG/PLG/GC ME was retracted by 3 mm and moved laterally over the sensing area of the biosensor. This position is taken as provisional zero distance. The

ME is then moved to the desired distance. $O_2^{\bullet-}$ was formed by a poly/PLG/PLG/GC ME from which it diffused to the biosensor positioned ca. 10 µm away and operated at E_{sens} = +0.13 V for detection of $O_2^{\bullet-}$. Afterwards, the solution was exchanged against a 10 mM ferrocenemethanol solution. The ME was moved over the insulating sheath and an approach curve was recorded. The clearly identifiable point of mechanical contact is then taken as zero distance (Fig. 48).

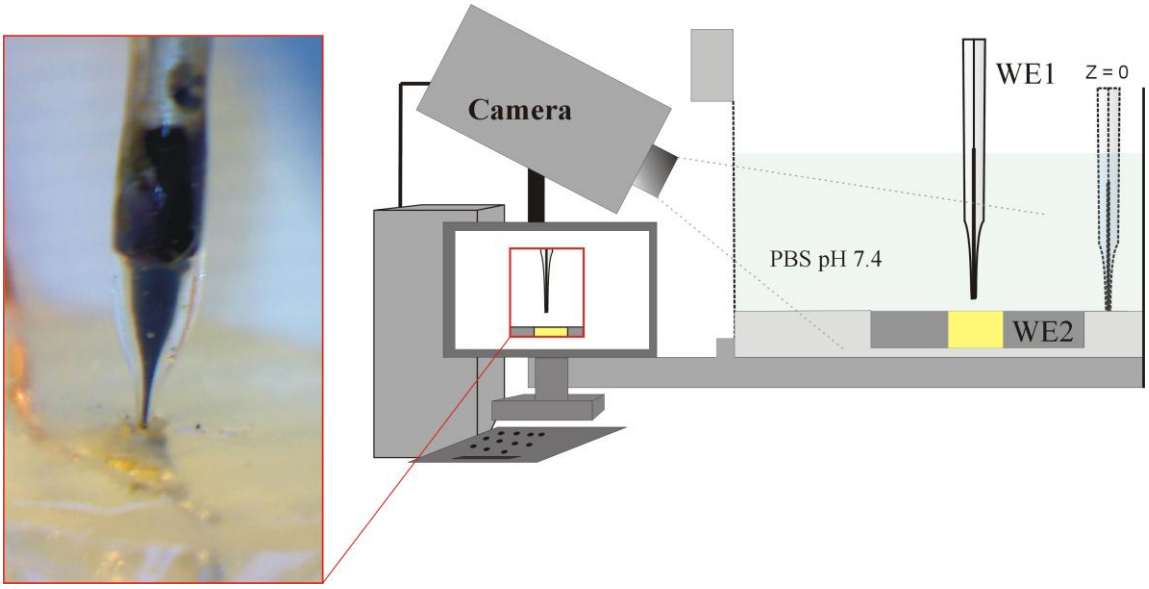

Figure 47: Positioning of modified-ME using camera-assisted SECM setup.

The electrochemical detection of $O_2^{\bullet-}$using the biosensor based on cyt c has been widely reported [93, 130, 212, 213]. The detection is performed as illustrated in the Fig. 49 in generation-collection mode (tip generation/substract collection). Horrock and co-workers described such investigation where a small generator electrode is used to produce a specified time-dependence flux of $O_2^{\bullet-}$, and the collector or detector is a large electrode [213]. It was observed that the electron transfer between cyt c and the gold electrode becomes rate-limiting at high concentration of $O_2^{\bullet-}$ [213], in other words the

quantity of cyt c loaded on gold modified with a SAM could be not enough to react with all $O_2^{\bullet-}$ present and cannot competes with the disproportionation reaction. Therefore, a large surface of collector was a typical approach in most of the experiments [213].

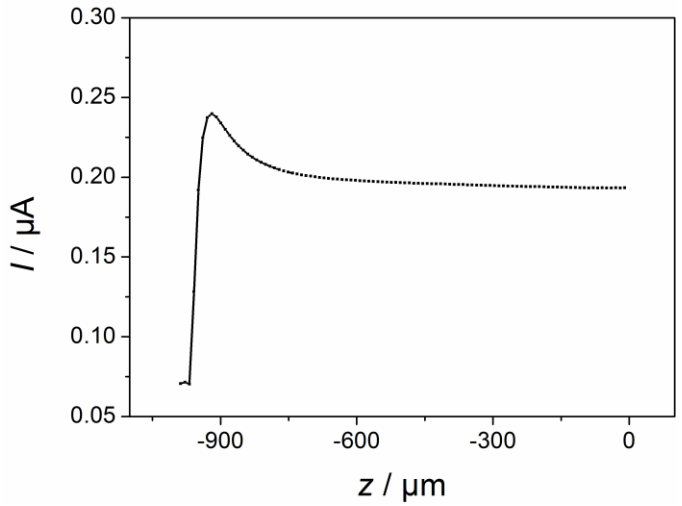

Figure 48: Approach curve recorded after the detection of $O_2^{\bullet-}$ using a polyPLG/PLG/GC ME (90µm) in 10 mM FcMeOH, E_T = + 0.46 V, v_T = 5 µm s^{-1}.

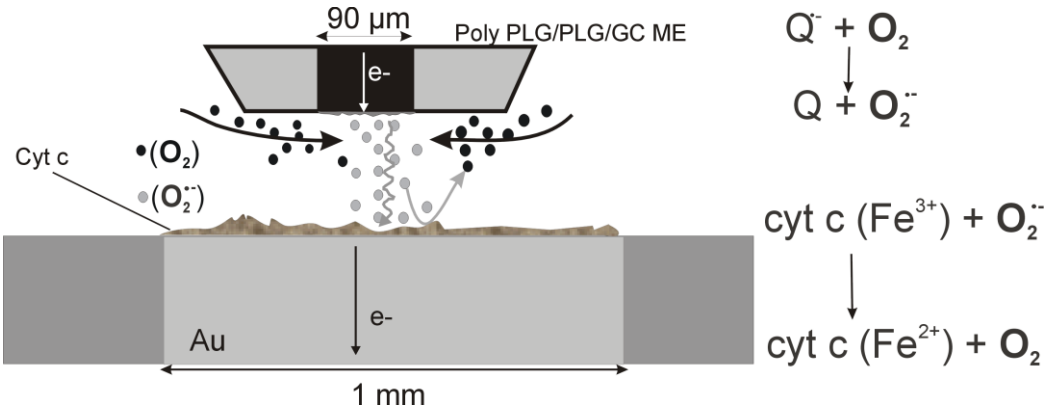

Figure 49: Detection of $O_2^{\bullet-}$ and regeneration of O_2 on a biosensor based on cyt c.

The distance between the modified ME and the biosensor was varied and at each distance a CA was executed at polyPLG/PLG/GC ME while the biosensor was held at a

constant potential value of +0.13 V suitable for detection of $O_2^{\bullet-}$. The particularity of this approach with two modified electrodes is the investigation of diffusion and detection of local $O_2^{\bullet-}$ concentrations. The CV of the biosensor showed a clearly discernible redox conversion of cyt c (Fe^{3+}/Fe^{2+}) at 0 V (Fig. 16). The current biosensor systems are, however, limited by the amount of cyt c immobilized on the surface of the electrode [212]. An investigation of modified electrodes by monolayer has clearly shown that the sensitivity of the sensor is directly proportional to the surface density of cyt c on the electrode [212]. Therefore, loading more cyt. c on the modified electrode surface could promote a significant improvement in sensitivity [212].

The polyPLG/PLG/GC ME was positioned at a distance of around 10 µm to the biosensor and two potentials were applied to the polyPLG/PLG/GC ME. At E_{gen} = 0 V no $O_2^{\bullet-}$ is formed. For E_{gen} = -0.8 V $O_2^{\bullet-}$ is formed, the transient current was recorded on a biosensor biased to E_{sens} = +0.13 V. The steady-state current observed for t > 20 s (Fig. 51 (1)) results from the competition between continuous formation of $O_2^{\bullet-}$ at the polyPLG/PLG/GC ME generator electrode and the spontaneous dismutation of $O_2^{\bullet-}$ in solution during which oxygen is regenerated. The detection was also performed at different d (Fig. 50). The steady-state current at d_1 = 5 µm reveals a higher current than at the d_1 = 10 µm. This reflects the transient concentration of $O_2^{\bullet-}$ and proves the decreasing concentration due to follow-up reactions during the diffusion from the generator to the biosensor.

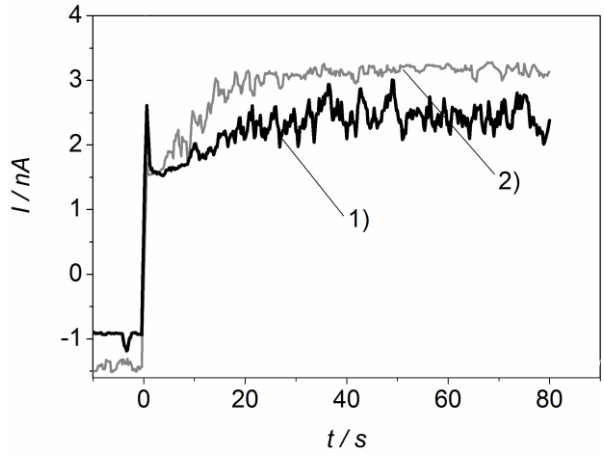

Figure 50: Chronoamperometric response at the biosensor (E_{sens}=+0.13 V) at a distance of (1) 10 µm and (2) 5 µm to the PLG polymer-modified GC ME of 90 mm diameter.

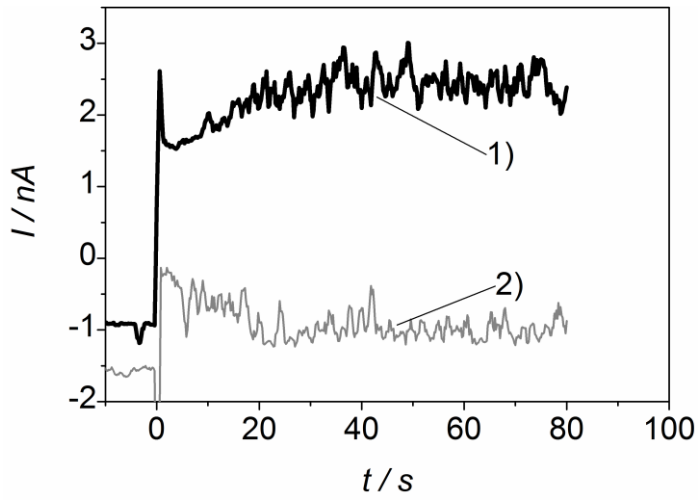

Figure 51: Chronoamperometric response of biosensor (E_{sens} = +0.13 V) (1) at the distance 10 µm in phosphate buffer pH 7.5 and (2) in presence of SOD.

A control measurement was carried out in a solution containing 0.1 mg/ml SOD in order to accelerate the disproportionation reaction of $O_2^{\bullet -}$. In this situation $O_2^{\bullet -}$ is removed from the solution faster than its diffusional transport from the generator to the biosensor. Therefore no oxidation currents are recorded at the biosensor, although $O_2^{\bullet -}$ is

still formed at the generator (Fig. 51 (2)). In fact, the reaction rate of disproportionation catalyzed reaction (Eq. (42); 6.4×10^9 M^{-1} s^{-1}) is much higher than the reaction between cyt c and $O_2^{\bullet-}$ (Eq. (43); 2.6×10^5 M^{-1} s^{-1}). Therefore, there is only H_2O_2 at the position of the biosensor [16, 93].

$$O_2^{\bullet-} + O_2^{\bullet-} + 2H^+ \xrightarrow{SOD} O_2 + H_2O_2 \quad (42)$$

$$O_2^{\bullet-} + \text{cyt c } (Fe^{3+}) \rightarrow O_2 + \text{cyt c } (Fe^{2+}) \quad (43)$$

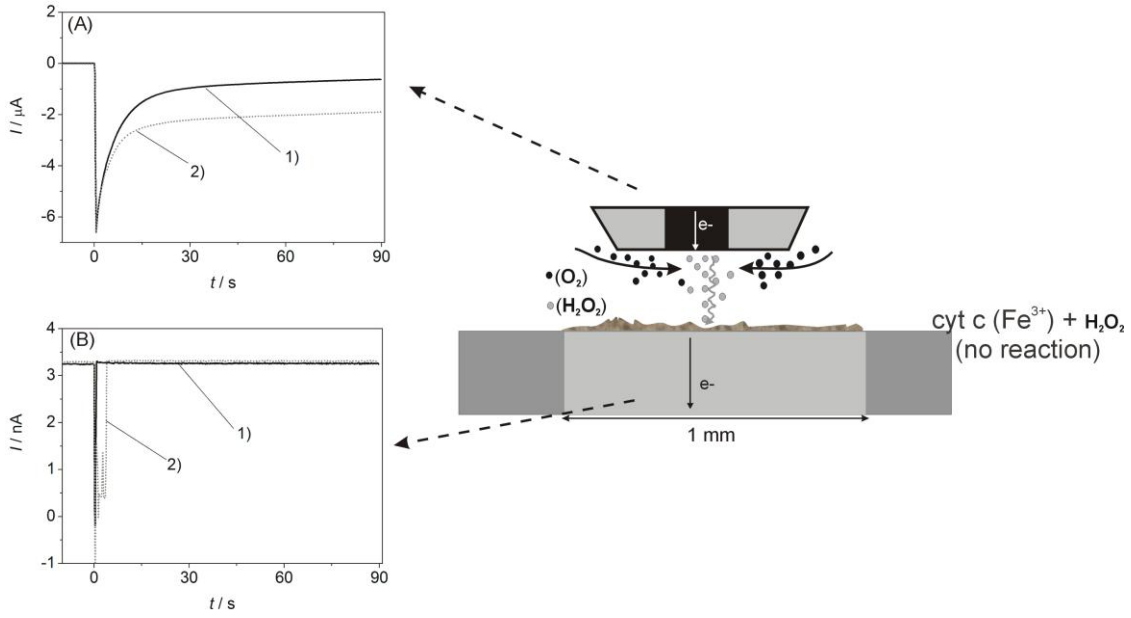

Figure 52: Chronoamperometric response of (A) a bare GC ME (250 µm diameter, E_{gen} = -0.8 V) at (1) 10 µm and (2) 1 mm distance to the biosensor. (B) Response of the biosensor (E_{sens} = +0.13 V) at (1) 10 µm and (2) 1 mm distance to the generator in 0.1 M aerated phosphate buffer pH 7.5.

In a second control measurement, a bare GC ME was used as generator positioned at the distance d = 10 µm and 1 mm from the biosensor. Except for capacitive coupling, there was no current when switching the potential of the generator to ORR.

The absence of any $O_2^{\bullet-}$ signal at the biosensor (Fig. 52B) proves the critical role of PLG polymer for the formation of $O_2^{\bullet-}$. On other hand, the transient generator currents can be compared for two different distances of 10 µm and 1 mm. The generator current is higher at d = 1 mm than at d = 10 µm. This reflects the hindered mass transport of O_2 to the bare GC. During each experiment, the CV of the biosensor was recorded after the generation-collection experiments, then compared to the CV of the fresh biosensor in order to prove that the surface was not damaged during the procedure (Fig. 53).

It is clear that the polyPLG/PG/GC ME is able to generate substantial fluxes $O_2^{\bullet-}$. Follow-up reactions will inevitably lead to the formation of H_2O_2. However, it cannot be decided in term of this investigation if H_2O_2 is also formed directly by heterogeneous reactions at the polymer or exclusively as a product of homogeneous disproportionation reactions. By carrying out a suitable strategy a polyPLG/PG/GC ME can be used as a generator of selective flux of $O_2^{\bullet-}$ or H_2O_2.

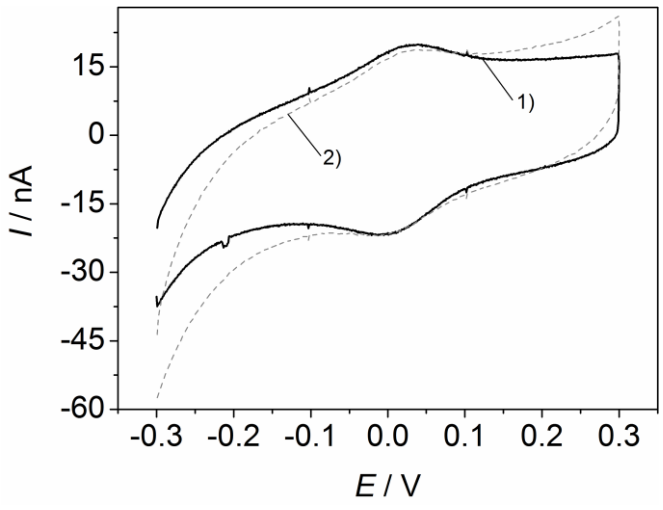

Figure 53: CV of biosensor before (1) and after detection (2) in 0.1 M phosphate buffer pH 7, v = 0.05 V s^{-1} vs. Ag/AgCl/3 M NaCl.

8.2 Local oxidative stress on cultured retinal pigment epithelium cells

Here the evaluation of the role of ROS in the death of cultured cells is described. Moreover, the cells death implies the morphological changes and allows an optical monitoring. Implication of ROS in the death process is undoubted since the antioxidant prevents the cell alterations. ROS was generated locally above the epithelium cells. The B6-RPE07 cells were selected by our partner in Neurobiology Department because of their high susceptibility to oxidative stress. They possess a strong mitochondrial metabolism and good resistance to many environmental factors. The PLG film was prepared on carbon fiber ME. The ME was positioned using a combination of motorized driver of microscope and the positioning piezo motor of the SECM setup. The focus was set on the cellular extension where the thickness of the cell is thin enough to obtain a good approximation (Fig. 54 (1)). Then using the motorized drive the focal plane of the microscope was moved to 25µm away above the cells. The polyPLG/PLG/CF ME was approaching using a piezo motor until a sharp image of the surface of ME was obtained. This position was used for further studies. The work was performed in serum free solution which does not contain an efficiency $O_2^{\bullet-}$ scavenged. Therefore, the production of $O_2^{\bullet-}$ cannot be neglected.

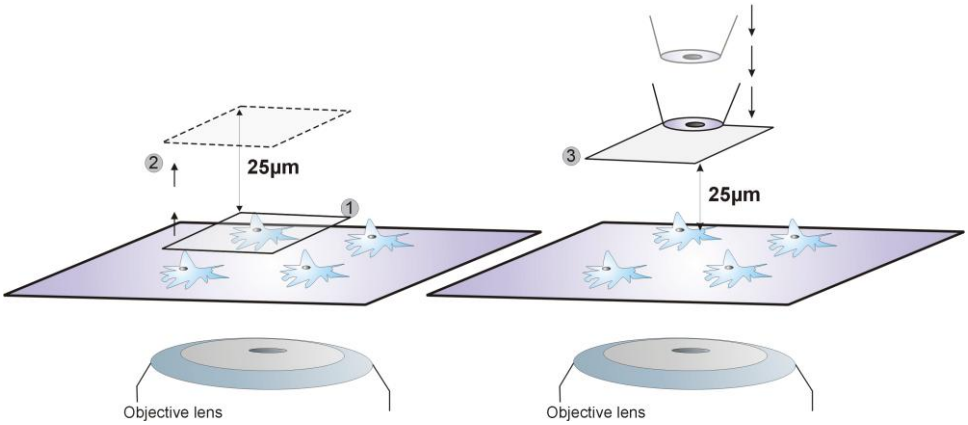

Figure 54: Positioning of the ME (30 µm diameter). The focal plane was first set to the cellular plane and then moved to a distance of 25 µm above the cells by using the motorized stage of the optical microscope. Finally, the ME was moved into focus by the motor of the SECM instrument.

To observe the effect of the local controlled short-term oxidative stress on mammalian B6-RPE07 cells, a polyPLG/PLG/CF ME with 30 µm diameter was used for local generation of ROS. The ROS were in-situ electrogenerated during ORR at polyPLG/PLG/CF ME and then diffuses from the ME to the cell located directly below (Fig. 55) causing local short-term oxidative stress.

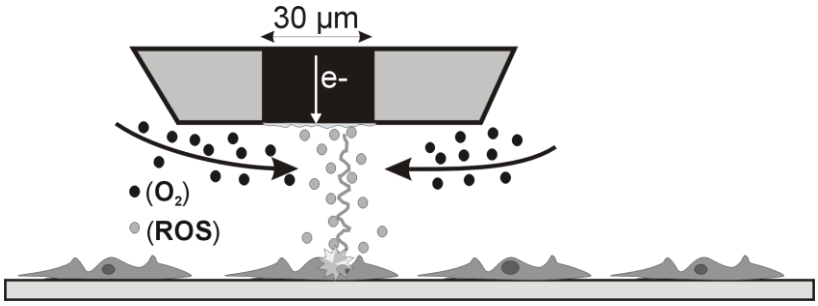

Figure 55: Schematic representation of local ROS generation above cultured cells using a polyPLG/PLG/CF ME.

The local oxidative stress was investigated by monitoring the morphological alteration of the cell. This was an easily accessible parameter compared to the effect on the mitochondrial structural rearrangement or metabolic adaption processes. Different morphological alterations were observed. A typical cell alteration is shown at Fig. 56. It was obtained after a 12 min pulse of ROS generation. In Fig. 56 the polyPLG/PLG/CF ME generator electrode was positioned at the distance of 25 µm above the cell as indicated by the arrow. After 12 min of ORR pulse, the B6-RPE07 cell below the tip of electrode started to round up and cellular processes were retracted. The surroundings cells seemed not to be affected. This clear local morphological changes were observed in 5% of the pulse experiments (n = 2). The local variation of the pH during this procedure cannot be excluded as well as the local decrease of oxygen concentration involved in the cellular metabolism. On other hand, with the same pulse time of ROS formation a slight alteration or loss of the cell adherence to the culture dish (Fig. 57) was observed in other runs. The morphological change in response to local ROS generation was comparable to the one elicited by the incubation of the cells with 0.5 M of H_2O_2 which was added directly to the culture medium (Fig. 58).

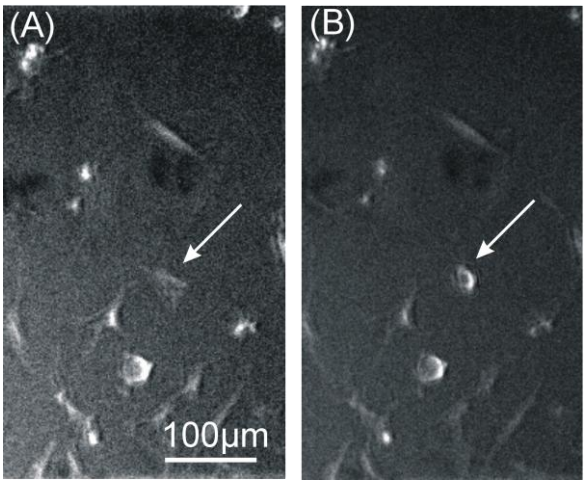

Figure 56: Morphological change of a B6-RPE07 cell to a local exposure of ROS generated at a polyPLG/PLG/CF ME. (A) Before ROS generation, (B) image after a 12 min pulse.

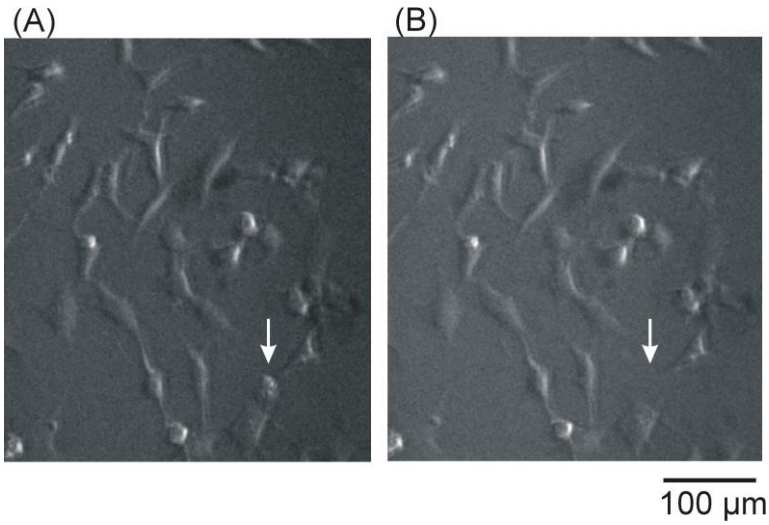

Figure 57: Minor alteration and cell lost of a B6-RPE07 cell to a local exposure of ROS generated at a polyPLG/PLG/CF ME. (A) Image before ROS generation, (B) image after a 12 min pulse.

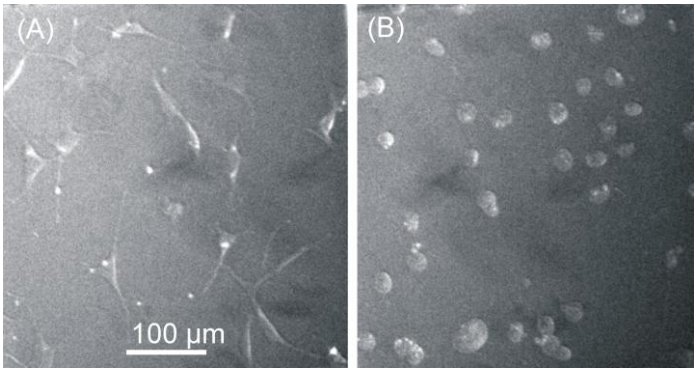

Figure 58: Optical images of the cells before (A) and 60 s after (B) the addition of 0.5 M of H_2O_2 to the cell culture media.

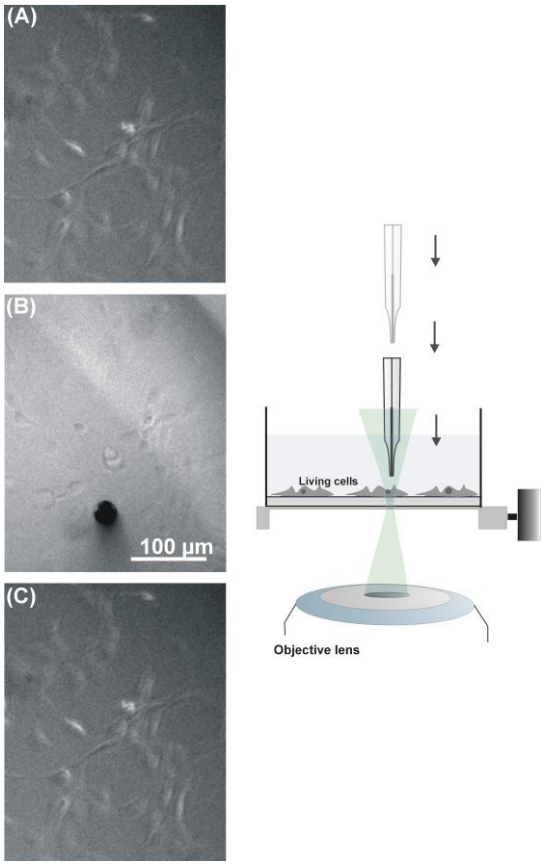

Figure 59: Control measurement of hydrodynamic effects during positioning of polyPLG/PLG/CF ME. (A) Cells before approaching the ME, (B) ME positioned 25 µm above the cells (cells are out of focus), (C) cells after retraction of ME.

Control measurements were performed for each experiment to test the hydrodynamic effects during movement of generator. No cell alteration or damage was observed during the movement of CF ME in the cell medium (Fig. 59A vs. Fig. 59C). A stress condition was also investigated when the cells were removed from incubator and lay down on the cell holder during 2 hours without any exposure to the ROS or movement of CF ME (Fig. 60). This investigation aimed to understand how the environment can influence the viability of the cells.

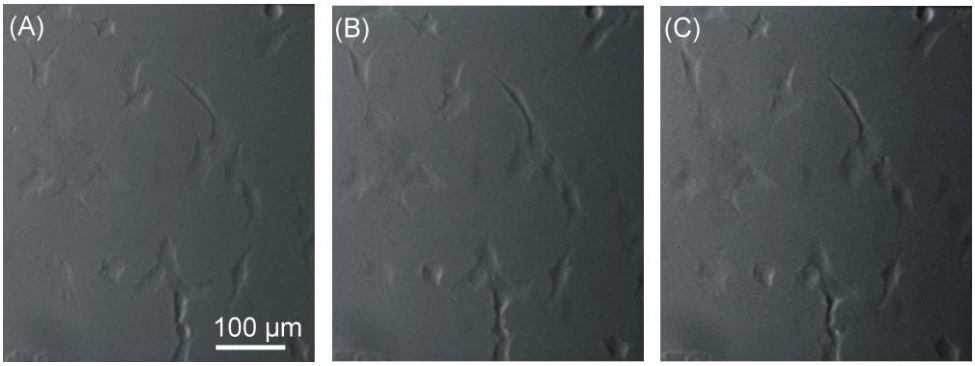

Figure 60: Optical images of morphological states of the cells at (A) 0 min, (B) 30 min and (C) 120 min after removal from the incubator.

Nonetheless, large varieties of cellular changes have been observed depending on the status of the cultured cells and minor compositional variation in the culture medium that may more or less effectively contribute to the scavenging of ROS. Morphological changes were visible only by detailed comparison of minor features of the cells such as slight retraction of cell processes in 35% of the attempts. Since the work is carried out in a buffer, the contributions of local pH changes could be considered as a minor effect compare to the overall small generation currents.

The procedure of local formation of ROS allows generation of low dosages of ROS that could be below the lethal concentrations that are used for bulk additions of H_2O_2. Another clear advantage compared to a bulk addition of H_2O_2 to the culture medium is the possibility to pre-select single cells for stress exposure. Furthermore, cells surroundings the area at a greater distance to the ME generator can be observed to assess how the stress signals are communicated in a cell population.

A prominent damage was also observed after shorter ROS generation pulses but this alteration was not reproducible and can be due of the status of the cell and the cell population, which make the local environnement not optimal for the cells (Fig. 61).

The CA recorded was used to make a semiquantitative evaluation of the amount of $O_2^{\bullet-}$ generated (Fig. 62). The transferred charge at the polyPLG/PLG/CF ME of 1.5 µC were transferred during 12 min (Fig. 62A). In another experiment 1.1 µC where transferred within 3 min using another poly/PLG/PLG/CF ME (Fig. 62B). This corresponds to a total amount of 1.1×10^{-11} mol of $O_2^{\bullet-}$ assuming that the transferred charge was exclusively used for the one-electron reduction of oxygen to $O_2^{\bullet-}$. This value forms an upper limit of the total $O_2^{\bullet-}$ dosage to the cells, because the charge includes the charge used to reduce quinone groups within the polyPLG/PLG film, the electrochemical reduction which may not lead to $O_2^{\bullet-}$ only. The dismutation will decrease the amount of $O_2^{\bullet-}$ and the $O_2^{\bullet-}$ or H_2O_2 diffuse to the outer edge of the insulating sheath, where they are rapidly diluted into the bulk solution. In other words, the upper limit of $O_2^{\bullet-}$ concentration can be given by the solubility of dioxygen in the culture medium under air (0.25 mM). However, the real concentration in the steady state cannot be deduced because the thin layer configuration of the culture dish and the generator electrode cause hindered diffusion of oxygen towards the generator.

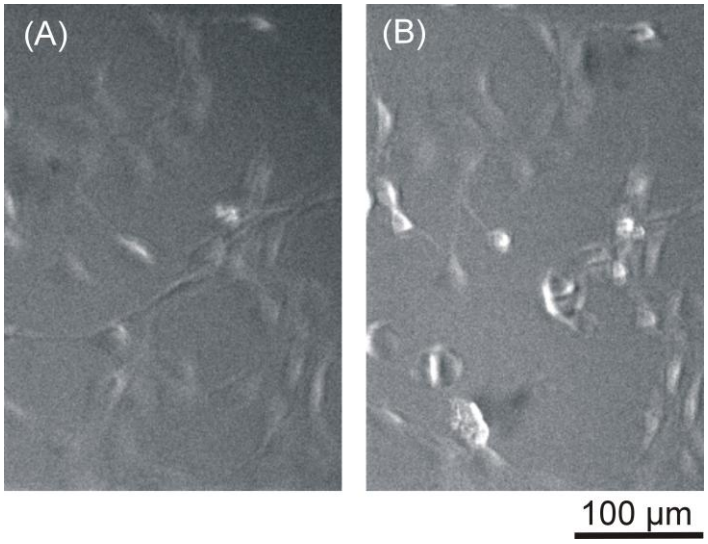

Figure 61: Optical images of cells (A) before and (B) after ROS generation during 3 min.

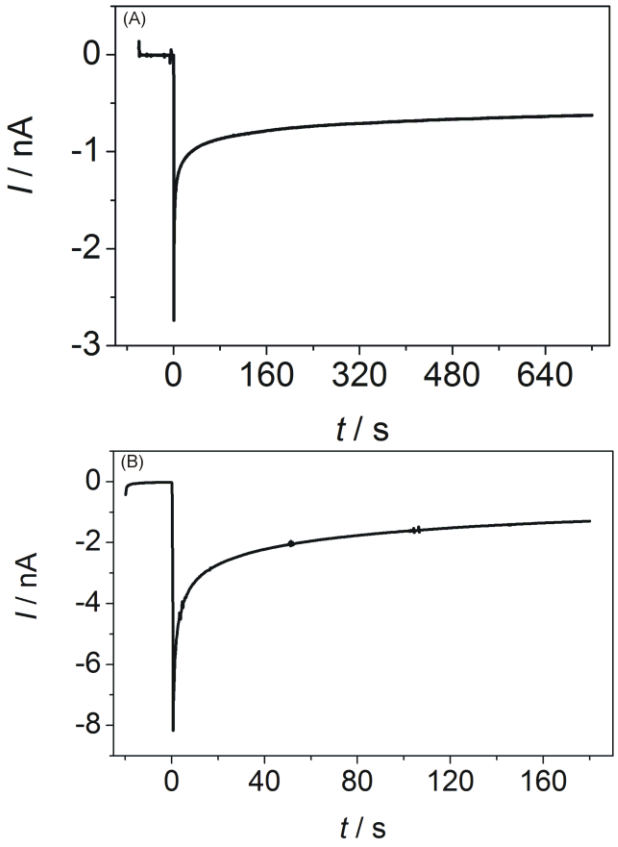

Figure 62: CA recorded at the generator MEs (30 µm diameter) during production of ROS in cell culture media at 25 µm (A) 12 min and (B) 3 min.

9 Summary and outlook

This thesis aimed to explore the formation of ROS during electrocatalysis or catalysis of ORR in different systems. ORR is undeniable the most important reaction in various domain such as in energy conversion. Two ROS were mainly investigated, $O_2^{\bullet-}$ and H_2O_2. A particular attention was paid to the formation of $O_2^{\bullet-}$ which is subject of many controversies that called for consideration of other possible pathways during ORR on different materials.

The first aspect (Chapter 6) of this thesis described the new approach for preparation of quinone-containing polymer modified electrode. The modification of the GC with a PLG monolayer by chemical grafting allows subsequent electropolymerization of a plumbagin polymer. The behavior observed during electropolymerization was different from that of direct electropolymerization on GC. In case of polyPLG/GC self limiting growth is observed, while the growth of polyPLG/PLG/GC is not limited and allows a free adjustment of the film thickness that contains electrochemically accessible quinone groups. The growth of the polymer on a grafted PLG monolayer apparently led to the permeability of this polymer. This is also reflected by the electrocatalysis of the ORR which was similar to PLG/GC and more effective than on directly polymerized polyPLG/GC films. The polyPLG/PLG/GC electrode was used as controllable source of ROS in later experiments of this thesis.

A strategy was developed to investigate the ROS generated during ORR. Instead of a classical technique such as rotating ring disc electrode technique to detect the ROS, SECM or fluorescence microscopy were used. The fluorescence microscopic approach developed in this thesis requires a selective chemical probe for each target oxygen-derived species and then allows a selective investigation. In chapter 7.1, formation of

H_2O_2 at the liquid|liquid interface was followed for the first time in real time using fluorescence microscopy and AUR as a sensitive and selective probe. The liquid|liquid interface was formed between two phase, one acidic aqueous phase and RTILs or organic phase. A strong electron donor such as DMFc was dissolved in non-aqueous phase and used to produce H_2O_2. An in-situ detection of H_2O_2 was possible by using AUR, which produced a fluorescent molecule after catalytic reaction with HRP. The effect of different cations of RTILs on the viscosity of the liquid has been highlighted by the diffusion of fluorescent molecule in different RTILs. The major intensity from fluorescent molecule was observed in non-aqueous phase induced by the partial extraction of the fluorophore to the organic phase. This work demonstrated that simple fuels can be generated at the RTIL|H_2O interface and the reduction power of DMFc in RTILs is large enough to carrier out this reactions in ionic liquid. A similar investigation was performed in DMFc in TFT|H_2O where the organic phase did not consist of ions. Reduction of dioxygen to H_2O_2 was carried out in this simple liquid|liquid two-phase system and also followed by fluorescence microscopy using AUR as H_2O_2-sensitive fluorescent dye. This system is in fact the simplest one for electron transfer reactions at soft interface since it involves only DMFc and two solvents. The thermodynamic calculations confirmed that this simple system provided favorable conditions for the formation of H_2O_2. Using $O_2^{\bullet-}$-sensitive fluorescent dye (NBD-Cl), formation of $O_2^{\bullet-}$ in lithium-oxygen batteries and at the polyPLG/PLG/GC electrode was investigated in chapter 7.2 and 7.3. Detection of $O_2^{\bullet-}$ during discharge in lithium-oxygen batteries was demonstrated at least as an soluble intermediate. The reaction with the fluorogenic compound NBD-Cl removes $O_2^{\bullet-}$and the stable reaction products diffuse away from the GDE. This implies the possibility of new reaction pathways involving $O_2^{\bullet-}$ as

intermediate and rise many questions. The high intensity fluorescence in the cracks of GDE is may be due to the fact that the solution layer probed is thicker in the cracks than above the opaque mesoporous carbon material of the GDE. Instead of RRDE technique, fluorescence microscopy was used to detect $O_2^{\bullet-}$ and H_2O_2 generated at the polyPLG/PLG/GC electrode. AUR as H_2O_2-sensitive fluorescent dye was used to detect H_2O_2 formed during CV and showed a strong variation over the electrode surface. The detection of $O_2^{\bullet-}$ was carried out during CA measurement using NBD-Cl. A precise background correction was applied and a clear difference of the signal was observed compare to the experiment performed in oxygen-free solution. These experiments, confirmed the generation of $O_2^{\bullet-}$ by a PLG compound known to produce mainly H_2O_2 as the final product. This suggest a mechanism which involves the formation of $O_2^{\bullet-}$ at pH 7 during ORR.

In chapter 8.1 diffusion and electrochemical detection of $O_2^{\bullet-}$ was conducted. The biosensor based on cyt c was used. An SECM setup assisted by camera was used to place the polyPLG/PLG/GC ME near the biosensor. At the 10 and 5 µm the $O_2^{\bullet-}$ was generated and diffuse to the biosensor, a current recorded during generation-collection mode at the biosensor shows the increase of the current and a steady state is reached faster at the 5 µm than at 10 µm working distance. A control measurement using SOD which accelerates the dispropornation reactions remove completely the $O_2^{\bullet-}$ from the solution and no current is observed.

An application of such alternative was described in chapter 8.2 with a local formation of ROS above the epithelial cells. A series of control measurements was performed to test the viability of the cells outside the incubator and also the stress situation during the vertical movement of the CF ME. A variety of the morphological

alterations were observed, from a clear round up of the cells to the small alterations of the cells extensions or the loss of adherence on the petri dish. The entire experiment was performed in serum-free solution to allow a formation of ROS.

A number of extensions to the work presented in this thesis are possible. A thickness-controlled polymer could be used as in the strategy of the preparation of polymer-imprinted nanoparticle, a study of ORR at different thickness value can be relevant to understand how the quinone interact with each other and the redox activity of the film at the different thickness. A quinone film can be also used in batteries which involve redox compounds. This polymer could be also used to encapsulate proteins and to prepare a biosensor since the quinone compounds could constitute a suitable bio-interface and facilitate the transfer of electrons. A formation of ROS at the liquid|liquid interface can be tested as one component of the oxygen-batteries where H_2O_2 could be used as fuel for the batteries. In lihium batteries the investigation of further formation of ROS could be also investigated using a selective approach in the way to understand the mechanism during ORR. Application of the local formation of ROS in the cellular environment using polyPLG/PLG/CF ME can be extended with a variety of experiment. Distance dependence, the effect of the time of exposure or the reaction at the different locations to investigate the cell communication during a stress situation are some possibilities. The effect of different dosage on the structure of mitochondria using fluorescence spectroscopy can be performed to investigate the adaptation of the cell to different dosage or to study the local necrosis process of the cell. Using different cell types could constitute a further experiment.

10 Appendix

10.1 Abbreviations

AUR	amplex ultra red
AFM	atomic force microscopy
Bio-SECM	bio-scanning electrochemical microscopy
CA	chronoamperometry
CV	cyclic voltammetry
CE	counter electrode
CLSM	confocal laser scanning microscopy
cyt c	cytochrome c
CF	carbon fiber
c_O, c_R	concentration of the oxidized and reduced form of the redox couple
DA, AD	digital-to-analog and analog-to-digital converter
DMFc	decamethylferrocene
GC	generation-collection mode
GDE	gas diffusion electrode
JUG	juglone
FcMeOH	ferrocenemethanol
ME	microelectrode
ORR	oxygen reduction reaction
Ox or O	oxidized form of redox couple

PLG	plumbagin
PLG/GC	plumbagin-modified glassy carbon
PolyPLG/GC	plumbagin polymer prepared on clean glassy carbon
PolyPLG/PLG/GC	plumbagin polymer prepared on plumbagin-modified glassy carbon
($Q/Q^{\bullet -}/QH_2$)	quinone/semiquinone/hydroquinone
RC	redox completion mode
RDE	rotating disk electrode
RE	reference electrode
Red or R	reduced form of redox couple
RNS	reactive nitrogen species
ROS	reactive oxygen species
RRDE	rotating ring disk electrode
RTIL	room temperature ionic liquid
SAM	self-assembled monolayer
SHE	standard hydrogen electrode
SECM	scanning electrochemical microscopy
SEM	scanning electron microscopy
SG/TC	substrate generation tip- collection
TG/SC	tip-generation substrate collection
UME	ultramicroelectrode
WE	working electrode

10.2 Symbols

Symbol	Quantity	Unit
a	Activity	[-]
A	Area	[cm^2]
α	Transfer coefficient	[-]
c^*	The bulk concentration of the redox active substance	[M]
D	Diffusion coefficient	[$cm^2\ s^{-1}$]
d	ME-sample separation	[µm]
Γ^*	Surface excess of species at equilibrium	[$mol.cm^{-2}$]
k_s°	Heterogeneous standard rate constant	[s^{-1}]
$E°'$	formal potential	[V]
E_{pa}	anodic peak potential	[V]
E_{pc}	Cathodic peak potential	[V]
E_{GDE}	Potential value at a gas-diffusion electrode	[V]
E_{gen}	Potential value at a PLG-polymer GC ME	[V]
E_{sens}	Potential value at a biosensor	[V]
E_T	Potential at the tip	[V]
i_T, $i_{T,\infty}$	ME current, Steady-state ME current	[A]
i_T	Peak current	[A]
ϕ	Galvani potential	[V]
ϕ_i	Potential drop across the inner layer	[V]

$\Delta_o^w\phi$	Interfacial (Galvani) potential difference	[V]
$\Delta_o^w\phi_i^{0'}$	Formal ion transfer potential	[V]
$\Delta_o^w\phi_i^0$	Standard ion transfer potential	[V]
F	Faraday constant	[C mol^{-1}]
k_s°	Heterogeneous standard rate constant	[-]
γ	Activity coefficient	[-]
ΔG_{tr}^o	Standard Gibbs transfer energy	[J mol^{-1}]
$\Delta G_{tr,i}^0$	Standard Gibbs energy of ions transfer	[J mol^{-1}]
g	Geometry-dependant factor related to electrode shape	[-]
λ_{max}	Maximum wavelength	[nm]
μ^o	Standard chemical potential	[J mol^{-1}]
n	Electron stoichiometry	[-]
R	Universal gas constant	[J K^{-1} mol^{-1}]
r_T	Radius of the active electrode area	[µm]
T	Temperature	[K]
t	time	[s]
v	Scan rate	[V s^{-1}]
v_T	Scan rate	[µm s^{-1}]
z	Charge number	[-]

11 Bibliography

[1] C. Song, J. Zhang, in *PEM Fuel Cell Electrocatalysts and Catalyst Layers: Fundamentals and Applications* (Ed.: J. Zhang), Springer London, London, **2008**.

[2] C. A. Hampel, *The encyclopedia of the chemical elements*, Reinhold Book Corp., New York, **1968**.

[3] E. John, *Nature's building blocks: an A-Z guide to the elements*, Oxford University Press, Oxford, **2001**.

[4] M. L'Her, in *Encyclopedia of Electrochemistry*, Wiley-VCH Verlag GmbH & Co. KGaA, **2007**.

[5] R. J. Mailloux, *Redox Biol.* **2015**, *4*, 381.

[6] K. Apel, H. Hirt, *Annu. Rev. Plant Biol.* **2004**, *55*, 373.

[7] R. Maria Giron, J. Marco-Martinez, S. Bellani, A. Insuasty, H. Comas Rojas, G. Tullii, M. R. Antognazza, S. Filippone, N. Martin, *J. Mater. Chem. A* **2016**, *4*, 14284.

[8] M. R. Tarasevich, A. Sadkowski, E. Yeager, in *Comprehensive Treatise of Electrochemistry: Volume 7 Kinetics and Mechanisms of Electrode Processes* (Eds.: B. E. Conway, J. O. M. Bockris, E. Yeager, S. U. M. Khan, R. E. White), Springer US, Boston, MA, **1983**.

[9] C. Zhang, F.-R. F. Fan, A. J. Bard, *J. Am. Chem. Soc.* **2009**, *131*, 177.

[10] C. Wang, X. Zhang, Y. Liu, *Appl. Surf. Sci.* **2015**, *358*, *Part A*, 28.

[11] R. Wang, T. Okajima, F. Kitamura, S. Kawauchi, N. Matsumoto, T. Thiemann, S. Mataka, T. Ohsaka, *J. Phys. Chem. A* **2004**, *108*, 1891.

[12] M. Gutowski, S. Kowalczyk, *Acta Biochim. Pol.* **2013**, *60*, 1.

[13] S. L. Richards, K. A. Wilkins, S. M. Swarbreck, A. A. Anderson, N. Habib, A. G. Smith, M. McAinsh, J. M. Davies, *J. Exp. Bot.* **2014**.

[14] L. A. Del Rio, *J. Exp. Bot.* **2015**, *66*, 2827.

[15] S. I. Liochev, *Free Radical Biol. Med.* **2013**, *60*, 1.

[16] H. Mattila, S. Khorobrykh, V. Havurinne, E. Tyystjärvi, *J. Photochem. Photobiol., B* **2015**, *152, Part B*, 176.

[17] V. I. Lushchak, *Chem.-Biol. Interact.* **2014**, *224*, 164.

[18] P. Fernández-Castro, M. Vallejo, M. F. San Román, I. Ortiz, *J. Appl. Chem. Biotechnol.* **2015**, *90*, 796.

[19] C. Amatore, S. Arbault, A. C. Michael, L. M. Borland ed., CRC Press, Boca Raton, FL, **2007**.

[20] L. Zuo, T. Zhou, B. K. Pannell, A. C. Ziegler, T. M. Best, *Acta Physiol.* **2015**, *214*, 329.

[21] J. J. Gao, K. H. Xu, B. Tang, L. L. Yin, G. W. Yang, L. G. An, *FEBS Journal* **2007**, *274*, 1725.

[22] N. Kishikawa, N. Ohkubo, K. Ohyama, K. Nakashima, N. Kuroda, *Anal. Bioanal. Chem.* **2008**, *393*, 1337.

[23] J. J. Inbaraj, C. F. Chignell, *Chem. Res. Toxicol.* **2004**, *17*, 55.

[24] A. Emadi, A. Le, C. J. Harwood, K. W. Stagliano, F. Kamangar, A. E. Ross, C. R. Cooper, C. V. Dang, J. E. Karp, M. Vuica-Ross, *Bioorg. Med. Chem.* **2011**, *19*, 7057.

[25] Y. Song, G. R. Buettner, *Free Radical Biol. Med.* **2010**, *49*, 919.

[26] M. Yuasa, K. Oyaizu, *Curr. Org. Chem.* **2005**, *9*, 1685.

[27] L. Michaelis, *Cold Spring Harbor Symp. Quant. Biol.* **1939**, *7*, 33.

[28] H. Tatsumi, H. Nakase, K. Kano, T. Ikeda, *J. Electroanal. Chem.* **1998**, *443*, 236.

[29] P. Schopfer, E. Heyno, F. Drepper, A. Krieger-Liszkay, *Plant Physiology* **2008**, *147*, 864.

[30] L. S. Hernandez-Munoz, M. Gomez, F. J. Gonzalez, I. Gonzalez, C. Frontana, *Org. Biomol. Chem.* **2009**, *7*, 1896.

[31] J. C. Forti, R. S. Rocha, M. R. V. Lanza, R. Bertazzoli, *J. Electroanal. Chem.* **2007**, *601*, 63.

[32] A. Sarapuu, K. Helstein, K. Vaik, D. J. Schiffrin, K. Tammeveski, *Electrochim. Acta* **2010**, *55*, 6376.

[33] A. Salimi, H. Eshghi, H. Sharghi, S. M. Golabi, M. Shamsipur, *Electroanalysis* **1999**, *11*, 114.

[34] K. Vaik, U. Mäeorg, F. C. Maschion, G. Maia, D. J. Schiffrin, K. Tammeveski, *Electrochim. Acta* **2005**, *50*, 5126.

[35] M. Mooste, E. Kibena, A. Sarapuu, L. Matisen, K. Tammeveski, *J. Electroanal. Chem.* **2013**, *702*, 8.

[36] G. Cohen, R. E. Heikkila, *J. Biol. Chem.* **1974**, *249*, 2447.

[37] A. J. Lambert, M. D. Brand, *J. Biol. Chem.* **2004**, *279*, 39414.

[38] G. Jürmann, D. J. Schiffrin, K. Tammeveski, *Electrochim. Acta* **2007**, *53*, 390.

[39] F. Mirkhalaf, K. Tammeveski, D. J. Schiffrin, *Phys. Chem. Chem. Phys.* **2004**, *6*, 1321.

[40] K. Vaik, A. Sarapuu, K. Tammeveski, F. Mirkhalaf, D. J. Schiffrin, *J. Electroanal. Chem.* **2004**, *564*, 159.

[41] A. Sarapuu, K. Vaik, D. J. Schiffrin, K. Tammeveski, *J. Electroanal. Chem.* **2003**, *541*, 23.

[42] J. M. Burns, W. J. Cooper, J. L. Ferry, D. W. King, B. P. DiMento, K. McNeill, C. J. Miller, W. L. Miller, B. M. Peake, S. A. Rusak, A. L. Rose, T. D. Waite, *Aquat. Sci.* **2012**, *74*, 683.

[43] G. Bartosz, *Clin. Chim. Acta* **2006**, *368*, 53.

[44] N. Soh, *Anal. Bioanal. Chem.* **2006**, *386*, 532.

[45] A. Gomes, E. Fernandes, J. L. F. C. Lima, *J. Biochem. Biophys. Methods* **2005**, *65*, 45.

[46] P. Wardman, *Free Radical Biol. Med.* **2007**, *43*, 995.

[47] S. Ben-Amor, A. Devin, M. Rigoulet, N. Sojic, S. Arbault, *Electroanalysis* **2013**, *25*, 656.

[48] A. Meunier, M. Bretou, F. Darchen, M. Guille Collignon, F. Lemaître, C. Amatore, *Electrochim. Acta* **2014**, *126*, 74.

[49] Y. Li, C. Sella, F. Lemaître, M. Guille-Collignon, L. Thouin, C. Amatore, *Electrochim. Acta* **2014**, *144*, 111.

[50] A. L. Sanford, S. W. Morton, K. L. Whitehouse, H. M. Oara, L. Z. Lugo-Morales, J. G. Roberts, L. A. Sombers, *Anal. Chem.* **2010**, *82*, 5205.

[51] B. C. Tripathy, R. Oelmüller, *Plant Signaling Behav.* **2012**, *7*, 1621.

[52] X. Yuan, A. N. Pham, C. J. Miller, T. D. Waite, *Environ. Sci. Technol.* **2013**, *47*, 8355.

[53] A. Ikhlaq, D. R. Brown, B. Kasprzyk-Hordern, *Appl. Catal., B* **2013**, *129*, 437.

[54] A. G. Crisostomo, R. B. Moreno, S. Navaratnam, J. A. Wilkinson, R. H. Bisby, *Free Radic. Res.* **2007**, *41*, 730.

[55] M. P. Murphy, *Biochem. J.* **2009**, *417*, 1.

[56] M. I. Heller, P. L. Croot, *Anal. Chim. Acta* **2010**, *667*, 1.

[57] X. Yuan, C. J. Miller, A. N. Pham, T. D. Waite, *Free Radical Biol. Med.* **2014**, *71*, 291.

[58] M. S. El- Deab, T. Ohsaka, *Electrochem. Commun.* **2002**, *4*, 288.

[59] M. Alvarez-Rizatti, K. Jüttner, *J. Electroanal. Chem.* **1983**, *144*, 351.

[60] R. R. Adžić, S. Strbac, N. Anastasijević, *Mater. Chem. Phys.* **1989**, *22*, 349.

[61] S. Štrbac, R. R. Adžić, *Electrochim. Acta* **1996**, *41*, 2903.

[62] M. Zhou, Y. Yu, K. Hu, M. V. Mirkin, *J. Am. Chem. Soc.* **2015**, *137*, 6517.

[63] J.-M. Noël, A. Latus, C. Lagrost, E. Volanschi, P. Hapiot, *J. Am. Chem. Soc.* **2012**, *134*, 2835.

[64] A. J. Bard, *J. Am. Chem. Soc.* **2010**, *132*, 7559.

[65] E. Lobyntseva, T. Kallio, N. Alexeyeva, K. Tammeveski, K. Kontturi, *Electrochim. Acta* **2007**, *52*, 7262.

[66] V. A. Roginsky, L. M. Pisarenko, W. Bors, C. Michel, *J. Chem. Soc., Perkin Trans. 2* **1999**, 871.

[67] Y. A. Ilan, G. Czapski, D. Meisel, *Biochim. Biophys. Acta* **1976**, *430*, 209.

[68] K. Öllinger, G. D. Buffinton, L. Ernster, E. Cadenas, *Chem. Biol. Interact.* **1990**, *73*, 53.

[69] T. W. Schultz, A. P. Bearden, *Bull. Environ. Contam. Toxicol.* **1998**, *61*, 405.

[70] E. J. Land, T. Mukherjee, A. J. Swallow, J. M. Bruce, *J. Chem. Soc., Faraday Trans. 1* **1983**, *79*, 391.

[71] C. Morin, T. Besset, J.-C. Moutet, M. Fayolle, M. Bruckner, D. Limosin, K. Becker, E. Davioud-Charvet, *Org. Biomol. Chem.* **2008**, *6*, 2731.

[72] M. Knüpling, J. T. Törring, S. Un, *Chem. Phys.* **1997**, *219*, 291.

[73] J. M. Robinson, T. Ohira, J. A. Badwey, *Histochem. Cell Biol.* **2004**, *122*, 293.

[74] X. Zhao, M. Zhang, Y. Long, Z. Ding, *Can. J. Chem.* **2010**, *88*, 569.

[75] C. M. Maier, P. H. Chan, *The Neuroscientist* **2002**, *8*, 323.

[76] Y. Groemping, K. Rittinger, *Biochem. J.* **2005**, *386*, 401.

[77] S. Arbault, P. Pantano, J. A. Jankowski, M. Vuillaume, C. Amatore, *Anal. Chem.* **1995**, *67*, 3382.

[78] L. Li, Q. Li, P. Chen, Z. Li, Z. Chen, B. Tang, *Anal. Chem.* **2016**, *88*, 930.

[79] N. S. Rajasekaran, P. Connell, E. S. Christians, L.-J. Yan, R. P. Taylor, A. Orosz, X. Q. Zhang, T. J. Stevenson, R. M. Peshock, J. A. Leopold, W. H. Barry, J. Loscalzo, S. J. Odelberg, I. J. Benjamin, *Cell* **2007**, *130*, 427.

[80] P. Korge, G. Calmettes, J. N. Weiss, *Biochim. Biophys. Acta, Bioenerg.* **2015**, *1847*, 514.

[81] M. Ghyczy, C. Torday, M. Boros, *The FASEB Journal* **2003**.

[82] A. Farhana, L. Guidry, A. Srivastava, A. Singh, M. K. Hondalus, A. J. C. Steyn, K. P. Robert, in *Advances in Microbial Physiology, Vol. Volume 57*, Academic Press, **2010**, pp. 43.

[83] B. Heyne, S. Ahmed, J. C. Scaiano, *Org. Biomol. Chem.* **2008**, *6*, 354.

[84] I. Snyrychova, F. Ayaydin, E. Hideg, *Physiol. Plant.* **2009**, *135*, 1.

[85] J. Petlicki, T. G. M. van de Ven, *J. Chem. Soc., Faraday Trans.* **1998**, *94*, 2763.

[86] M. J. Green, H. A. O. Hill, D. G. Tew, N. J. Walton, *FEBS Letters* **1984**, *170*, 69.

[87] C. Calas-Blanchard, G. Catanante, T. Noguer, *Electroanalysis* **2014**, *26*, 1277.

[88] H. A. O. Hill, D. G. Tew, N. J. Walton, *FEBS Letters* **1985**, *191*, 257.

[89] K. Tanaka, Y. Muto, *Bioelectrochem. Bioenerg.* **1992**, *29*, 143.

[90] C. Amatore, S. Arbault, C. Bouton, K. Coffi, J.-C. Drapier, H. Ghandour, Y. Tong, *ChemBioChem* **2006**, *7*, 653.

[91] S. Gáspár, in *Oxidative Stress: Diagnostics, Prevention, and Therapy, Vol. 1083*, American Chemical Society, **2011**.

[92] C. Amatore, S. Arbault, Y. Chen, C. Crozatier, I. Tapsoba, *Lab Chip* **2007**, *7*, 233.

[93] B. Ge, F. Lisdat, *Anal. Chim. Acta* **2002**, *454*, 53.

[94] S. Ben-Amor, E. Vanhove, F. Sékli Belaïdi, S. Charlot, D. Colin, M. Rigoulet, A. Devin, N. Sojic, J. Launay, P. Temple-Boyer, S. Arbault, *Electrochim. Acta* **2014**, *126*, 171.

[95] Š. Mesároš, Ž. Vaňková, S. Grunfeld, A. Mesárošová, T. Malinski, *Anal. Chim. Acta* **1998**, *358*, 27.

[96] F. Lemaître, M. Guille Collignon, C. Amatore, *Electrochim. Acta* **2014**, *140*, 457.

[97] A. Schulte, W. Schuhmann, *Angew. Chem. Int. Ed.* **2007**, *46*, 8760.

[98] L. Hofler, D. Koley, J. Wu, C. Xi, M. E. Meyerhoff, *RSC Advances* **2012**, *2*, 6765.

[99] H. Ren, A. Colletta, D. Koley, J. Wu, C. Xi, T. C. Major, R. H. Bartlett, M. E. Meyerhoff, *Bioelectrochemistry* **2015**, *104*, 10.

[100] H. Ren, M. A. Coughlin, T. C. Major, S. Aiello, A. Rojas Pena, R. H. Bartlett, M. E. Meyerhoff, *Anal. Chem.* **2015**, *87*, 8067.

[101] Y. Wu, Z. Zhou, M. E. Meyerhoff, *J. Biomed. Mater. Res., Part A* **2007**, *81A*, 956.

[102] Y. Wang, J.-M. Noël, J. Velmurugan, W. Nogala, M. V. Mirkin, C. Lu, M. Guille Collignon, F. Lemaître, C. Amatore, *Proc. Natl. Acad. Sci.* **2012**, *109*, 11534.

[103] C. G. Zoski, *J. Electrochem. Soc.* **2016**, *163*, H3088.

[104] G. Wittstock, M. Burchardt, S. E. Pust, Y. Shen, C. Zhao, *Angew. Chem. Int. Ed.* **2007**, *46*, 1584.

[105] A. J. Bard, F. R. F. Fan, J. Kwak, O. Lev, *Anal. Chem.* **1989**, *61*, 132.

[106] R. C. Engstrom, M. Weber, D. J. Wunder, R. Burgess, S. Winquist, *Anal. Chem.* **1986**, *58*, 844.

[107] J. Kwak, A. J. Bard, *Anal. Chem.* **1989**, *61*, 1221.

[108] R. J. Forster, T. E. Keyes, in *Handbook of Electrochemistry*, Elsevier, Amsterdam, **2007**.

[109] A. J. Bard, L. P. Faulkner, *Electrochemical methodes, Fundamentals and Applications*, John Wiley & Sons, New York, Chichester, Brisbane, Toronto, **1980**.

[110] J. L. Amphlett, G. Denuault, *J. Phys. Chem. B* **1998**, *102*, 9946.

[111] Y. Shao, M. V. Mirkin, *J. Phys. Chem. B* **1998**, *102*, 9915.

[112] M. V. Mirkin, F.-R. F. Fan, A. J. Bard, *J. Electroanal. Chem.* **1992**, *328*, 47.

[113] A. J. Bard, M. V. Mirkin, P. R. Unwin, D. O. Wipf, *J. Phys. Chem.* **1992**, *96*, 1861.

[114] C. Lefrou, *J. Electroanal. Chem.* **2006**, *592*, 103.

[115] R. Cornut, C. Lefrou, *J. Electroanal. Chem.* **2007**, *608*, 59.

[116] R. Cornut, C. Lefrou, *J. Electroanal. Chem.* **2008**, *621*, 178.

[117] P. Sun, F. O. Laforge, M. V. Mirkin, *Phys. Chem. Chem. Phys.* **2007**, *9*, 802.

[118] D. T. Pierce, P. R. Unwin, A. J. Bard, *Anal. Chem.* **1992**, *64*, 1795.

[119] D. T. Pierce, A. J. Bard, *Anal. Chem.* **1993**, *65*, 3598.

[120] G. Wittstock, K.-j. Yu, H. B. Halsall, T. H. Ridgway, W. R. Heineman, *Anal. Chem.* **1995**, *67*, 3578.

[121] K. Eckhard, X. Chen, F. Turcu, W. Schuhmann, *Phys. Chem. Chem. Phys.* **2006**, *8*, 5359.

[122] X. Chen, K. Eckhard, M. Zhou, M. Bron, W. Schuhmann, *Anal. Chem.* **2009**, *81*, 7597.

[123] M. Michalak, M. Kurel, J. Jedraszko, D. Toczydlowska, G. Wittstock, M. Opallo, W. Nogala, *Anal. Chem.* **2015**, *87*, 11641.

[124] J. Li, J. Yu, *Bioelectrochemistry* **2008**, *72*, 102.

[125] A. Pailleret, J. Oni, S. Reiter, S. Isik, M. Etienne, F. Bedioui, W. Schuhmann, *Electrochem. Commun.* **2003**, *5*, 847.

[126] S. Dongmo, J. Witt, G. Wittstock, *Electrochim. Acta* **2015**, *155*, 474.

[127] N. Arroyo-Currás , A. J. Bard, *J. Phys. Chem. C* **2015**, *119*, 8147.

[128] G. K. Kiema, S. Ssenyange, M. T. McDermott, *J. Electrochem. Soc.* **2004**, *151*, C142.

[129] M. M. Ardakani, E. P. Karami, R. H. Zare, M. Hamzehloo, *Microchim. Acta* **2007**, *159*, 165.

[130] A. Krylov, M. Beissenhirtz, H. Adamzig, F. Scheller, F. Lisdat, *Anal. Bioanal. Chem.* **2004**, *378*, 1327.

[131] A. Yarman, B. Neumann, M. Bosserdt, N. Gajovic-Eichelmann, F. W. Scheller, *Biosensors* **2012**, *2*, 189.

[132] M. Chen, E. Muckersie, M. Robertson, M. Fraczek, J. V. Forrester, H. Xu, *Invest. Ophthalmol. Visual Sci.* **2008**, *49*, 3699.

[133] M.-C. Pham, A. Hachemi, J.-E. Dubois, *J. Electroanal. Chem.* **1984**, *161*, 199.

[134] M.-C. Pham, J.-E. Dubois, *J. Electroanal. Chem.* **1986**, *199*, 153.

[135] M.-C. Pham, P.-C. Lacaze, J.-E. Dubois, *J. Electroanal. Chem.* **1978**, *86*, 147.

[136] A. J. Downard, M. J. Prince, *Langmuir* **2001**, *17*, 5581.

[137] H.-H. Yang, R. L. McCreery, *Anal. Chem.* **1999**, *71*, 4081.

[138] H.-G. Hong, M. D. Porter, *J. Electroanal. Chem.* **2005**, *578*, 113.

[139] C. Saby, B. Ortiz, G. Y. Champagne, D. Bélanger, *Langmuir* **1997**, *13*, 6805.

[140] A. Dekanski, J. Stevanović, R. Stevanović, B. Ž. Nikolić, V. M. Jovanović, *Carbon* **2001**, *39*, 1195.

[141] G. Ilangovan, K. Chandrasekara Pillai, *J. Solid State Electrochem.* **1999**, *3*, 357.

[142] G. E. Cabaniss, A. A. Diamantis, W. R. Murphy, R. W. Linton, T. J. Meyer, *J. Am. Chem. Soc.* **1985**, *107*, 1845.

[143] G. Ilangovan, K. Chandarasekara Pillai, *J. Electroanal. Chem.* **1997**, *431*, 11.

[144] N. M. Pontikos, R. L. McCreery, *J. Electroanal. Chem.* **1992**, *324*, 229.

[145] S. Thiagarajan, T.-H. Tsai, S.-M. Chen, *Biosens. Bioelectron.* **2009**, *24*, 2712.

[146] R. J. Taylor, A. A. Humffray, *J. Electroanal. Chem.* **1973**, *42*, 347.

[147] W. J. Blaedel, R. A. Jenkins, *Anal. Chem.* **1975**, *47*, 1337.

[148] R. C. Engstrom, *Anal. Chem.* **1982**, *54*, 2310.

[149] J. C. Harfield, C. Batchelor-McAuley, R. G. Compton, *Analyst* **2012**, *137*, 2285.

[150] G. March, S. Reisberg, B. Piro, M. C. Pham, M. Delamar, V. Noel, K. Odenthal, D. B. Hibbert, J. J. Gooding, *J. Electroanal. Chem.* **2008**, *622*, 37.

[151] A. J. Bard, L. R. Faulkner, *Electrochemical Methods: Fundamentals and Applications*, 2nd ed., John Wiley & Sons, New York, **2001**.

[152] A. P. Brown, F. C. Anson, *Anal. Chem.* **1977**, *49*, 1589.

[153] P. T. Lee, D. Lowinsohn, R. G. Compton, *Analyst* **2014**, *139*, 3755.

[154] R. B. Smith, C. Canton, N. S. Lawrence, C. Livingstone, J. Davis, *New J. Chem.* **2006**, *30*, 1718.

[155] K. Gong, X. Zhu, R. Zhao, S. Xiong, L. Mao, C. Chen, *Anal. Chem.* **2005**, *77*, 8158.

[156] M. Ferreira, H. Varela, R. M. Torresi, G. Tremiliosi-Filho, *Electrochim. Acta* **2006**, *52*, 434.

[157] M. Gattrell, D. W. Kirk, *J. Electrochem. Soc.* **1993**, *140*, 903.

[158] M.-C. Pham, B. Piro, E. A. Bazzaoui, M. Hedayatullah, J.-C. Lacroix, P. Novák, O. Haas, *Synth. Met.* **1998**, *92*, 197.

[159] L. A. A. Newton, E. Cowham, D. Sharp, R. Leslie, J. Davis, *New J. Chem.* **2010**, *34*, 395.

[160] F. Bruno, M. C. Pham, J. E. Dubois, *Electrochim. Acta* **1977**, *22*, 451.

[161] M. Gattrell, D. W. Kirk, *Can. J. Chem. Eng.* **1990**, *68*, 997.

[162] N. Belhadj Tahar, R. Abdelhédi, A. Savall, *J. Appl. Electrochem.* **2008**, *39*, 663.

[163] E. Laviron, *J. Electroanal. Chem.* **1979**, *101*, 19.

[164] J. Jedraszko, W. Nogala, W. Adamiak, S. Dongmo, G. Wittstock, H. H. Girault, M. Opallo, *Chem. Commun.* **2015**, *51*, 6851.

[165] W. Adamiak, J. Jedraszko, W. Nogala, M. Jönsson-Niedziolka, S. Dongmo, G. Wittstock, H. H. Girault, M. Opallo, *J. Phys. Chem. C* **2015**, *119*, 20011.

[166] P. Schwager, S. Dongmo, D. Fenske, G. Wittstock, *Phys. Chem. Chem. Phys.* **2016**, *18*, 10774.

[167] S. Dongmo, J. Leyk, C. Dosche, C. Richter-Landsberg, U. Wollenberger, G. Wittstock, *Electroanalysis* **2016**, *28*, 2400.

[168] R. M. Allen, D. E. Williams, *Faraday Discuss.* **1996**, *104*, 281.

[169] B. Su, I. Hatay, F. Li, R. Partovi-Nia, M. A. Méndez, Z. Samec, M. Ersoz, H. H. Girault, *J. Electroanal. Chem.* **2010**, *639*, 102.

[170] P. Wasserscheid, W. Keim, *Angew. Chem., Int. Ed.* **2000**, *39*, 3772.

[171] R. Marcilla, J. A. Blazquez, R. Fernandez, H. Grande, J. A. Pomposo, D. Mecerreyes, *Macromol. Chem. Phys.* **2005**, *206*, 299.

[172] J. J. H. Davis, *Chem. Lett.* **2004**, *33*, 1072.

[173] P. Wasserscheid, T. Welton, in *Ionic Liquids in Synthesis*, Wiley-VCH Verlag GmbH & Co. KGaA, **2003**.

[174] M. J. Earle, K. R. Seddon, in *Clean Solvents, Vol. 819*, American Chemical Society, **2002**.

[175] U. Kragl, M. Eckstein, N. Kaftzik, *Curr. Opin. Biotechnol.* **2002**, *13*, 565.

[176] S. Park, R. J. Kazlauskas, *Curr. Opin. Biotechnol.* **2003**, *14*, 432.

[177] C. E. Song, *Chem. Commun.* **2004**, 1033.

[178] Z. Yang, W. Pan, *Enzyme Microb. Technol.* **2005**, *37*, 19.

[179] K. Fujita, M. Forsyth, D. R. MacFarlane, R. W. Reid, G. D. Elliott, *Biotechnol. Bioeng.* **2006**, *94*, 1209.

[180] P. Wang, S. M. Zakeeruddin, J.-E. Moser, R. Humphry-Baker, M. Grätzel, *J. Am. Chem. Soc.* **2004**, *126*, 7164.

[181] Y. Wang, K. Zaghib, A. Guerfi, F. F. C. Bazito, R. M. Torresi, J. R. Dahn, *Electrochim. Acta* **2007**, *52*, 6346.

[182] N. Papageorgiou, Y. Athanassov, M. Armand, P. Bonho⁄te, H. Pettersson, A. Azam, M. Grätzel, *J. Electrochem. Soc.* **1996**, *143*, 3099.

[183] K. Xu, *Chem. Rev.* **2004**, *104*, 4303.

[184] R. Kawano, M. Watanabe, *Chem. Commun.* **2005**, 2107.

[185] R. F. de Souza, J. C. Padilha, R. S. Gonçalves, J. Dupont, *Electrochem. Commun.* **2003**, *5*, 728.

[186] W. Nernst, E. H. Riesenfeld, *Ann. Phys.* **1902**, *313*, 600.

[187] E. H. Riesenfeld, *Ann. Phys.* **1902**, *313*, 609.

[188] E. H. Riesenfeld, *Ann. Phys.* **1902**, *313*, 616.

[189] P. Peljo, H. H. Girault, in *Encyclopedia of Analytical Chemistry*, John Wiley & Sons, Ltd, **2006**.

[190] F. Reymond, D. Fermín, H. J. Lee, H. H. Girault, *Electrochim. Acta* **2000**, *45*, 2647.

[191] A. Volkov, D. Deamer, *Liquid-Liquid Interfaces: Theory and Methods*, CRC Press, **1996**.

[192] P. Schwager, D. Fenske, G. Wittstock, *J. Electroanal. Chem.* **2015**, *740*, 82.

[193] G. Girishkumar, B. McCloskey, A. C. Luntz, S. Swanson, W. Wilcke, *J. Phys. Chem. Lett.* **2010**, *1*, 2193.

[194] R. Black, B. Adams, L. F. Nazar, *Adv. Energy Mater.* **2012**, *2*, 801.

[195] J. Lu, L. Li, J.-B. Park, Y.-K. Sun, F. Wu, K. Amine, *Chem. Rev.* **2014**, *114*, 5611.

[196] Y.-C. Lu, B. M. Gallant, D. G. Kwabi, J. R. Harding, R. R. Mitchell, M. S. Whittingham, Y. Shao-Horn, *Energy Environ. Sci.* **2013**, *6*, 750.

[197] H.-G. Jung, Y. S. Jeong, J.-B. Park, Y.-K. Sun, B. Scrosati, Y. J. Lee, *ACS Nano* **2013**, *7*, 3532.

[198] M. D. Bhatt, H. Geaney, M. Nolan, C. O'Dwyer, *Phys. Chem. Chem. Phys.* **2014**, *16*, 12093.

[199] V. S. Bryantsev, V. Giordani, W. Walker, M. Blanco, S. Zecevic, K. Sasaki, J. Uddin, D. Addison, G. V. Chase, *J. Phys. Chem. A* **2011**, *115*, 12399.

[200] V. S. Bryantsev, J. Uddin, V. Giordani, W. Walker, D. Addison, G. V. Chase, *J. Electrochem. Soc.* **2013**, *160*, A160.

[201] Z. Peng, S. A. Freunberger, L. J. Hardwick, Y. Chen, V. Giordani, F. Bardé, P. Novák, D. Graham, J.-M. Tarascon, P. G. Bruce, *Angew. Chem., Int. Ed.* **2011**, *50*, 6351.

[202] C. Degrand, L. L. Miller, *J. Electroanal. Chem.* **1981**, *117*, 267.

[203] R. O. Olojo, R. H. Xia, J. J. Abramson, *Anal. Biochem.* **2005**, *339*, 338.

[204] F. Terrier, *Chem. Rev.* **1982**, *82*, 77.

[205] G. A. Artamkina, M. P. Egorov, I. P. Beletskaya, *Chem. Rev.* **1982**, *82*, 427.

[206] M. I. Walash, N. El-Enany, H. C. B. I. O. R. Askar, *Luminescence* **2015**, *30*, 1119.

[207] A. A. Al-Majed, F. Belal, M. A. Abounassif, N. Y. Khalil, *Microchim. Acta* **2003**, *141*, 1.

[208] M. Saran, W. Bors, *Chem.-Biol. Interact.* **1994**, *90*, 35.

[209] H. Jin, D. A. Heller, M. Kalbacova, J.-H. Kim, J. Zhang, A. A. Boghossian, N. Maheshri, M. S. Strano, *Nat. Nanotechnol.* **2010**, *5*, 302.

[210] P. Manning, C. J. McNeil, J. M. Cooper, E. W. Hillhouse, *Free Radical Biol. Med.* **1998**, *24*, 1304.

[211] C. E. Berger, B. R. Horrocks, H. K. Datta, *J. Endocrinol.* **1998**, *158*, 311.

[212] M. K. Beissenhirtz, F. W. Scheller, F. Lisdat, *Anal. Chem.* **2004**, *76*, 4665.

[213] C. E. M. Berger, H. K. Dattaa, B. R. Horrocks, *Phys. Chem. Chem. Phys.* **2011**, *13*, 5288.

12 Own publications and conference contributions

12.1 Publications

- (2015): Saustin Dongmo, Julia Witt and Gunther Wittstock, **Electropolymerization of quinone-polymers onto grafted quinone monolayers: a route towards non-passivating, catalytically active film**, Electrochimica Acta, 155, 474-48

- (2015): Justyna Jedraszko, Wojciech Nogala, Wojciech Adamiak, Saustin Dongmo, Gunther Wittstock, Hubert H. Girault and Marcin Opallo, **Catalysis at the room temperature ionic liquid|water interface: H_2O_2 generation**, Chemical Communications, 51, 6851-6853

- (2015): Adamiak Wojciech; Jedraszko Justyna; Nogala Wojciech; Jönsson-Niedziółka Martin; Dongmo Saustin; Wittstock Gunther; Girault Hubert; Opallo Marcin; **A Simple Liquid–Liquid Biphasic System for Hydrogen Peroxide Generation**; The Journal of Physical Chemistry C, 119, 20011-20015

- (2016): Patrick Schwager; Saustin Dongmo; Daniela Fenske and Gunther Wittstock; **Reactive oxygen species formed in organic lithium-oxygen batteries**; Physical Chemistry Chemicals Physics, 18, 10774 – 10780

- (2016): Saustin Dongmo, Janina Leyk, Carsten Dosche, Christiane Richter-Landsberg, Ulla Wollenberger, Gunther Wittstock; **Electrogeneration of $O_2^{\bullet-}$ and H_2O_2 using polymer-modified microelectrodes in the environment of living cells**; Electroanalysis, 28 (10), 2400-2407

- Saustin Dongmo, Gunther Wittstock and Izabella Brand, **In situ determination of structural changes in redox-active plumbagin polymer film on a glassy carbon electrode using PM IRRAS under electrochemical control** (in preparation)

12.2 Oral presentations in national and international conferences

- S. Dongmo, J. Leyk, C. Dosche, C. Richter-Landsberg, U. Wollenberger, G. Wittstock; "Controlled release of ROS using polymer-modified microelectrode in the cell environment: Investigation of local oxidative stress", GDCh Electrochemistry 2016, 26 - 28 September 2016, Goslar-Germany.

- S. Dongmo, C. Dosche, G. Wittstock; "Detection of superoxide radical generated during electrocatalysis of oxygen reduction on polymer-modified electrode using scanning electrochemical microscopy and fluorescence microscopy", XXIII International Symposium on Bioelectrochemistry and Bioenergetics, 14-18 June, 2015, Malmö-Sweden.

- S. Dongmo, J. Witt, C. Dosche, G. Wittstock, T. Dietz, U. Wollenberger; "Detection of hydrogen peroxide and superoxide radical during electrocatalysis of oxygen reduction on quinone-containing polymer-modified electrode", PhD Workshop on Bioelectrochemistry and Bioanalysis, 20-21 November 2014, Luckenwalde-Germany.

- S. Dongmo, J. Witt, C. Dosche, G. Wittstock, T. Dietz, U. Wollenberger; "Detection of hydrogen peroxide and superoxide radical during electrocatalysis of oxygen reduction on polymer-modified electrode", GDCh Electrochemistry 2014, 22 - 24 September 2014, Mainz-Germany.

12.3 Posters in national and international conferences

- S. Dongmo, I. Brand, W. Nogala, M. Opallo, G. Wittstock; "PM-IRRAS and SECM investigations of redox polymer as organic active material for batteries", GDCh Electrochemistry 2016, 26 – 28 September 2016, Goslar-Germany.
- S. Dongmo, J. Leyk, C. Dosche, C. Richter-Landsberg, U. Wollenberger, G. Wittstock; "Local oxidative stress by controlled release of ROS using polymer-modified microelectrode", The 67th Annual Meeting of the International Society of Electrochemistry, 21-26 August 2016, The Hague-The Netherlands.
- S. Dongmo, C. Dosche, G. Wittstock; "Superoxide radical generated during electrocatalysis of oxygen reduction on quinone-containing polymer-modified electrodes", 11th ECHEMS, 15-18 June 2015, Bad Zwischenahn-Germany.

13 Fellowship, Grant and Award

- Best Poster Prize (symposium 4, The 67th Annual Meeting of the International Society of Electrochemistry, 21-26 August 2016, The Hague)
- DAAD Scholarship (2012-2016)
- IPID4all (Mobile Doctorates in System Integration of Renewable Energy) grant for research stay in Institute of Physical Chemistry, Polish Academic of Sciences Warsaw, Poland (2015)
- Graduate School travel grants (2015)
- GDCh travel grants (2014, 2016)
- AGEF travel grants (2014, 2015 and 2016)
- The Pelle foundation scholarship (2010)

14 Curriculum vitae

Personal information

Name(s):	Saustin Dongmo
Address(es):	Faculty of Mathematics and Natural Sciences Institute of Chemistry Carl-von-Ossietzky-Str.9-1, D-26111 Oldenburg/Germany.
Telephone(s):	+49(0)441 7983977/(+49)17684226901
E-mail:	saustin.dongmo@uni-oldenburg.de/dongmosaustin@daad-alumni.de
Nationality:	Cameroonian
Date of birth:	25 July 1985 at Douala-Cameroon
Family status:	Married and one son
Language	English (Fluent), German (Conversional), French (Excellent), Yemba (Mother tongue)
Gender:	Male

Education and training

Since April 2013	PhD student; *Physical Chemistry (Wittstock group, https://www.uni-oldenburg.de/en/pc2/)* Carl Von Ossietzky University of Oldenburg-Germany

1.10.2012-	German language course (intensive course);
31.03.2013	Carl Duisberg Centrum of Berlin-Germany
2009-2011	Post-graduate Teaching Diploma;
	Chemistry and Didactic;
	Higher Teacher Training College University of Yaoundé 1-Cameroon
2007-2009	Master Diploma;
	Physical Chemistry;
	University of Yaoundé 1-Cameroon
2004-2007	Bachelor Diploma;
	Chemistry;
	University of Dschang-Cameroon

Research stay and working visit

02.2014	Work visit and training at the University of Potsdam, Institute of Biology and Biochemistry , Topic of interest: preparation of biosensor based on cytochrome c
11.2015	Work visit and training at the Polish Academy of Science , Institute of Physical Chemistry, Topic of interest: simple route of preparation of nanoelectrode and 4-dimensional SECM investigation at the modified electrode surface

Professional experience

04.2013-2016	Scientific co-worker in Wittstock group (Tutor during Laboratory courses) Department of Physical Chemistry, University of Oldenburg,

Germany.

Topic: Langmuir Blodgett technique and self assembled monolayer

PMIRRAS measurement

Preparation of microelectrode and nanoelectrode

SECM technique

Biosensor

In-situ detection using Fluorescence microscopy

Electropolymerization and surface modification

2008-2012 Graduate assistant at the University of Yaoundé 1-Cameroon

Ich versichere hiermit, dass ich diese Arbeit selbstständig verfasst und nur die angegebenen Quellen und Hilfsmittel benutzt habe. Während der Dissertation sind die unter "Publications" aufgelisteten Veröffentlichungen entstanden. Die Dissertation hat weder zu Teilen noch in Gänze einer anderen wissenschaftlichen Hochschule zur Begutachtung in einem Promotionsverfahren vorgelegen.

Oldenburg, den 08.12.2016

Saustin Dongmo